The salty truth behind gassy ponds: stratification and greenhouse gas emissions in urban stormwater ponds in southern Ontario

by

Rayden Laliberte

A thesis

presented to the University of Waterloo

in fulfillment of the

thesis requirement for the degree of

Master of Science

in

Geography (Water)

Waterloo, Ontario, Canada, 2025

© Rayden Laliberte 2025

Author’s Declaration

I hereby declare that I am the sole author of this thesis. This is a true copy of the thesis, including any required final revisions, as accepted by my examiners.

I understand that my thesis may be made electronically available to the public.

Abstract

Urban stormwater management ponds are established end-of-pipe components of green stormwater management infrastructure in North America. The main aim of this infrastructure is to protect our cities and homes from storm flooding and to clean the water before introducing it to protected ecosystems. While created for stormwater management, stormwater ponds provide key ecosystem services in urban areas, such as storing carbon, preserving biodiversity, and enhancing the connection to nature for the surrounding communities. Regardless of these services, stormwater ponds also accumulate large loads of organic matter, nutrients, and contaminants from their catchment and undergo a range of aerobic to anaerobic microbial processes that create and release significant amounts of greenhouse gases (GHGs) such as methane (CH_4), carbon dioxide (CO_2), and nitrous oxide (N_2O). Pond design and catchment inputs may affect the processes and the GHG exchanges from the ponds. Therefore, this study aims to understand the processes that drive GHG emissions under the different design and contaminant conditions of depth and road salt concentration in four ponds over a study period from June - November and April - May the following year with no sampling over the winter months. The high salt ponds had greater stratification induced by road salt density gradient impact then their low salt counterparts, which was reflected in water specific conductivity and dissolved oxygen (DO), the stratification indexes calculated from the water column density gradients of each sample location, and the redox water quality sampling profiles. The CH_4 emissions of the high salt ponds were also higher than their low salt counterparts, with the shallow ponds having higher emissions then the deep ponds, while the CO_2 and N_2O emissions were not driven by depth or road salt. A redundancy analysis showed that there were six significant predictors for the GHG emissions: specific conductivity, temperature, pH, dissolved CH_4 concentration, DO, and pond depth. CO_2 emissions were associated with deeper, cooler, low-conductivity conditions, whereas CH_4 diffusive emission and N_2O emissions were associated with high-conductivity, low-oxygen waters and ebullitive CH_4 emission aligned with warm, higher pH environments. These findings highlight the complex and dynamic role of stormwater management infrastructure in urban GHG emissions and the importance of understanding the processes that govern them.

Key words: stormwater management ponds, water quality stratification, road salt, greenhouse gas emissions

Acknowledgments

I would like to express my gratitude to my supervisor Dr. Maria Strack, for her guidance, support, and encouragement throughout the period of this research. I am also grateful to my committee members, Dr. Merrin Macrae and Dr. Bruce MacVicar, for their insightful comments and support. My sincere thanks to the Department of Geography and Environmental Management for providing the resources and environment needed to complete this work.

This project would not have been possible without the help and support of many individuals in the lab and in the field. I would like to thank Akshara Withanage, Allison Yang, Ellie Harrison, Syd Higgins, Yimeng Wang, Kiki Kimber, Cody Palmer, and Maryam Bayatvarkeshi for the countless hours and help spent on data collection. Fieldwork would not have been possible without immense support. I wish to thank all the members in our lab for sharing their ideas, offering help when needed, and listening when I needed to share my thoughts and feelings; it all meant more to me then I can properly express. I would additionally like to thank Thiruni Thirimanne for her help in compiling watershed characteristics.

I acknowledge that my research was conducted on the traditional lands of the Neutral, Anishinaabeg, and Haudenosaunee peoples.

This research is a part of RISE (Residential Development Impact Scorecard for the Environment) project. I am grateful to all the parties involved in this project, particularly the participating cities for their generous support throughout the research. The RISE project was undertaken with the financial support of the Government of Canada's Climate Action and Awareness Fund. Special thanks to the City of Kitchener and City of Waterloo for their assistance with site access, providing site information and documents, and background information.

I acknowledge that artificial intelligence tools (ChatGPT version 5.0) were used solely for obtaining guidance in generating and troubleshooting R codes and language refinement.

Content

Author's Declaration ii
Abstract iii
Acknowledgments iv
List of Figures viii
List of Tables xii
Chapter 1: Literature Review 1
1.1 Introduction 1
1.2 Urban Stormwater Ponds 2
1.3 Carbon and Greenhouse Gas Exchange in Stormwater Ponds 3
1.3.1 Carbon Dioxide 4
1.3.2 Methane 5
1.3.3 Nitrous Oxide 7
1.4 Road Salt: Contaminant of Concern 9
1.5 Knowledge-Led Decision Making 9
1.6 Research Gap 11
Chapter 2: Stratification in Urban Stormwater Ponds in Southern Ontario 13
2.1 Introduction 13
2.1.1 Biogeochemical Pond Conditions 13
2.1.2 Road Salt: Contaminant of Concern 15
2.2 Methods 16
2.2.1 Site Selection & Study Design 16
2.2.2 Pond Water Quality 18
2.2.3 Dissolved Methane Concentration 21
2.2.4 Pond Level Monitoring 21
2.2.5 Data Analysis 22
2.3 Results 23

2.3.1 Temporal Patterns of Water Chemistry at the Deepest Point 24
2.3.2 Spatial Variation in Water Chemistry 32
2.3.3 Variation in Water Chemistry and Redox Conditions among Ponds 38
2.4 Discussion 40
2.5 Conclusion 44
Chapter 3: Greenhouse Gas Emissions from Salt Impacted Stormwater Management Ponds in Southern Ontario 45
3.1 Introduction 45
3.2 Methods 47
3.2.1 Site Selection & Study Design 47
3.2.2 Pond Water Quality 49
3.2.3 Greenhouse Gas Fluxes 50
3.2.4 Dissolved Gas Concentration 52
3.2.5 Data Analysis 53
3.3 Results 56
3.3.1 Environmental Conditions 56
3.3.2 Dissolved CH_4 and N_2O Concentrations 57
3.3.3 Greenhouse Gas Exchange 58
3.3.4 Environmental Controls on GHG Exchange 64
3.4 Discussion 72
3.4.1 Methane Fluxes 73
3.4.2 Carbon Dioxide Fluxes 75
3.4.3 Nitrous Oxide Fluxes 76
3.4.4 Management Implications 77
3.5 Conclusion 78
Chapter 4: Summary and Conclusion 79

4.1 Water Quality & Stratification 79
4.2 Greenhouse Gas Exchange 80
4.3 Limitations & Future Research Needs 80
4.3.1 Site Selection 80
4.3.2 Water Quality & Stratification 81
4.3.3 Greenhouse Gas Exchange 82
4.4 Implications 83
References 84
Appendix A: Chapter 2 Supplemental Figures & Tables 91
Appendix B: Chapter 3 Supplemental Figures & Tables 103

List of Figures

Figure 1.1 Redox cascade and energy layers within an aquatic ecosystem. 6
Figure 2.1. Example of sampling design showing flow transect (Inlet, Middle, Outlet) and depth transect (Deep, Medium, Shallow). In this pond, the transects shared a sampling point where the outlet location of the flow transect was also the deep sampling point for the depth transect. No sampling was conducted at the locations marked as "Pond features". 18
Figure 2.2. Pond sampling schematic – demonstrating the water column sampling profiles. 19
Figure 2.3 Engineered shallow ponds' hydrograph of the pond water level and climate station precipitation of the a) shallow and low salt and b) shallow and high salt pond, the deepest location time series contours with the c) the temperature at depth for the shallow & low salt pond, d) the temperature at depth for the shallow & high salt pond, e) the specific conductivity at depth for the shallow & low salt pond, f) the specific conductivity at depth for the shallow & high salt pond, g) the dissolved oxygen at depth for the shallow & low salt pond, h) the dissolved oxygen at depth for the shallow & high salt pond. Black points indicated the dates and depths of measurements. Interpolation was completed using Natural Neighbour in Surfer®. 26
Figure 2.4 Naturalized deep ponds' hydrograph of the pond water level and climate station precipitation of the a) deep and low salt and b) deep and high salt pond, deepest location time series contours, c) the temperature at depth for the deep & low salt pond, d) the temperature at depth for the deep & high salt pond, e) the specific conductivity at depth for the deep & low salt pond, f) the specific conductivity at depth for the deep & high salt pond, g) the dissolved oxygen at depth for the deep & low salt pond, h) the dissolved oxygen at depth for the deep & high salt pond. Black points indicate the dates and depth of measurements. Contours were created using Natural Neighbour in Surfer®. 29
Figure 2.5 Stratification index over time per pond, highlighting both differences within and among engineered and naturalized ponds and the impact of seasonal trends on the

stratification index for all sample locations (each as an individual point) on each measurement date. The dashed line is the 0.287 kg m^{-3} m^{-1} mixing threshold below which ponds are thought to be well-mixed (Holgerson et al., 2022). 31
Figure 2.6 Stratification index by pond for all sampling locations for the entire study period. The centreline in the boxplot given the median, with top and bottom of the box indicating 25th and 75th quartiles, and whiskers illustrating 10th and 90th percentiles. Letters above the boxes indicate the Tukey pairwise comparisons where ponds are significantly different from each other if they share no letters. 32
Figure 2.7 Engineered shallow ponds flow transect contours - Summer 2024, a) the specific conductivity at depth in the shallow & low salt pond, b) the specific conductivity at depth in the shallow & high salt pond, c) the DO at depth in the shallow & low salt pond, d) the DO at depth in the shallow & high salt pond. Black points indicate the depth and the location along the flow transect of the measurements. Contours were created using Natural Neighbour in Surfer®. 33
Figure 2.8 Naturalized deep ponds flow transect contours - Summer 2024, a) the specific conductivity at depth in the deep & low salt pond, b) the specific conductivity at depth in the deep & high salt pond, c) the DO at depth in the deep & low salt pond, d) the DO at depth in the deep & high salt pond. Black points indicate the depth and the location along the flow transect of the measurements. Contours were created using Natural Neighbour in Surfer®. 35
Figure 2.9 Engineered shallow ponds flow transect contours - Spring 2025, a) the specific conductivity at depth in the shallow & low salt pond, b) the specific conductivity at depth in the shallow & high salt pond, c) the DO at depth in the shallow & low salt pond, d) the DO at depth in the shallow & high salt pond. Black points indicate the depth and the location along the flow transect of the measurements. Contours were created using Natural Neighbour in Surfer®. 36
Figure 2.10 Naturalized deep ponds flow transect contours - Spring 2025, a) the specific conductivity at depth in the deep & low salt pond, b) the specific conductivity at depth in the deep & high salt pond, c) the DO at depth in the deep & low salt pond, d) the DO at

depth in the deep & high salt pond. Black points indicate the depth and the location along the flow transect of the measurements. Contours were created using Natural Neighbour in Surfer®. 37
Figure 2.11. Depth profiles of redox reactive ions, Fe (II) and dissolved CH4 measured in the deepest point in each pond during the growing & nongrowing season, July 21-23 and October 10-24, 2024, respectively. Plots are ordered according to the typical redox cascade from high to low energy. 39
Figure 3.1. Site Selection - Deep & Low Salt Pond illustrating GHG emission sampling locations. No measurements were made at the pond features locations. 49
Figure 3.2. The floating chamber used to measure the different GHG fluxes on the pond's water surface. 52
Figure 3.3 Boxplots depicting the diffusive CH_4 (a), ebullitive CH_4 (b), and total CH_4 (c) at the GHG exchange sample locations across the ponds. Ponds are significantly different from each other if they share no letters in common, Results from the LME model can be found in Table 3.5. 61
Figure 3.4 Boxplot depicting the CO_2 fluxes at the GHG exchange sample location across the ponds. Ponds are significantly different from each other if they share no letters in common. Results from the LME model can be found in Table 3.5. 63
Figure 3.5 Boxplot depicting the N_2O fluxes at the GHG exchange sample location across the ponds. Ponds are significantly different from each other if they share no letters in common. Results from the LME model can be found in Table 3.5. 64
Figure 3.6 Scatterplot depicting the relationship between the water column stratification index & diffusive CH_4 (a), ebullitive CH_4 (b), and total CH_4 fluxes (c) across the ponds, with the solid lines showing significant relationships with strong explanatory power ($R^2m > 0.1$) and the dotted lines showing significant relationships with no explanatory power ($R^2m < 0.1$). 68
Figure 3.7. Scatterplot depicting the relationship between the water column stratification index and CO_2 fluxes across the ponds, with the solid lines showing significant

relationships with strong explanatory power ($R^2m > 0.1$) and the dotted lines showing significant relationships with no explanatory power ($R^2m < 0.1$). 69
Figure 3.8 Scatterplot depicting the relationship between the water column stratification index & log N_2O Fluxes across the ponds, with the solid lines showing significant relationships with strong explanatory power ($R^2m > 0.1$) and the dotted lines showing significant relationships with no explanatory power ($R^2m < 0.1$). 70
Figure 3.9. Redundancy analysis investigating environmental controls on GHG fluxes. RDA1 (61% of constrained variance) represented a conductivity–oxygen gradient, and RDA2 (35% of constrained variance) reflects a temperature–pH gradient. Pond identities (type) are abbreviated as shallow & low salt (SLS), shallow & high salt (SHS), deep & low salt (DLS), and deep & high salt (DHS). CH4Eb represents the ebullitive CH_4 fluxes, CH4Diff represents the diffusive CH_4 fluxes, N2O represents the N_2O fluxes, and CO2 represents the CO_2 fluxes. Temp represents water temperature, pH represents water pH, dissolvedCH4 represents the dissolved CH_4 concentrations, DO represents the dissolved oxygen concentration, SpecCond represents the specific conductivity concentration of the water, and Pond_Depth_m represents the pond depth where that sample is. 72

List of Tables

Table 2.1 Physical characteristics of the 4 study sites in the Kitchener-Waterloo area, ON. 17

Table 2.2. Summary statistics of environmental variables[a] at the top and bottom of the water columns across all sample locations of each pond. 24

Table 2.3. Summary statistics of pond stratification index (kg m^{-3} m^{-1}). 30

Table 3.1. Summary mean of environmental variables at the top and bottom of the water columns across all sample locations of each pond. 56

Table 3.2. Water column integrated (Total) and sample depth (Average) dissolved CH_4 and N_2O concentration descriptive statistics (Standard Deviation: SD, Minimum: Min, Maximum: Max) across all locations per pond. 57

Table 3.3. Pond flux descriptive statistics (Standard Deviation: SD, Minimum: Min, Maximum: Max) across all locations per pond. 58

Table 3.4. Sum of ebullition contribution to the sum of total pond CH_4 fluxes. 59

Table 3.5 LME model outputs for the GHG Fluxes ~ Pond x Sampling Location. 60

Table 3.6 LME model outputs for GHG Flux ~ Pond * Stratification Index, with variance explained by the fixed effects (R^2m) and variance explained by fixed and random effects (R^2c). If stratification index was found not to be significant when pond identity was a fixed effect, then it was removed and GHG Flux ~ Stratification Index was run. 65

Chapter 1: Literature Review

1.1 Introduction

Climate change caused by global warming is one of the most important issues of the 21st century due to it causing substantial damages and continuously growing irreversible losses (Calvin et al., 2023). Due to the rising average temperatures and extreme weather, Canada, and in particular Ontario are experiencing infrastructure damages, economic disruptions, ecosystem structure and function transformation, and harm to human health and well-being (Climate Risk Institute, 2023). Adapting to the impacts of climate change in Canada has been a priority for decades and continues to be so, with continually renewed national climate goals and international participation (Warren & Lulham, 2021). The main driver of global warming as identified by the IPCC is the loss of carbon storage and increasing concentrations of greenhouse gases (GHG) in the atmosphere (Calvin et al., 2023), and our best way to manage climate change is with adaptive solutions that both reduce our emissions while mitigating climate change effects (Robertson et al., 2025). Wetlands are one such solution, with their ability to store carbon and capture GHGs, as well as safely storing and slowly releasing received precipitation, groundwater flow, and surface water flow (Price et al., 2023; Ramsar Convention Secretariat, 2016). Additionally, wetlands filter the water that moves through them by capturing and storing the nutrients, while also providing critical habitat to a range of aquatic and terrestrial species (Hotte et al., 2011; Neubauer & Megonigal, 2021). Wetlands are extremely valuable ecosystems that provide multiple services that are becoming increasingly important as the impacts of climate change worsen, and thus they have begun to be incorporated into our designs and plans for the future in different ways (Robertson et al., 2025).

1.2 Urban Stormwater Ponds

One way wetlands and their functions are being incorporated into cities and urban areas is through stormwater management (SWM) infrastructure (Birch et al., 2022; Ontario Ministry of the Environment, 2003). Ontario implements a range of SWM infrastructure, broadly grouped into lot level, conveyance, and end of pipe systems (Ontario Ministry of the Environment, 2003). End of pipe systems consist of wet ponds, constructed wetlands, and dry ponds, with wet ponds having the greatest percentage of its' volume provided in deep water (> 0.5 m) zones, while wetlands are dominated by shallow zones (<0.5 m) (Ontario Ministry of the Environment, 2003, 2016a). Among the end of pipe infrastructure options, wet ponds are the most widely implemented in Ontario, as they provide multiple ecosystem services, while requiring less land area than constructed wetlands (Ontario Ministry of the Environment, 2016b). Accordingly, this thesis explores stormwater management ponds (SWMPs), with particular attention to their functional performance within the urban landscape.

SWMPs are widely implemented in southern Ontario's urban landscapes both to replace wetland losses due to development and to introduce wetland functions and services into areas previously lacking in them (Audet et al., 2020; Birch et al., 2022). SWMPs are designed and implemented in urban areas to improve water quality, provide aquatic habitat and to support carbon storage through vegetation and sediment capturing infrastructure (Kaushal et al., 2014; Marques et al., 2024; Ontario Ministry of the Environment, 2003). Concurrently to these services, SWMPs have been engineered to meet strict hydrologic volume requirements, making them a commonly used component of municipal stormwater planning (Ontario Ministry of the Environment, 2003). As climate change intensifies pressures on built environments, infrastructure that can deliver multiple ecosystem services while maintaining public safety is increasingly valuable (Marques et al., 2024; Price et al., 2023; Robertson et al., 2025). However, growing research raises questions about whether SWMPs consistently deliver these anticipated benefits across all

functional domains (Birch et al., 2022; Kati & Jari, 2016; Malyan et al., 2021; Marques et al., 2024).

1.3 Carbon and Greenhouse Gas Exchange in Stormwater Ponds

An urban pond's most significant GHG exchanges are carbon dioxide (CO_2) and CH_4; however, depending on the nitrogen loading to the system, nitrous oxide (N_2O) could also have a significant exchange (Malyan et al., 2022). In both natural and anthropogenic ponds and wetlands, gas exchange with the atmosphere is governed by the concentration gradient between the water column and the overlying air, as well as the solubility of the gas; for methane (CH_4) since its solubility is so low, ebullition (bubbling) can also be an important emission pathway. The concentration of each gas reflects the net balance between its production and consumption within the system, so the emissions ultimately depend on how these processes interact themselves, as well as with physical controls such as solubility (Neubauer & Megonigal, 2021). Stormwater management ponds, however, receive substantial anthropogenic inputs, particularly nutrient loads, that exceed what natural systems of similar size or morphology would typically experience. These elevated inputs stimulate higher rates of microbial production, often resulting in greater emissions and altered ratios of GHGs compared with natural waterbodies of comparable physical characteristics (Audet et al., 2020; Badiou et al., 2019; D'Acunha & Johnson, 2019; Fan et al., 2022; Grinham et al., 2018; Herrero Ortega et al., 2019; Kaushal et al., 2014; Peacock et al., 2019). GHG emissions from SWMPs in urban environments have received minor attention even though as urbanization and development continues to expand locally and globally, their quantity and spatial extent will continue to increase (Audet et al., 2020; Birch et al., 2022).

1.3.1 Carbon Dioxide

CO_2 is one the most important long lived GHGs, yet it does not have a single, well-defined atmospheric lifetime because it is continuously exchanged among the atmosphere, terrestrial biosphere, and oceans (Prentice et al., 2021). Its removal depends on multiple biogeochemical processes operating over timescales ranging from seconds to centuries (Filonchyk et al., 2024; Prentice et al., 2021). By definition, CO_2 is the reference compound used in calculating global warming potential (GWP) for all other compounds, and therefore has a GWP of 1 (Masson-Delmotte & Intergovernmental Panel on Climate Change, 2023).

In aquatic systems, CO_2 is produced through several pathways. The breakdown of organic matter, derived from both within the system, autochthonous sources, and upstream or catchment inputs, allochthonous sources, is the primary driver of the CO_2 produced aquatic systems. Aerobic respiration is the primary mechanism generating CO_2, although anaerobic metabolism and the oxidation of CH_4 by methanotrophs also contribute to CO_2 concentrations (Filonchyk et al., 2024; Neubauer & Megonigal, 2021). When CO_2 builds up in the water column above saturation levels, it is emitted to the atmosphere mainly via diffusion due to its high solubility within water (Holgerson, 2015; Neubauer & Megonigal, 2021). Conversely, aquatic plants, including emergent, submerged, and floating species, can partially offset these emissions through photosynthesis taking up CO_2, at times drawing the system into a temporary net-CO_2 sink (Holgerson, 2015; Neubauer & Megonigal, 2021).

In SWMPs, these carbon cycling processes are intensified by the large influx of watershed allochthonous organic matter and nutrients their design is intended to capture (Ontario Ministry of the Environment, 2003). The continuous deposition of organic carbon provides substantial substrate for microbial respiration, enhancing CO_2 production. Additionally, the elevated nutrient loads can stimulate primary production, increasing plant biomass and decomposition rates, further contributing to CO_2 production within the sediments and water column (Filonchyk et al., 2024; Kumar et al., 2019; Malyan et al., 2022). Additionally, CH_4 produced within the pond's anoxic zone can be oxidized to CO_2 as it encounters

oxygenated water near the surface, providing another CO_2 production pathway (Holgerson, 2015; Neubauer & Megonigal, 2021). Concurrently, CO_2 uptake by aquatic vegetation and algal communities may offset a portion of these emissions, particularly during periods of high productivity (Gorsky et al., 2019). Therefore, while SWMPs function as effective pollutant capture systems, their biogeochemical conditions also position them as active and dynamic sites of CO_2 production, transformation, and exchange. The studies on urban ponds reported mean (standard deviation: SD) CO_2 fluxes of 628 (795) mg m^{-2} d^{-1} (Audet et al., 2020), 493.7 (529.6) mg m^{-2} d^{-1} (Davidson et al., 2024), 62.5 mg m^{-2} h^{-1} (1500 mg m^{-2} d^{-1}, if this rate is assumed for 24 hours, Gorsky et al., 2019), and 752 mg m^{-2} d^{-1} (Peacock et al., 2019). Across the studies, the primary controls on CO_2 fluxes were vegetation cover (Audet et al., 2020), pH (Gorsky et al., 2019), and silicon and calcium concentrations, suggesting groundwater input (Peacock et al., 2019).

1.3.2 Methane

CH_4 is an important GHG with an atmospheric lifetime of approximately 11.8 years, a GWP of 82.5 years over 20 years and 29 over 100 years (Masson-Delmotte & Intergovernmental Panel on Climate Change, 2023). Despite its short lifetime, CH_4 traps a substantial amount of heat energy and is responsible for 30% of the global warming impact (Filonchyk et al., 2024; Masson-Delmotte & Intergovernmental Panel on Climate Change, 2023).

Methanogenesis is the final step of anaerobic organic matter decomposition and produces CH_4 through a form of anaerobic respiration performed by methanogens, a subset of microbes that belong to the domain of Archaea (Lyu et al., 2018; Neubauer & Megonigal, 2021). Organic matter decomposition and nutrient cycling in aquatic systems depend heavily on oxygen availability (Neubauer & Megonigal, 2021). As dissolved oxygen (DO) concentrations decline with depth within a pond, the water column transitions from oxic near the surface to anoxic near the sediment layer. As ponds typically have limited oxygen sources and replenishment, restricted to surface diffusion or the inflow of oxygen rich water, they often experience oxygen depletion. Under these low oxygen conditions, as seen

in Figure 1.1, microbial communities shift to alternative terminal electron acceptors (TEA) to sustain their respiration (Loewen & Jackson, 2024; Neubauer & Megonigal, 2021). This descent follows the redox cascade, wherein microbes preferentially utilize the TEA that yields the greatest energy until it becomes depleted, subsequently shifting to the next most favourable TEA. Over time, this progression of reductive processes moves from oxygen to nitrate (NO_3^-), manganese and iron oxides (MnO_2 and $Fe(OH)_3$), sulphate (SO_4^{-2}), and finally to CO_2. Once CO_2 is the only remaining TEA, methanogenesis becomes the dominant metabolic pathway, producing CH_4 as the final by-product (Holgerson et al., 2022; Neubauer & Megonigal, 2021). This redox driven progression underpins the biogeochemical functions of a pond, connecting DO dynamics directly GHG production potential.

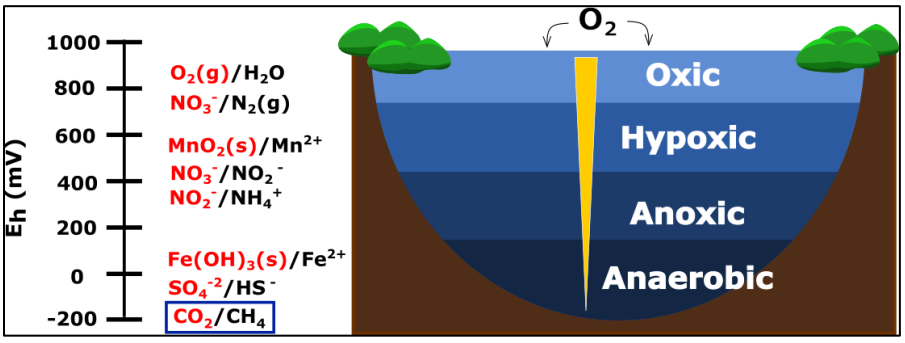


Figure 1.1 Redox cascade and energy layers within an aquatic ecosystem.

In aquatic systems >0.5 m and <4 m deep, such as ponds (Holgerson et al., 2022; Ontario Ministry of the Environment, 2003), CH_4 is emitted through four principal pathways: diffusive flux, ebullitive flux, storage flux, and plant mediated transport (Bastviken et al., 2008). Of these, diffusion and ebullition are a pond's primary CH_4 emission pathways into the atmosphere (Grinham et al., 2018; Neubauer & Megonigal, 2021; Żygadłowska et al., 2024). Diffusive flux occurs when CH_4 produced in the sediment moves along a concentration gradient through the water column to the atmosphere. Once reaching the surface, the dissolved CH_4 diffuses into the atmosphere. However, a portion of produced

CH_4 is oxidized when it encounters the oxic layer of the water column, reducing the amount of CH_4 ultimately emitted (Holgerson, 2015; Venetz et al., 2024).

In contrast, ebullition occurs when CH_4 molecules produced within the sediment accumulate rather than dissolve into the water column due to CH_4's low solubility. As these molecules accumulate, their combined buoyancy eventually exceeds the pressure of the overlying sediment and water, allowing them to escape as bubbles that rise through the water column. This rapid release to the atmosphere limits the opportunity for CH_4 oxidation compared with CH_4 diffusion (Bastviken et al., 2008; Grinham et al., 2018; Neubauer & Megonigal, 2021; Żygadłowska et al., 2024). Another transport pathway that circumvents CH_4 oxidation is plant mediated transport. Many wetland plants use pressurized ventilation, an adaptive mechanism that vents oxygen rich air to their roots, resulting in soil pore water CH_4 diffused into the rhizome being transported upward through the plant material and released directly to the atmosphere (Armstrong & Armstrong, 1991; Sorrell & Boon, 1994; Villa et al., 2020). These pathways lead to high CH_4 production and exchange in SWMPs due to their biogeochemical conditions. The studies on urban ponds reported mean (SD) CH_4 fluxes of 15 (70) mg m^{-2} d^{-1} (Audet et al., 2020), 26.75 (35.26) mg m^{-2} d^{-1} (Davidson et al., 2024), 15.1 mg m^{-2} h^{-1} (362 mg m^{-2} d^{-1} assuming 24 hours of emission; Gorsky et al., 2019), and 30.3 mg m^{-2} d^{-1} (Peacock et al., 2019). Across the studies, the primary controls on CH_4 fluxes were water temperature (Audet et al., 2020), maximum depth and surface area (Gorsky et al., 2019), and total phosphorus and total organic carbon concentration (Peacock et al., 2019).

1.3.3 Nitrous Oxide

N_2O is the third most important GHG emitted from ponds, with an atmospheric lifetime of 109 years in the atmosphere and a GWP of 273 over both 20 and 100 year timescales (Masson-Delmotte & Intergovernmental Panel on Climate Change, 2023). In addition to its high GWP, N_2O emissions are also the most significant ozone depleting emissions (Ravishankara et al., 2009).

In aquatic environments, N_2O production is controlled by microbial nitrogen transformation pathways, primarily nitrification and denitrification, processes where ammonium (NH_4^+) and nitrates (NO_3^-) are used as reactants and N_2O is released as a product (Lunau et al., 2013; Malyan et al., 2021; Neubauer & Megonigal, 2021). The processes are strongly influenced and driven by the availability and quality of the dissolved inorganic nitrogen and the oxygen availability within the system (Davidson et al., 2000; Qiao et al., 2020). Nitrification is the aerobic oxidation of NH_4^+ to NO_3^-, producing intermediate products including N_2O and nitric oxide (NO). Denitrification, by contrast, is the anaerobic reduction of NO_3^- to nitrogen gas (N_2), with N_2O and NO formed as intermediates (Davidson et al., 2000). Owing to its high solubility, N_2O produced through either pathway dissolves readily into the surrounding water, and emissions occur predominantly through diffusive flux across the air–water interface (Hefting et al., 2003).

The production of N_2O, a byproduct of both microbial denitrification and microbial nitrification processes, is largely determined by the nitrogen availability and redox state of the system (Davidson et al., 2000). Wetlands exposed to elevated nutrient loading exhibit substantially higher N_2O emissions (Hefting et al., 2003; Moseman-Valtierra et al., 2011). Since SWMPs are designed to intercept and retain nutrient rich runoff in urban areas (Ontario Ministry of the Environment, 2003), their N_2O emissions are expected to be elevated compared to those of natural systems (Li et al., 2024). Beyond nutrient loads, several biogeochemical factors further influence N_2O dynamics in wetlands, including water level variability, the availability of electron acceptors and donors, hydrogen sulfide concentrations, temperature, and pH (Cornwell et al., 1999; Joye & Hollibaugh, 1995; Megonigal et al., 2014). Many of these conditions are altered in SWMPs relative to natural wetlands, contributing to potentially elevated and variable N_2O production (Haq et al., 2018; Malyan et al., 2021). Therefore, while SWMPs function as effective pollutant capture systems, their biogeochemical conditions also position them as active and dynamic sites of N_2O production, transformation, and exchange. The studies on urban ponds reported mean (SD) N_2O fluxes of 0.19 (0.63) mg m^{-2} d^{-1} (Audet et al., 2020), 0.11 (0.09) mg m^{-2} d^{-1} (Davidson et al., 2024), and 0.0042 mg m^{-2} h^{-1} (0.10 mg m^{-2} h^{-1} assuming 24 hours of

emissions; Gorsky et al., 2019). Among these, only Audet et al. (2020) identified a primary driver of N_2O fluxes, reporting that nitrate concentrations were a key control.

1.4 Road Salt: Contaminant of Concern

Due to the temperate nature of Canada, and Southern Ontario in particular, road salt is often applied to roads and parking lots in the winter months when the temperature falls below 0 °C to reduce the risk of vehicular accidents due to the ice and snow. In 2019, ECCC reported an annual usage of 4,240,983.86 tonnes of total solid salt (ECCC, 2023b). While road salt is applied to ensure the safety of drivers in the winter by increasing the melting temperature of snow and ice (Pollock & The Conversation, 2019), the applied salt is often flushed into stormwater management infrastructure and it can then either remain in a pond or leave through the pond's outflow (Snodgrass et al., 2017). Road salt is now considered one of the most prevalent contaminants of concern for urban waterbodies within southern Ontario due to the decades of application and growing urbanization (Kaushal et al., 2022). When the road salt stays in a pond's water, it can lead to water column stratification by amplifying the density differences of the water, beyond just the typical temperature stratification that occurs within the pond (Loewen & Jackson, 2024). This stratification can reduce the mixing between the water layers, leading to increased oxygen depletion within a pond, creating zones that have thicker layers of anoxic water that resists mixing and remain at a lower energy level for longer, providing greater opportunity for CH_4 production and exchange (Dupuis et al., 2019).

1.5 Knowledge-Led Decision Making

Urban residential developments commonly incorporate and assign cultural value blue–green infrastructure such as SWM ponds, wetlands, and other aquatic features designed to mitigate flooding and regulate stormwater quantity and quality (Kati & Jari, 2016). Although these systems provide essential hydrologic and water-quality functions, as well as cultural

values, they also act as biogeochemical reactors that can emit GHGs through microbial processes and redox-driven transformations. Emerging research indicates that constructed ponds and wetlands can serve as notable sources of CO_2, CH_4, and N_2O in urban landscapes, yet their contribution to municipal GHG budgets remains poorly quantified. Understanding the physical and chemical factors that regulate GHG production in these systems is therefore critical for informing sustainable urban design and management strategies.

Two key characteristics strongly influence the redox reactions and nutrient availability in urban ponds: water depth and salinity (or specific conductivity) (Dupuis et al., 2019; Holgerson, 2015; Holgerson et al., 2022; Kaushal et al., 2022; Kinsman-Costello et al., 2023; Peacock et al., 2019; Ray & Holgerson, 2023). Depth plays a central role in regulating thermal and chemical layering, which in turn shapes oxygen availability, redox gradients, and the spatial organization of microbial processes associated with GHG production. Stormwater ponds vary widely in their engineered depths depending on design objectives, ranging from shallow basins (~1 m) to deep wet ponds (~3 m or more), resulting in substantial differences in stratification potential and internal biogeochemical dynamics (Ontario Ministry of the Environment, 2003).

Salinity is another major driver of density stratification, particularly in cold-climate regions where extensive road salt use elevates chloride concentrations in receiving waterbodies. Elevated salinity increases water density and can strengthen or prolong stratification, reducing vertical mixing and promoting anoxic conditions conducive to CH_4 generation and other anaerobic metabolic reactions (Craig & Zhu, 2018; Dupuis et al., 2019; Haq et al., 2018; Kim & Koretsky, 2013; Loewen & Jackson, 2024; Schuler & Relyea, 2018).

Together, pond depth and salinity represent two influential and controllable factors that shape redox structure, carbon cycling, and GHG emissions in urban stormwater systems. Clarifying how these characteristics interact to regulate stratification and biogeochemical function will support broader efforts to quantify and mitigate the climate impacts of urban development and stormwater infrastructure.

1.6 Research Gap

SWMPs are widely implemented as end-of-pipe infrastructure in residential developments, yet their role as sources of GHGs remains insufficiently characterized. While their primary purpose is to control flooding, protect downstream water quality, and moderate peak flows, these systems also act as biogeochemical reactors where organic matter degradation, microbial activity, and redox processes influence the production and release of CH_4, CO_2, and N_2O. As residential development continues to expand, the cumulative contribution of these ponds to municipal GHG budgets may become increasingly important; however, the governing mechanisms behind these emissions are not well understood.

A growing body of literature indicates that road-salt-driven salinity increases have important consequences for aquatic systems (Findlay & Kelly, 2011; Schuler & Relyea, 2018; Szklarek et al., 2022). Elevated specific conductance is known to strengthen water-column density gradients, enhancing thermal and chemical stratification, particularly in small to mid-sized waterbodies typical of SWM systems (Dupuis et al., 2019; Loewen & Jackson, 2024; Radosavljevic et al., 2022; Sibert et al., 2015). This stratification can create persistent anoxic zones at depth (Dupuis et al., 2019), fostering conditions that favour CH_4 production and altering carbon and nitrogen cycling pathways. Despite this, few empirical studies have directly measured how salinity-driven stratification influences GHG fluxes, and even fewer have assessed these relationships in the cold temperate climates where road salt use is highest.

In parallel, pond depth and structural design vary considerably across municipalities. Deeper ponds (e.g., 3 m) may be more prone to pronounced and long-lasting stratification, whereas shallow ponds (e.g., 1 m) may mix frequently and exhibit weaker chemical gradients. Hydrologic connectivity—such as the number of inlets, outlet elevation, and seasonal flow conditions—further modulates stagnation potential and redox behaviour. Despite these well-recognized physical differences, there is limited research examining

how pond depth interacts with salinity to drive stratification patterns and influence GHG production.

Another critical research gap is the spatial heterogeneity of GHG emissions within ponds. Inlet zones receiving fresher, oxygenated stormwater may behave very differently from sheltered shorelines or from deeper, central basins. While conceptual models suggest that GHG fluxes should vary substantially across these zones based on redox dynamics, nutrient inputs, and organic matter availability, few studies have systematically compared GHG emissions across distinct pond locations.

Collectively, these gaps limit the ability of municipalities, planners, and developers to design or retrofit stormwater systems that minimize GHG emissions. With increasing pressure to integrate climate mitigation into urban infrastructure planning (Climate Risk Institute, 2023; ECCC & Canda Water Agency, 2018; Ontario Ministry of the Environment, 2016a; *RISE*, 2023; Warren & Lulham, 2021), there is a clear need for research that explicitly measures the combined influence of salinity, depth, and within-pond spatial variability on GHG fluxes. Understanding these processes will be essential for evidence-based decision-making within the broader context of climate-forward residential development.

Therefore, this study aims to understand the biogeochemical and physicochemical controls on the GHG emissions from road salt impacted stormwater ponds in Southern Ontario. The specific objectives of this study are to: (1) determine if a high salt content stratifies the water column within a pond and create thicker anoxic sections (Chapter 2:), (2) assess if road salt interferes with the typical redox cascade in a pond (Chapter 2), (3) determine how the addition of road salt effects GHG emissions from the ponds (Chapter 3), and (4) determine if the location within a pond has a significant effect on GHG emissions (Chapter 3). Results can be used to advance smarter and more sustainable urban stormwater management design and planning that reduces GHG emissions and considers the water quality of these systems.

Chapter 2: Stratification in Urban Stormwater Ponds in Southern Ontario

2.1 Introduction

Adapting to the impacts of climate change in Canada has been a priority for decades and continues to be so, with continually renewed national climate goals and international participation (Warren & Lulham, 2021). In Ontario, climate change is anticipated to significantly impact the stormwater management (SWM) systems and infrastructure, infrastructure that protects the health, safety, and property of our cities (Ontario Ministry of the Environment, 2003). Both long-term increases in accumulated precipitation and intense short-term storm events are identified as some of the most impactful stressors on SWM infrastructure in the region (Climate Risk Institute, 2023).

Artificial waterbodies, including stormwater management ponds (SWMPs) and urban wetlands, are integral components of these systems. Engineered for SWM purposes, they differ from natural waterbodies in their water chemistry and carbon cycling, with smaller artificial systems often showing higher per-area emissions of greenhouse gases (Grinham et al., 2018). Understanding how these small, constructed ponds function under changing climatic and land cover conditions is therefore essential for effective water quality management, undiminished nutrient redistribution, natural habitat and aquatic biodiversity, and balanced greenhouse gas cycling. However, SWMPs in urban environments have received minor attention to their dominant water quality processes and chemical functions, even though as urbanization and development continues to expand, their quantity and spatial extent will continue to increase (Audet et al., 2020; Birch et al., 2022).

2.1.1 Biogeochemical Pond Conditions

External factors such as sunlight, wind, surface water input, or groundwater input can create uneven energy distribution across horizontal layers in water bodies, producing

gradients in physiochemical properties like density, oxygen concentration, and turbidity (Davidson et al., 2024; Holgerson et al., 2022; Loewen & Jackson, 2024). When these differences are large enough, mixing between layers is reduced, resulting in stratification. Shallow water bodies are often considered to be well mixed, but ponds can become stratified through various mechanisms, though thermal stratification is the most common in natural systems (Holgerson et al., 2022). Stratification, in turn, can influence biogeochemical processes and drive a range of ecosystem responses (Davidson et al., 2024; Dupuis et al., 2019).

As SWMPs receive substantial inputs of nutrients and contaminants from stormwater inflow originating from the watershed they manage, they are considered important areas for urban biogeochemical processing (Peacock et al., 2019). Organic matter decomposition and nutrient cycling pathways within a wetland or pond vary depending on the oxygen availability (Neubauer & Megonigal, 2021). As the concentration of dissolved oxygen (DO) decreases with depth within a pond, the water column transitions from an oxic system near the surface to an anoxic system closer to the sediment layer. Given ponds typically have limited oxygen sources and replenishment, either through surface diffusion or the inflow of oxygen rich water, they often experience oxygen depletion, forcing the microbial communities to use alternative terminal electron acceptors (TEA) to sustain organic matter cycling (Loewen & Jackson, 2024; Neubauer & Megonigal, 2021). This descent follows the redox cascade wherein microbes utilize the TEA that provides the most energy until that compound becomes depleted, subsequently shifting to the next most favourable TEA. Over time, this progression of reductive processes moves from reduction of oxygen to nitrate (NO_3^-), manganese and iron oxides (MnO_2 and $Fe(OH)_3$), sulphate (SO_4^{-2}), and finally to CO_2. When only CO_2 remains as an available TEA, methanogenesis becomes the dominant metabolic pathway, producing CH_4 as the final by-product (Holgerson et al., 2022; Neubauer & Megonigal, 2021). This redox driven sequence within the metabolism of the microbial communities underpins the biogeochemical functions of a pond, connecting DO dynamics directly to oxidation-reduction potential.

2.1.2 Road Salt: Contaminant of Concern

Due to the temperate nature of Canada, and Southern Ontario in particular, road salt is often applied to roads and parking lots in the winter months when the temperature falls below 0 °C to reduce the risk of vehicular accidents due to the ice and snow. In 2019, Environment and Climate Change Canada (ECCC) reported an annual usage of 4.2 million tonnes of total solid salt across Canada (ECCC, 2023b). While necessary for road safety in the winter, the applied salt is often flushed into stormwater management infrastructure from impervious surfaces and can either accumulate in a pond or leave through the pond's outflow (Snodgrass et al., 2017). Due to the decades of application and the growing urbanization, road salt is now considered one of the most prevalent contaminants of concern for urban waterbodies within southern Ontario (Kaushal et al., 2022; Loewen & Jackson, 2024; Szklarek et al., 2022). When road salt is retained and accumulates in a pond's water column, it can alter the pond's physical structure by enhancing density driven stratification beyond the typical temperature induced layering (Loewen & Jackson, 2024). This stratification exacerbates oxygen depletion within a pond, creating zones that accelerate redox progression and remain in a reduced state for longer (Dupuis et al., 2019).

With climate change driving more extreme weather, maintaining reliable and resilient SWM infrastructure has become increasingly critical. SWMPs not only protect water quality, reduce flooding, provide urban aquatic habitat and biodiversity, but may also contribute to urban carbon sequestration (Alikhani et al., 2021; Lehner et al., 2024). However, there remains a significant gap in knowledge regarding the biogeochemical mechanisms governing the water quality in road salt impacted urban wetlands and SWMPs. Therefore, this research aims to address that gap by understanding and identifying the biogeochemical and physicochemical controls of the GHG emissions from road salt impacted SWMPs in Southern Ontario. The specific objectives of this study are to: (1) determine if a high salt content (inferred from electrical conductivity) stratifies the water column within a pond and creates thicker anoxic sections, (2) assess if high electrical conductivity interferes with the typical redox cascade in a pond. Results can be used to

advance smarter and more sustainable urban stormwater management design and maintenance.

2.2 Methods

2.2.1 Site Selection & Study Design

Research was conducted in SWMPs located in Kitchener (43° 27´ 11˝N, 80° 29´ 42˝W) and Waterloo (43° 29´N, 80° 31´W), Ontario, two cities undergoing continuous urban growth and development. The study was conducted across four ponds: with low/high water electrical conductivity, as an indicator of salinity, orthogonal to low/high water depth to ensure both variables, water depth and salinity, were investigated. In May 2024, 24 ponds were selected based on descriptions provided by the municipalities and were visited to determine depth and electrical conductivity or specific conductivity (EC). Ponds were chosen to minimize differences in depth and maximize difference EC within each depth category (Table 2.1). During the main sampling period in 2024 the shallow & low salt pond had a maximum specific conductivity of 730 µS/cm, the shallow & high salt pond had a maximum specific conductivity of 7500 µS/cm, the deep & low salt pond had a maximum specific conductivity of 970 µS/cm, and the deep & high salt pond had a maximum specific conductivity of 2750 µS/cm. The shallow ponds are highly designed and engineered systems with pipe inlets and outlet control structures, and the deep ponds consist of a re-naturalized open-water wetland connected to a creek during mid to high flow conditions, and a natural pond integrated into the city's stormwater network, representing the low-salinity and high-salinity ponds, respectively.

Table 2.1 Physical characteristics of the 4 study sites in the Kitchener-Waterloo area, ON.

Pond	Region	Latitude; Longitude	Surface Area (km^2)	P:A ratio (km^{-1})	Installation year	Catchment Area (km^2)	Level of Design	Maximum Depth (m)	Sediment Depth (m): Inlet, Middle, Outlet
Shallow & Low Salt	Waterloo	43° 29'52.18"N 80° 34'25.43"W	0.0071	55.6	1995	0.337	Engineered wet pond	1.0-1.1	0.75, 0.25, 0.25
Shallow & High Salt	Waterloo	43° 30'57.81"N 80° 31'21.40"W	0.0041	60.4	1998	0.249	Engineered wet pond	1.1-1.3	0.8, 0.65, 0.55
Deep & Low Salt	Kitchener	43° 23'12.82"N 80° 27'44.30" W	0.0033	97.4	2010 (Retrofitted)	8.38[a]	Re-naturalized wet pond	3.0-4.0	0.7, 0.35, 0.35
Deep & High Salt	Kitchener	43° 25'57.64"N 80° 29'58.46"W	0.0235	38.2	No records	8.57[a]	Natural wet pond	3.5-4.0	1.3, 0.65, 0.8

a. Values were determined using a delineation algorithm (Thirimanne, 2025), as the records either did not specify a catchment area or there were no records available, so there may be inconsistencies in the deep pond catchment areas.

Within each pond two sampling transects were identified, one from the inlet to the outlet (flow transect), and another from the deepest point to the nearest shore (depth transect), (Figure 2.1; Appendix A: Figure A.1 – A.3). The transect following the pond's flow had three sampling locations, and the transect following the pond's depth had three to four sampling locations, depending on the size of the pond. The two transects shared one location, the deepest location for the depth transect and the middle or the outlet for the flow transect. The ponds underwent sampling campaigns throughout the ice-free period: twice a month from June to August (peak microbial activity), once a month from September to November (less microbial activity due to cooler temperatures), and finally three times in the spring (transition of microbial activity due to warming temperatures) for a total of 12 sampling rounds.

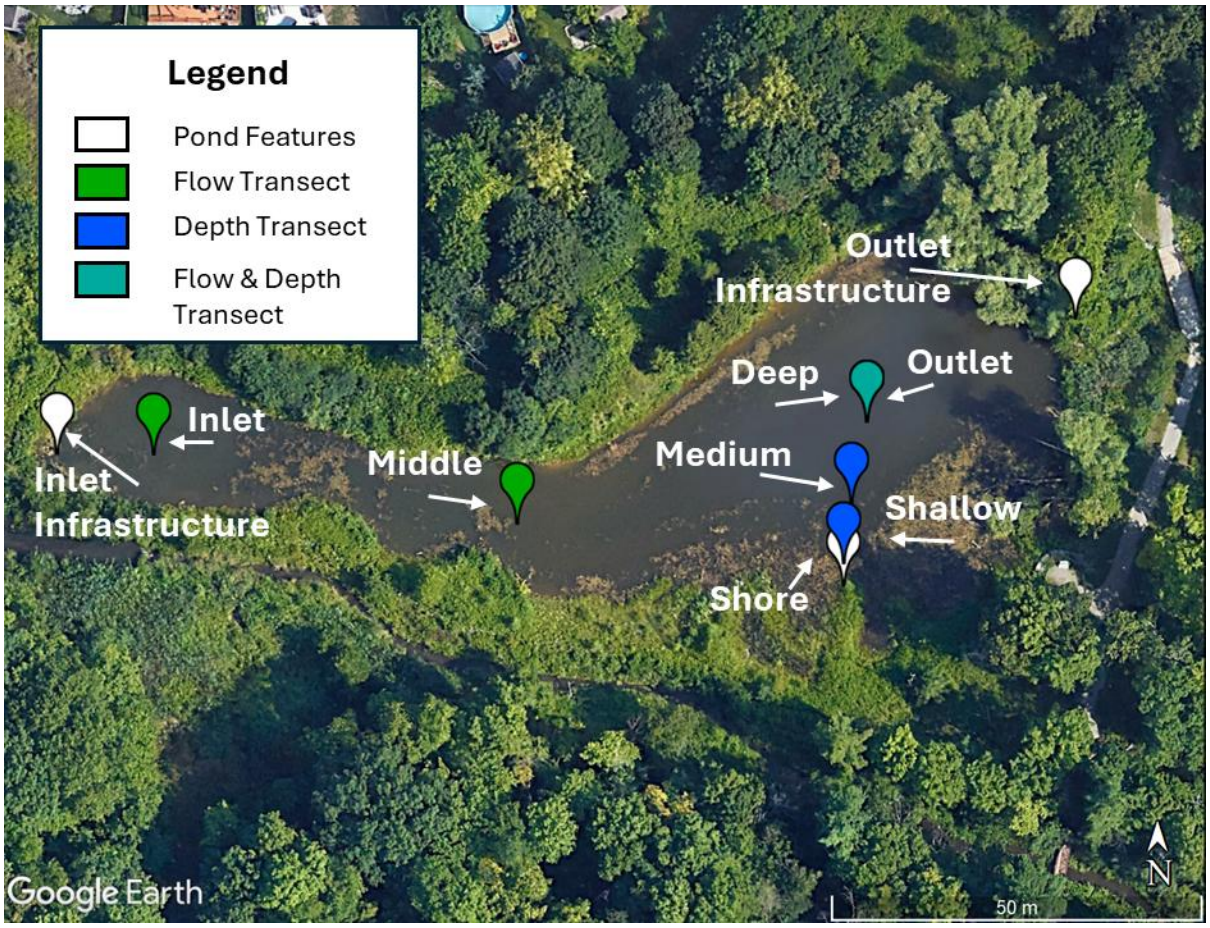


Figure 2.1. Example of sampling design showing flow transect (Inlet, Middle, Outlet) and depth transect (Deep, Medium, Shallow). In this pond, the transects shared a sampling point where the outlet location of the flow transect was also the deep sampling point for the depth transect. No sampling was conducted at the locations marked as "Pond features".

2.2.2 Pond Water Quality

Water chemistry was measured using a handheld ProQuatro YSI probe equipped with sensors for temperature, pH, conductivity/specific conductivity, and DO. These variables were measured at each sampling location at depths of 10 cm, 20 cm, 40 cm, 60 cm, 80 cm, 100 cm, 150 cm, 200 cm, 250 cm, 300 cm, 350 cm, and 10 cm above the sediment (Figure 2.2). At locations where water was shallower than 350 cm, sampling was conducted from the surface down following this pattern until 10 cm above the sediment was reached. Prior to each sampling campaign the YSI was calibrated according to manufacturer instructions

(*606962-ProQuatro-User-Manual-English.Pdf*, n.d.). The DO measurements exceeding the saturation limits specified in the instrument user manual were retained and not adjusted. Supersaturated DO conditions can occur in systems with high aquatic plant biomass due to associated photosynthetic activity and therefore could not be confidently attributed to sensor error (Koop-Jakobsen & Gutbrod, 2019; YSI Environmental, 2005). While this approach resulted in DO concentrations that are higher than those commonly reported in literature, similar magnitudes have been observed in similar pond systems (Withanage, 2025).

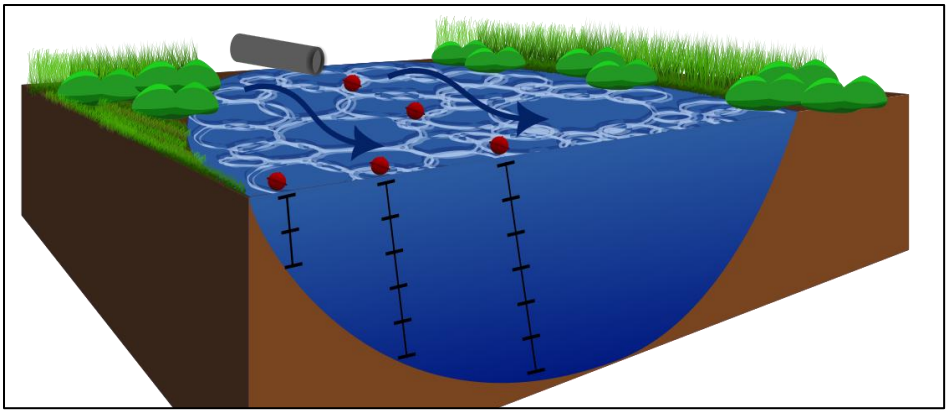


Figure 2.2. Pond sampling schematic – demonstrating the water column sampling profiles.

To better characterize pond nutrient content and oxidation - reduction potential, two water quality sampling events were also conducted: one in the growing season (GS) (July 21-23, 2024) and one in the nongrowing season (NGS) (October 10-24, 2024). Aligned with the primary objective of evaluating how the ponds stratified along the redox gradient, water quality sampling was focused to a single sampling location, the deepest point in each pond, to allow greater emphasis on sampling frequency along the vertical water columns. Additionally, due to logistical constraints, some redox - sensitive elements were sampled less frequently than others, limiting the level of interpolation possible for certain profiles, specific sampling for each event in the Appendix A (Table A.1).

Water samples were collected with vinyl tubing connected to a manual syringe pump and a four-way stopcock. The tubing had an inner diameter of ¼", a length of 5 m (vol ~ 160 mL), and was attached to the outside of the YSI probe with one opening in line with the sensor heads and the other connected to the four-way stopcock in the boat. 60 mL syringes were used to flush the tubing three times (vol ~ 180 mL) before each sample is taken to purge the tubing of the previous water and to rinse the tubing with the water at the current sample depth. The sampling then followed the protocol for sampling the water column from boats & aircrafts (Canadian Council of Ministers of the Environment, 2011) . Water samples were collected into Corning 50 mL sampling bottles that were new and sanitized by the seller or were acid washed in a 10% sulphuric acid bath for a minimum of 24 hours, then rinsed five times with DI water (Canadian Council of Ministers of the Environment, 2011). Water samples were analyzed for anions Chloride, Bromide (indicators of salt input), Nitrite, Nitrate, Phosphate (macronutrients), and Sulphate (indicator of salt input, nutrient and redox), cations Sodium, Calcium (indicators of salt input), Iron, Manganese, and Sulfur (indicators of redox). The inorganic element Iron (II) (redox) was also measured. Water samples for inorganic anions, inorganic cations, dissolved ammonium, and dissolved iron were filtered after or during collection following the Aqueous Analysis Laboratory (AAL) protocols at the University of Waterloo. Inorganic anions were filtered in the laboratory using 0.22 µm syringe filters, while inorganic elements and dissolved ammonium were filtered in the laboratory with 0.45 µm filters. Dissolved iron samples were filtered in the field using 0.45 µm filters. All samples were refrigerated after filtration and delivered to the AAL within five days of collection. Inorganic elements were analyzed using Inductively Coupled Plasma–Optical Emission Spectrometry (ICP-OES; Thermo Scientific iCAP 6300), inorganic anions were quantified using a Capillary Ion Chromatograph System (Dionex ICS-125000 with autosampler), and dissolved ammonium and dissolved iron were determined using a Gallery™ Discrete Analyzer (Thermo Scientific). The minimum detection levels for the sampled elements can be found in the Appendix A (Table A.2)

2.2.3 Dissolved Methane Concentration

The concentration of dissolved CH_4 was determined at each sampling location at depth along the water column for the entire sampling period except for three ponds in late August 2024 and spring 2025, using the headspace equilibration method (Peacock et al., 2019). A 60 mL syringe was connected to the tubing and stopcock assembly described for the water quality sampling earlier in the Section: 2.2.2, and water was withdrawn from the YSI water variable specified depths, excluding the intervals 10 cm below the surface and 10 cm above the sediment. After purging the water in the tube from the previous sample, the tube was cleared once with the desired water and then a syringe was filled up to 30 mL with sample water and 30 mL of ambient air. The syringe was then vigorously shaken for 180 seconds, and the headspace was transferred to an appropriate cleaned and pre-evacuated glass vial (Exetainer, Labco Ltd., UK). Finally, the collected headspace gas samples were analysed by injecting a set volume, 10 mL, into a GHG analyzer (LICOR, LI7810) with the signal compared to a series of known standards (1, 5, 50 , and 1000 ppm) to measure the headspace GHG concentration. Quality control of the headspace concentration data was completed using the PEDRO software (Newton et al., 2025). The headspace concentration data was trimmed to the injection time and when the concentration peak is clearly visible. The PEDRO software then calculated the concentration of the injected samples by taking the area under the curve of the flux peaks and using the established volume, determined the CH4 concentration of the headspace sample. Any concentrations that resulted in a headspace concentration less than zero were removed.

2.2.4 Pond Level Monitoring

Water level variation in the ponds was monitored using Solinst Junior Level Loggers. Loggers were deployed at the deepest point in the engineered shallow ponds; at the middle and outlet locations in the low and high salt ponds, respectively, at the medium sampling location in the deep & low salt pond; and at the medium-A sampling location in the deep &

high salt pond (Figure 2.1; Appendix A: Figure A.1 – A.3). The loggers recorded pressure changes in meters at 10-minute intervals from deployment in late June 2024 until the October 2024 sampling event, after which recording intervals were changed to hourly intervals until removal in May 2025. Water level measurements were corrected for atmospheric pressure using data from the Kitchener-Waterloo NAVCAN weather station (ECCC & NAVCAN, 2024) and underwent manual quality control to remove any errors. Continuous logging was maintained for all ponds from June 2024 to May 2025, except for the shallow & low salt pond, where the logger was lost during winter 2025 and could not be recovered.

2.2.5 Data Analysis

To understand how stratification varied among the ponds, the water variables measured by the YSI were compared between the high salt ponds and the low salt ponds. To assist in visualization of the changes along the flow path and at depth within and across the ponds, depth profile plots were created in R (R Core Team, 2023) and contour plots were created in Surfer® (Golden Software, LLC, n.d.) to visually identify trends. Supporting the depth profile contour plots, hydrographs of the pond water level changes and regional precipitation patterns were created in R (ECCC & NAVCAN, 2024; R Core Team, 2023). Additionally, the density gradient of each sample location for each sampling event was calculated according to Holgerson et al. (2022) to calculate a stratification index. Temperature, electrical conductivity (converted to salinity), and air pressure data from the Kitchener-Waterloo NAVCAN weather station (ECCC & NAVCAN, 2024) were used to calculate water density at each sampled depth. Salinity was determined using the gsw (*CRAN: Package Gsw*, n.d.) package in R, and density was calculated using the rLakeAnalyzer package (Winslow et al., 2019). The density gradient (kg m^{-3} m^{-1}) was computed as the difference between the top and bottom layer densities divided by the distance between them. These density gradients were then compared across ponds using ANOVA followed by Tukey pairwise comparisons when significant ($p<0.05$). The headspace gas concentrations

measured using the GHG analyser described in the Section: 2.2.3 were converted to dissolved gas concentrations using the neonDissGas (Cawley, 2007) package in R. Profiles of redox reactive anions, cations and dissolved CH_4 concentration were plotted for each pond for the growing season and non-growing season water quality sampling dates. As only one profile in each pond was measured on each date, differences between ponds were assessed visually and key variations in concentrations described.

2.3 Results

Pond characteristics and water chemistry varied among sampled ponds as seen in the measured in-situ environmental conditions per pond for the shallowest and deepest point in the water column (Table 2.2, Table A.3). In general, the high salt ponds had higher EC than the low salt ponds at the same depth and a greater difference between DO and EC measured at 10 cm depth and 10 cm above the sediment layers. The predominant cations and anions were sodium and chloride for the high salt ponds, magnesium for the deep & low salt pond, and manganese for the low salt ponds, with the concentrations for all measured water quality variables summarized in Appendix A (Table A.4).

Table 2.2. Summary statistics of environmental variables[a] at the top and bottom of the water columns across all sample locations of each pond.

		Shallow & Low Salt	Shallow & High Salt	Deep & Low Salt	Deep & High Salt
Parameter	Depth				
Water Column Depth (m)		0.89 (0.19)	0.96 (0.20)	2.06 (0.86)	2.12 (1.18)
Temperature (°C)	10 cm[b]	17.88 (6.59)	17.19 (6.44)	18.26 (5.87)	19.48 (5.89)
	10 cm as[b]	16.12 (4.85)	15.61 (4.78)	15.88 (5.13)	16.35 (5.85)
DO (mg/L)	10 cm	10.44 (4.21)	13.42 (3.73)	7.65 (2.51)	8.76 (2.6)
	10 cm as	7.34 (5.81)	7.03 (5.69)	5.53 (4.23)	4.59 (3.88)
pH	10 cm	8.62 (0.55)	8.15 (0.35)	8.1 (0.33)	8.41 (0.42)
	10 cm as	8.1 (0.56)	7.54 (0.52)	7.74 (0.35)	7.67 (0.59)
EC (µS/cm)	10 cm	726.44 (175.71)	4208.46 (867.07)	849.85 (197.22)	1380.15 (267.11)
	10 cm as	771.25 (145.96)	5625.1 (2381.59)	876.18 (186.87)	1765.29 (745.86)

a. Values are given as mean (standard deviation) across all sampling locations and dates sampled for each pond for the specified depth.
b. "10 cm" refers to 10 cm below the water surface and "10 cm as" refers to 10 cm above the sediment layer.

2.3.1 Temporal Patterns of Water Chemistry at the Deepest Point

The hydrographs and time series contours show the water quality variables measured along a depth profile at the deepest sample location for the highly engineered shallow ponds (Figure 2.3) and the naturalized deep ponds (Figure 2.4) over the entire sampling period from June 2024 to May 2025, with the pause in sampling over the 2025 winter season outlined in gray. A hydrograph of the pond water levels, alongside the regional precipitation pattern, was included to illustrate periods of water and nutrient input to the ponds from the surrounding urban catchments (Figure 2.3a, b)(Figure 2.4a, b). The temperature, specific conductivity, and DO variables were chosen to demonstrate the extent of stratification that was occurring in ponds throughout the sampling campaign, as temperature shows the thermal stratification, the specific conductivity shows the salt stratification, and the DO shows the impact of both to the oxygen access within the pond, and therefore an indication of redox potential. The time series contours for the water pH in these locations and over the sampling period can be found in Appendix A (Figure A.4 – A.7).

The thermal profiles indicate that the shallow & low salt pond exhibited distinct temperature stratification during June and early July, with only minor surface stratification observed in early August (Figure 2.3c, d). For the remaining sampling events, the water column generally had similar temperature throughout the water column. In contrast, the shallow & high salt pond demonstrated strong and persistent thermal stratification from June through August, followed by well-mixed conditions between September and November. In spring 2025, temperature profiles showed only weak stratification compared to the more pronounced thermal gradients observed during summer 2024 for both ponds.

Specific conductivity in the shallow & low salt pond varied among sampling events, with occasional stratification observed in July and August (Figure 2.3e). However, most sampling event profiles indicated similar salinity throughout the water column. Even during spring 2025 when overall conductivity increased, specific conductivity remained weakly stratified. In contrast, the shallow & high salt pond exhibited pronounced conductivity stratification during most 2024 sampling events, only diminishing once in November above 80 cm (Figure 2.3f). Following the 2025 winter, conductivity increased substantially, and the water column became strongly stratified, reaching near-brackish levels (U.S. Geological Survey, 2021) at the pond bottom.

DO patterns reflected similar seasonal trends as the thermal and specific conductivity stratification (Figure 2.3g, h). The shallow & low salt pond exhibited stronger stratification in June and July, which weakened during the peak summer period as the water column mixed, reflecting seasonal turnover during late summer to fall (September to November) and again in spring (April to May) (Figure 2.3g). In contrast, the shallow & high salt pond remained stratified throughout the 2024 sampling period, with low DO concentrations close to the surface observed in June, July and September (Figure 2.3h). In spring 2025, partial turnover increased DO concentrations to approximately 80 cm depth, while low oxygen persisted near the bottom of the pond, indicating incomplete vertical mixing of the water column in this system during multiple spring sampling events.

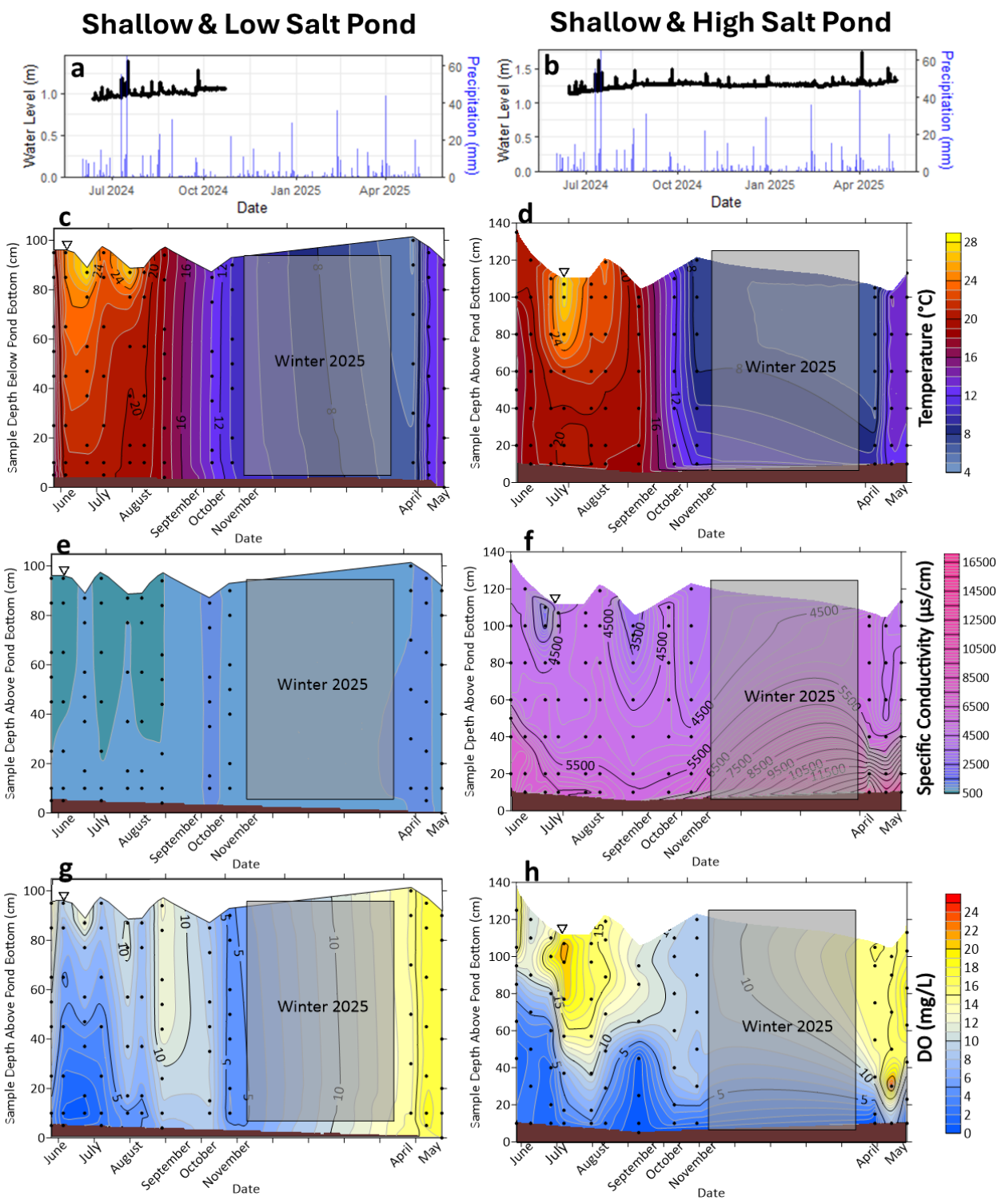


Figure 2.3 Engineered shallow ponds' hydrograph of the pond water level and climate station precipitation of the a) shallow and low salt and b) shallow and high salt pond, the deepest location time series contours with the c) the temperature at depth for the shallow & low salt pond, d) the temperature at depth for the shallow & high salt pond, e) the specific

conductivity at depth for the shallow & low salt pond, f) the specific conductivity at depth for the shallow & high salt pond, g) the dissolved oxygen at depth for the shallow & low salt pond, h) the dissolved oxygen at depth for the shallow & high salt pond. Black points indicated the dates and depths of measurements. Interpolation was completed using Natural Neighbour in Surfer®.

The deep & low salt pond exhibited temperature stratification from June through early August (Figure 2.4c), with lower overall temperatures compared to the shallow ponds. From late August to November, temperature profiles were uniform throughout the water column. During spring 2025, gradual increases in stratification were observed from early April to May. Similarly, the deep & high salt pond displayed strong thermal stratification between June, and early August characterized by a greater temperature range than the deep & low salt pond, with warmer surface waters and cooler bottom waters (Figure 2.4d). From late August to November, the water column became more thermally mixed, although some residual stratification persisted. In spring 2025, the deep & high salt pond exhibited somewhat stronger stratification than the deep & low salt pond, though the difference between them was not substantial.

The deep & low salt pond showed no significant specific conductivity stratification throughout most of the sampling period (Figure 2.4e). A marked change occurred after the early July sampling event, corresponding to the flushing of a beaver dam during a large storm, which altered the conductivity conditions within the pond. In spring 2025, slight stratification was observed; however, conductivity levels remained comparable to early summer 2024 and did not exceed previous concentrations. In contrast, the deep & high salt pond exhibited elevated specific conductivity near the bottom of the water column in June and early July (Figure 2.4f). Conductivity decreased through the remainder of 2024, resulting in well-mixed conditions for specific conductivity by fall. In spring 2025, stratification re-emerged, with elevated conductivity at shallower depths, 200 to 250 cm below the surface, showing concentrations similar to those measured in June 2024.

The deep & low salt pond exhibited observable DO stratification in June, July, and September 2024, while profiles from late fall appeared largely uniform with depth (Figure 2.4g). In spring 2025, DO concentrations varied among sampling events, but the vertical profiles remained well mixed. The October and November 2024 and April and May 2025 sampling periods had similar DO throughout the water column indicating mixing associated with seasonal turnover. In contrast, the deep & high salt pond showed pronounced DO stratification in early summer 2024, corresponding with elevated specific conductivity during the same period (Figure 2.4h). Although low DO concentrations persisted through summer, stratification diminished towards fall, with turnover evident in October and November. In spring 2025, partial turnover increased DO concentrations to depths of 250–300 cm, while the bottom water layers remained oxygen-depleted, indicating incomplete vertical mixing during multiple spring sampling events.

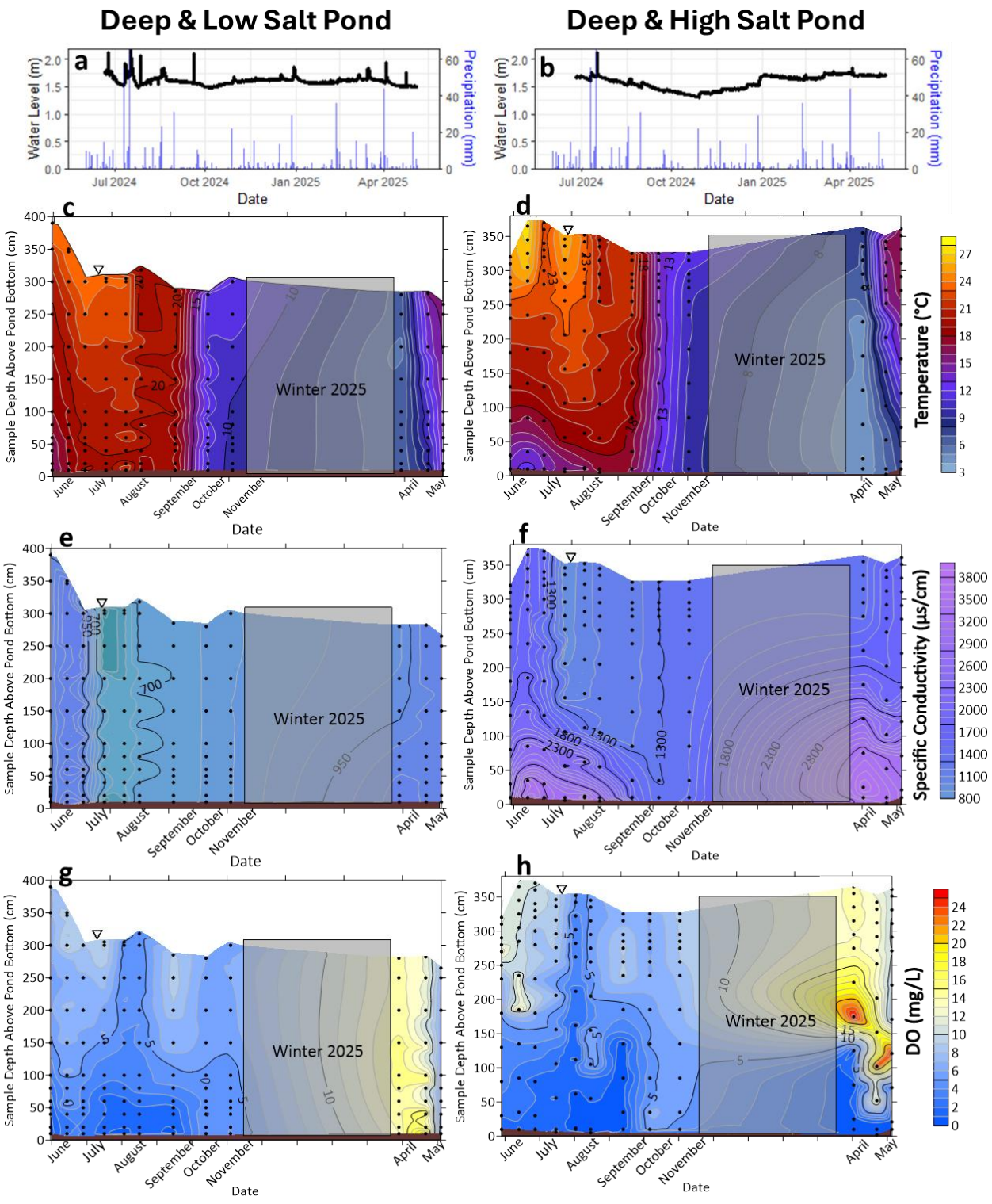


Figure 2.4 Naturalized deep ponds' hydrograph of the pond water level and climate station precipitation of the a) deep and low salt and b) deep and high salt pond, deepest location time series contours, c) the temperature at depth for the deep & low salt pond, d) the temperature at depth for the deep & high salt pond, e) the specific conductivity at depth for

the deep & low salt pond, f) the specific conductivity at depth for the deep & high salt pond, g) the dissolved oxygen at depth for the deep & low salt pond, h) the dissolved oxygen at depth for the deep & high salt pond. Black points indicate the dates and depth of measurements. Contours were created using Natural Neighbour in Surfer®.

The summary statistics for the stratification index, which was calculated using the gsw (*CRAN: Package Gsw*, n.d.) and rLakeAnalyzer (Winslow et al., 2019) packages that used the temperature and salinity of the water columns measured at every sample location per pond, can be found in Table 2.3.

Table 2.3. Summary statistics of pond stratification index (kg m^{-3} m^{-1}).

Statistic	Shallow & Low Salt	Shallow & High Salt	Deep & Low Salt	Deep & High Salt
Mean	0.78	1.5	0.35	0.48
Standard Deviation	1.23	1.70	0.36	0.40
Minimum	-0.062	-0.044	-0.038	-0.19
Maximum	7.37	7.70	1.41	1.37
Range	7.43	7.74	1.44	1.56

The variation in stratification index over time across the engineered and naturalized ponds (Figure 2.5) supported the variation in the stratification seen in the temporal water quality sampling contours. As expected, due to the higher specific conductivity highlighted in the time series contours, the shallow & high salt pond and the deep & high salt pond had higher average stratification indexes than their low salt counterparts, with a percent difference of 63% and 27%, respectively (Figure 2.6). Additionally, due to the nature of calculating the stratification indexes by dividing the difference in water density by the distance of the sampled water column, the engineered shallow ponds had a greater range and average stratification index than the deeper ponds. There was a significant difference in stratification index among ponds (ANOVA, $F = 32.52$, $p < 0.0001$), with pairwise comparisons indicating that the shallow & high salt pond had a significantly higher stratification index than all other ponds.

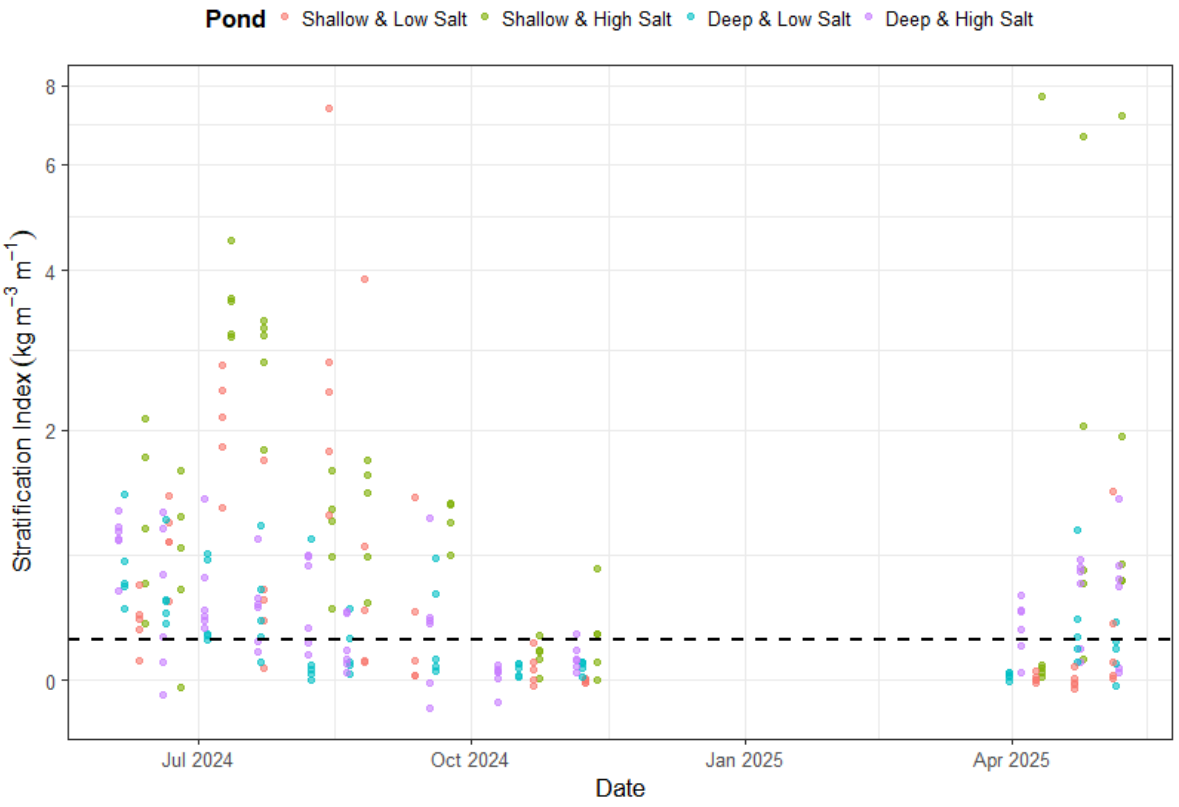


Figure 2.5 Stratification index over time per pond, highlighting both differences within and among engineered and naturalized ponds and the impact of seasonal trends on the stratification index for all sample locations (each as an individual point) on each measurement date. The dashed line is the 0.287 kg m^{-3} m^{-1} mixing threshold below which ponds are thought to be well-mixed (Holgerson et al., 2022).

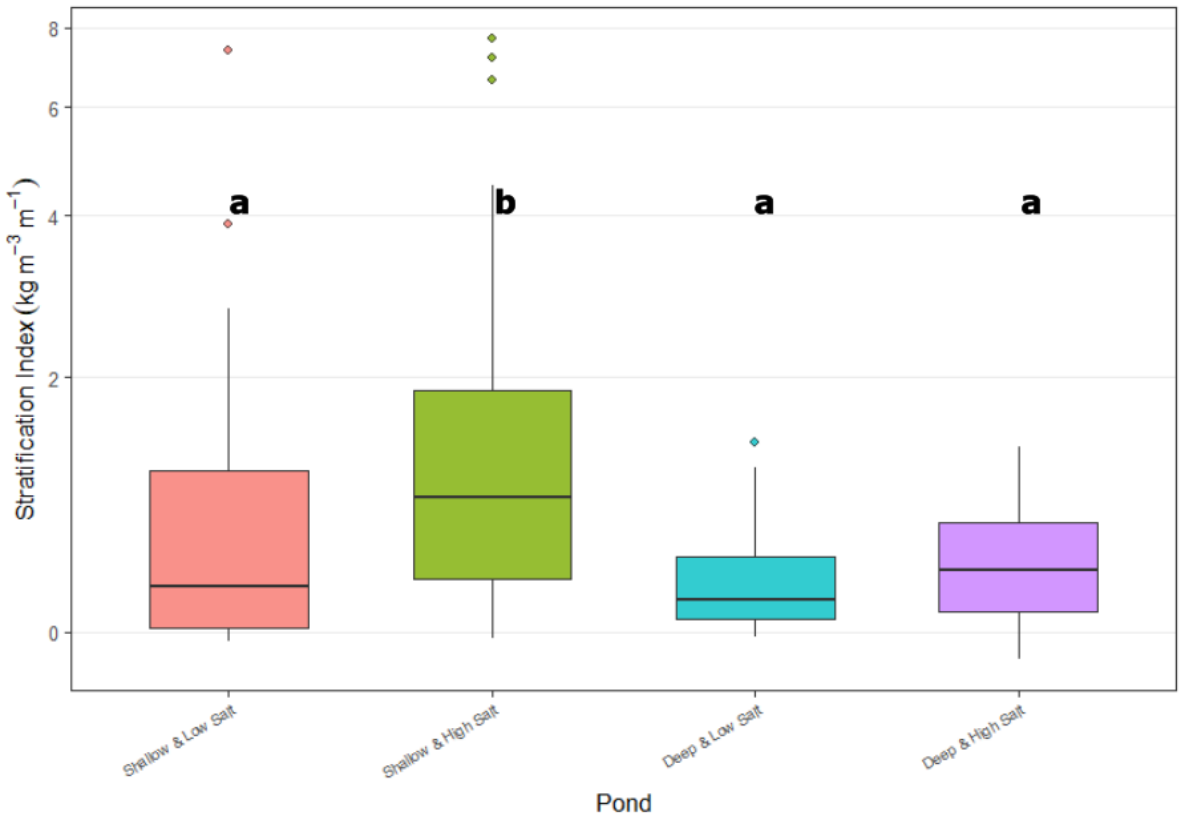


Figure 2.6 Stratification index by pond for all sampling locations for the entire study period. The centreline in the boxplot given the median, with top and bottom of the box indicating 25th and 75th quartiles, and whiskers illustrating 10th and 90th percentiles. Letters above the boxes indicate the Tukey pairwise comparisons where ponds are significantly different from each other if they share no letters.

2.3.2 Spatial Variation in Water Chemistry

Considering variation in specific conductivity and DO from the inflow to outflow of each pond (flow transects), contours show the water quality variables in the summer measured from the sample location by the pond's inflow, the sample location in the middle of the pond, and the sample location by the outlet of the pond for the engineered shallow ponds (Figure 2.7) and the naturalized deep ponds (Figure 2.8). The late July sample round was chosen to visualize the differences in the ponds' specific conductivity and DO concentration and stratification in the summer along this flow path. The specific conductivity profiles in the engineered shallow ponds suggests differences in flushing

capacity between the low and high salt systems. In the low salt pond, specific conductivity decreased along the water column from the deepest middle point toward the surface at the outlet, indicating effective flushing (Figure 2.7a). Contrastingly, the high salt pond showed only slight surface flushing at the outlet (Figure 2.7b). The DO profiles in both ponds indicate insufficient flow to mix and oxygenate the bottom of the water column (Figure 2.7c, d). For further details on the stratification conditions within the shallow ponds the specific conductivity and DO profiles for the depth transect during the sampling event can be found in Appendix A (Figure A.8 & A.9).

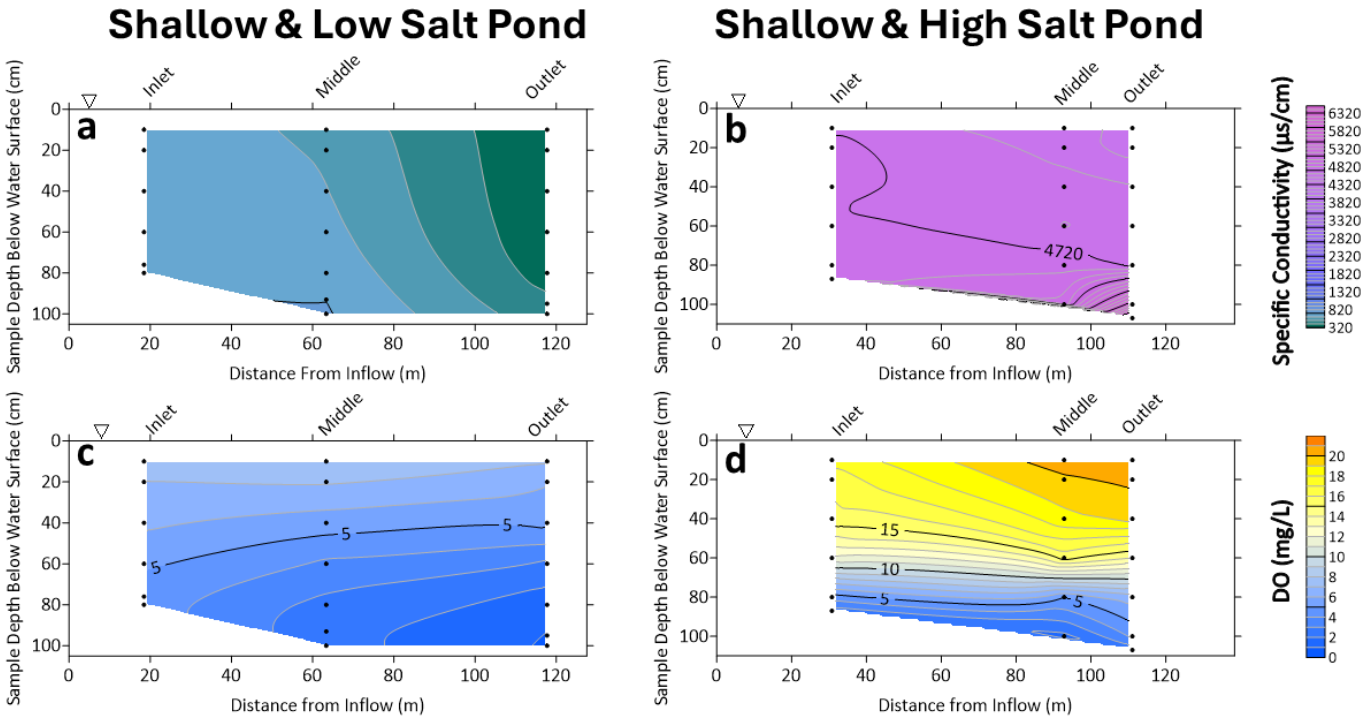


Figure 2.7 Engineered shallow ponds flow transect contours - Summer 2024, a) the specific conductivity at depth in the shallow & low salt pond, b) the specific conductivity at depth in the shallow & high salt pond, c) the DO at depth in the shallow & low salt pond, d) the DO at depth in the shallow & high salt pond. Black points indicate the depth and the location along the flow transect of the measurements. Contours were created using Natural Neighbour in Surfer®.

The specific conductivity profiles in the naturalized deep ponds revealed distinct differences between the low and high salt systems. In the low salt pond, there was no proof that specific conductivity did not vary with flow direction or position relative to the inlet, though DO was slightly higher at both the inlet and outlet, indicating some influence of incoming and outgoing water (Figure 2.8a, c). In contrast, the high salt pond exhibited strong trapping of high specific conductivity water in the deepest zone, with flushing occurring only in the upper ~100 cm of the water column, likely due to the outlet sitting at that depth (Figure 2.8b). DO patterns were less affected by inlet and outlet flow, and high DO levels appeared more wind driven (Figure 2.8d). Together these patterns suggest that road salt accumulates at depth in deep ponds when the inlet and outlet structures are shallower than the deepest point, and that flow through the system is not the primary control on DO levels. For further details on the stratification conditions within the deep ponds the specific conductivity and DO profiles for the depth transect during the sampling event can be found in Appendix A (Figure A.10 & A.11).

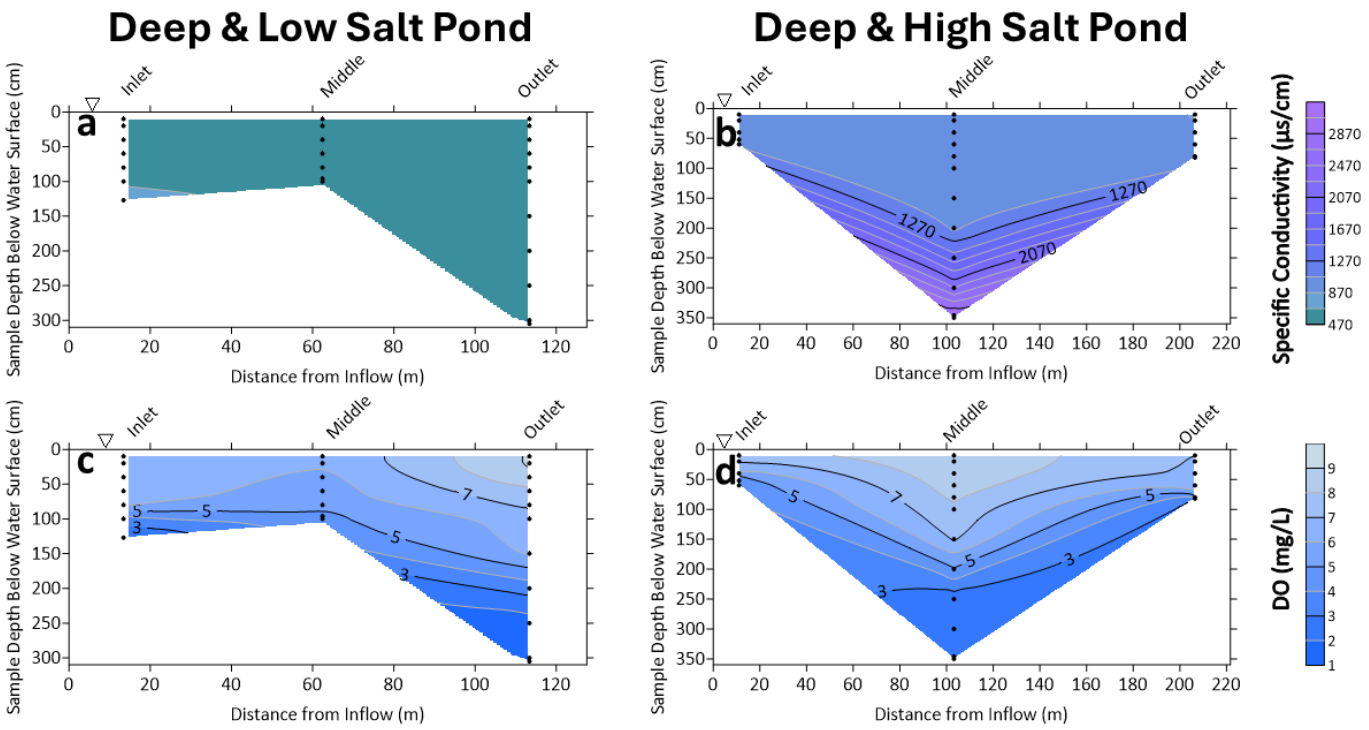


Figure 2.8 Naturalized deep ponds flow transect contours - Summer 2024, a) the specific conductivity at depth in the deep & low salt pond, b) the specific conductivity at depth in the deep & high salt pond, c) the DO at depth in the deep & low salt pond, d) the DO at depth in the deep & high salt pond. Black points indicate the depth and the location along the flow transect of the measurements. Contours were created using Natural Neighbour in Surfer®.

To capture the effects of winter-derived inputs and the resulting spring conditions on the spatial variation in specific conductivity and DO along each pond's flow transect, the contours show the water quality variables measured in the spring for the engineered shallow ponds (Figure 2.9) and the naturalized deep ponds (Figure 2.10). The early April sample round, round 10, was chosen to visualize the differences in the ponds' DO and specific conductivity levels and stratification in the spring along this flow path. The specific conductivity and DO profiles in the engineered shallow ponds show broadly similar patterns between the low and high salt systems, with a few key differences. The low salt pond was well mixed for both specific conductivity and DO (Figure 2.9a, c), indicating greater mixing in the spring then the summer. The high salt pond also appeared more well

mixed for both specific conductivity and DO in the spring then the summer (Figure 2.9b, d), but there was a continuous stratified layer across the seasons at the bottom of the deepest location. For further details on the stratification conditions within the shallow ponds the specific conductivity and DO profiles for the depth transect during the sampling event can be found in Appendix A (Figure A.12 & A.13).

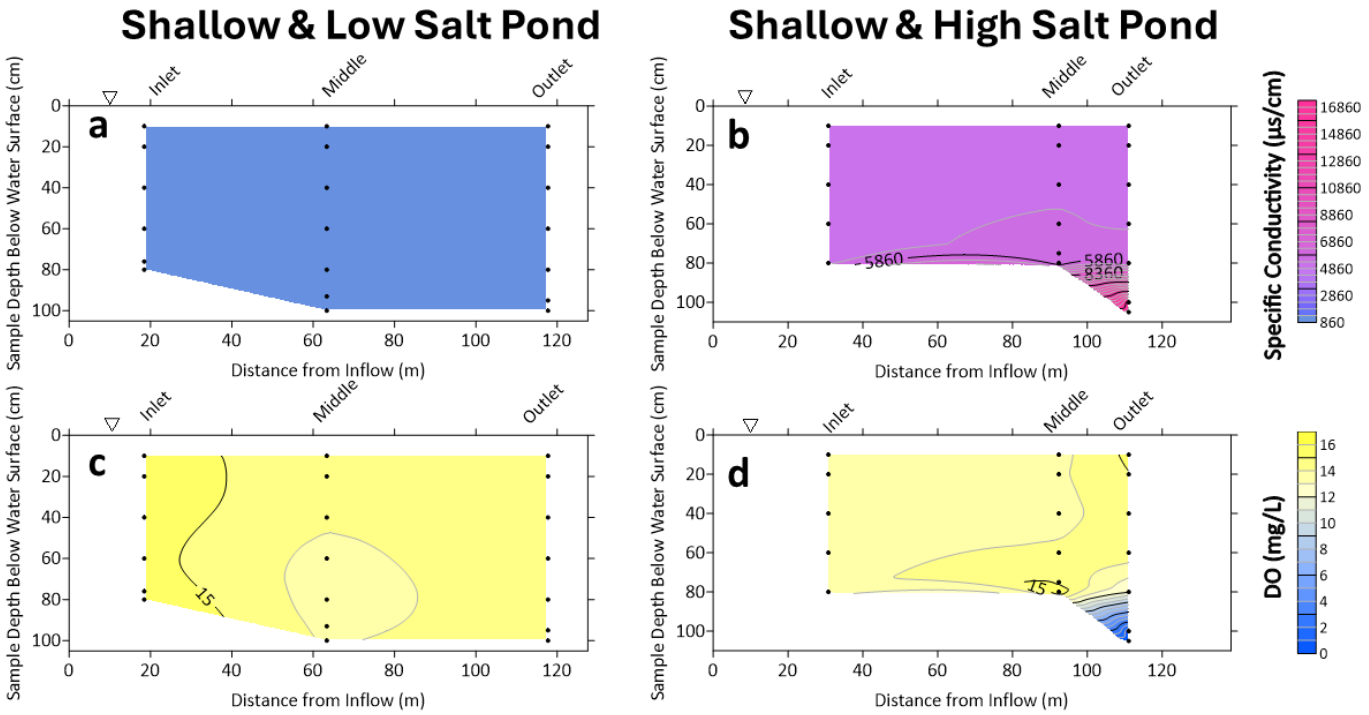


Figure 2.9 Engineered shallow ponds flow transect contours - Spring 2025, a) the specific conductivity at depth in the shallow & low salt pond, b) the specific conductivity at depth in the shallow & high salt pond, c) the DO at depth in the shallow & low salt pond, d) the DO at depth in the shallow & high salt pond. Black points indicate the depth and the location along the flow transect of the measurements. Contours were created using Natural Neighbour in Surfer®.

The specific conductivity and DO profiles in the naturalized deep ponds reveal distinctly different patterns between the low and high salt systems. The low salt pond's contour shows a well mixed system along the flow transect and with depth for both specific conductivity and DO (Figure 2.10a, c), indicating greater mixing in the spring then the

summer. Contrastingly, the high salt pond shows strong stratification along the flow transect for both the specific conductivity and the DO (Figure 2.10b, d). As in the summer profiles, mixing does not extend below the outlet depth, but in the spring the inlet exhibits the higher, more strongly stratified specific conductivity, and stratification in the middle begins closer to the surface. The DO levels at the inlet and outlet are well mixed in the spring, similar to the low salt pond, yet the deepest location remains highly stratified with the bottom reaching near 0 mg/L. With pond turnover only extending to ~150 cm above the sediment, the stratification from the summer had remained and even reduced the mixed depth in the spring. For further details on the stratification conditions within the deep ponds the specific conductivity and DO profiles for the depth transect during the sampling event can be found in Appendix A (Figure A.14 & A.15).

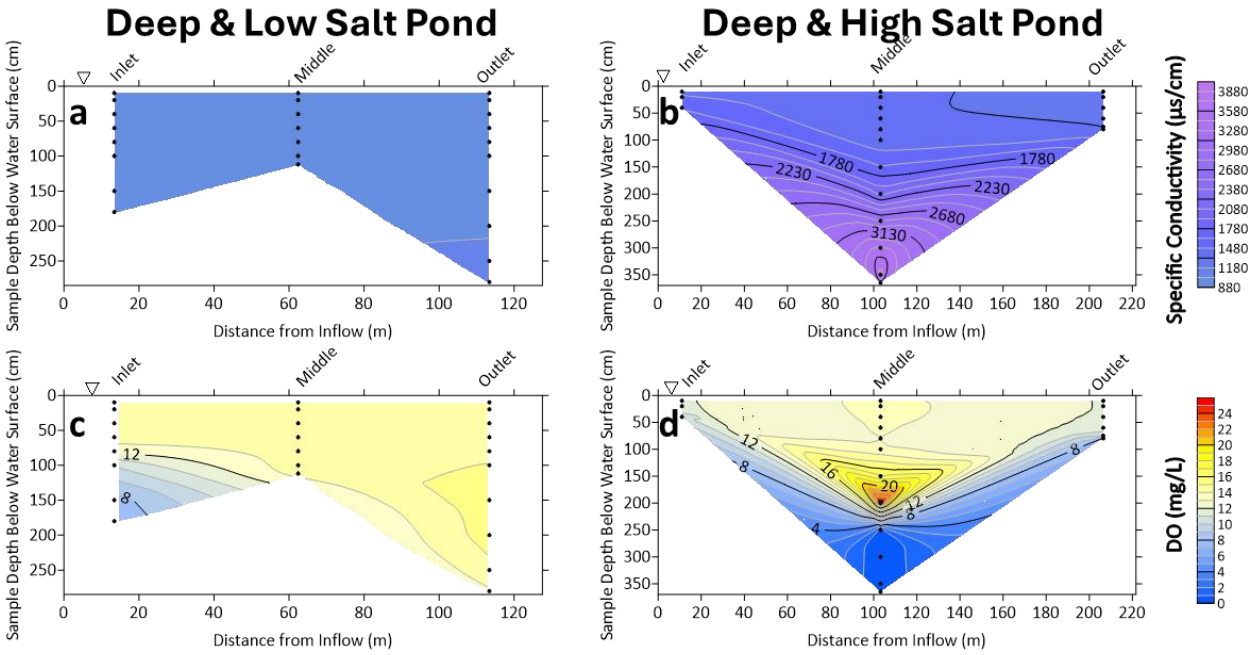


Figure 2.10 Naturalized deep ponds flow transect contours - Spring 2025, a) the specific conductivity at depth in the deep & low salt pond, b) the specific conductivity at depth in the deep & high salt pond, c) the DO at depth in the deep & low salt pond, d) the DO at depth in the deep & high salt pond. Black points indicate the depth and the location along the flow transect of the measurements. Contours were created using Natural Neighbour in Surfer®.

2.3.3 Variation in Water Chemistry and Redox Conditions among Ponds

Overall, the data shows clear redox stratification was evident in the engineered shallow ponds during the GS, with nitrate & nitrite and Mn concentrations increasing or decreasing with depth depending on oxidation potential, while the naturalized deeper ponds showed more uniform profiles (Figure 2.11). Nitrate & nitrite concentrations were generally higher in the shallow ponds, with the greatest concentrations in the shallow & high salt pond that began declining halfway down the water column. Mn and Fe (II) exhibited classic redox-controlled trends, with both metals increasing near the sediment where DO concentrations were low. These patterns were strongest in the shallow ponds and during the NGS, reflecting seasonal oxygen depletion and reduced redox potential. In the deep ponds, Fe (II) spikes at depth indicated localized low-energy zones, particularly in the deep & high salt pond, where concentrations rose sharply near the bottom during the GS. SO_4^{2-} concentrations were highest in the high salt systems and declined with depth, consistent with sulfate-reducing conditions. Seasonal variability was most evident in the shallow ponds, with generally higher SO_4^{2-} levels during the NGS, suggesting shifts in sulfur cycling linked to redox transitions. CH_4 profiles showed the strongest spatial and seasonal variability, with concentrations increasing with depth and peaking near the sediment, particularly in the deep & high salt pond during the GS. Shallow ponds displayed more variable CH_4 distributions, influenced by stratification strength and redox gradients. Elevated surface CH_4 concentration across all ponds suggests upward diffusion and accumulation at the air–water interface. Together, these profiles indicate that pond depth and salinity strongly modulate redox structure and biogeochemical gradients, with stratification during the GS driving vertical segregation of electron acceptors and enhancing concentrations of reduced species and CH_4 production near the sediment.

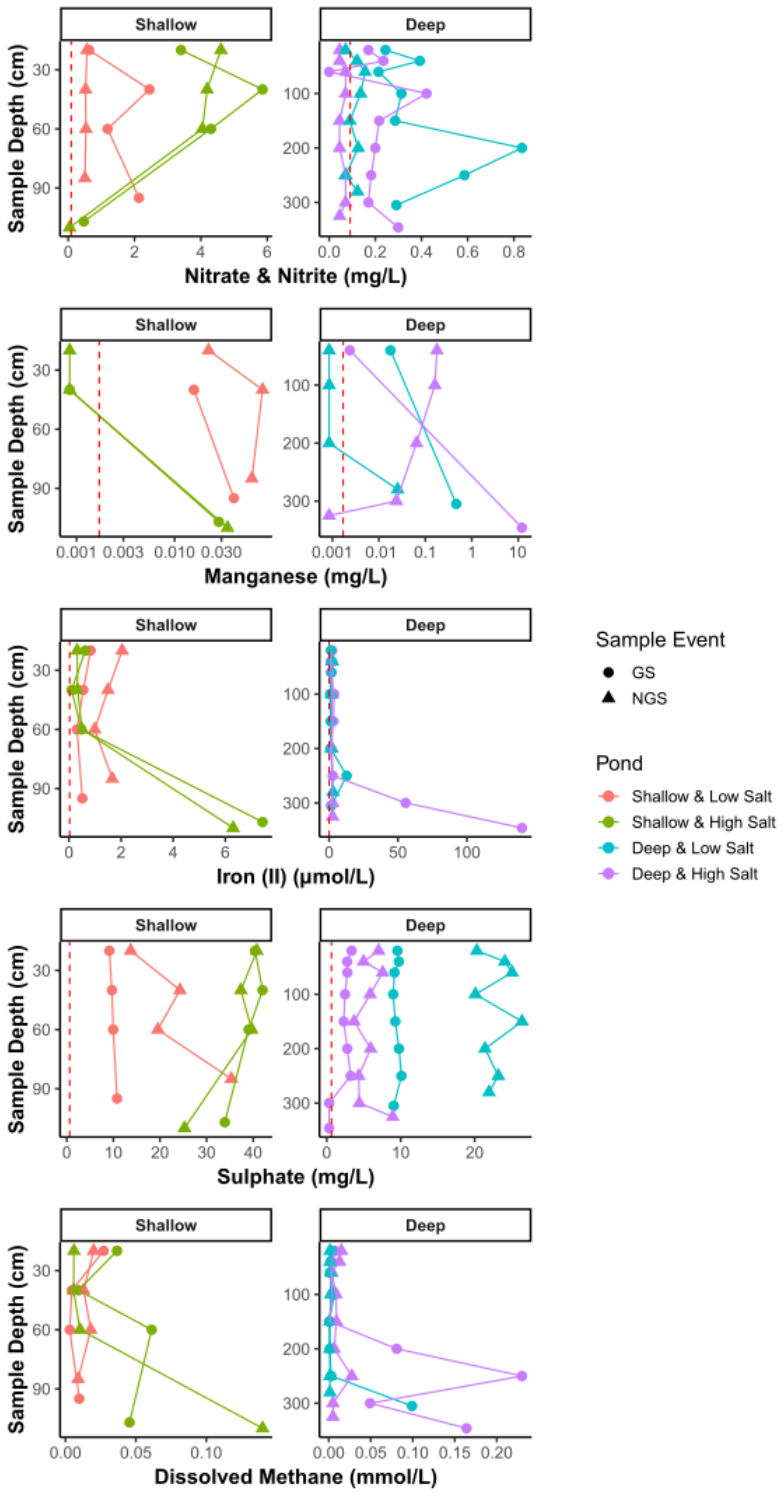


Figure 2.11. Depth profiles of redox reactive ions, Fe (II) and dissolved CH4 measured in the deepest point in each pond during the growing & nongrowing season, July 21-23 and October 10-24, 2024, respectively. Plots are ordered according to the typical redox cascade from high to low energy.

2.4 Discussion

Understanding how engineered and naturalized SWMPs respond to urban contaminants is essential for improving water quality, reducing flooding impacts, providing urban aquatic habitats and upholding its biodiversity, refining carbon budgets, and guiding the future design of more resilient urban aquatic ecosystems. These systems were engineered or incorporated into our infrastructure to protect downstream environments, yet their internal conditions and ecological functions are increasingly shaped by the urban stressors they are meant to manage. Here we focus on the effect of road salt accumulation, as indicated by specific conductivity, on stratification and redox conditions in engineered and naturalized SWMPs in southern Ontario. Within a single continuous urban area, the ponds in this study exhibited specific conductivity values spanning an order of magnitude, reflecting a gradient of road salt exposure and containment (Figure 2.3 & Figure 2.4). This variation provided an opportunity to evaluate how elevated salinity from road salt inputs alter the internal structure and functioning of SWMPs designed and incorporated into our infrastructure as freshwater ecosystems for inland catchments. The findings clearly show that elevated salinity promotes strong and persistent stratification, supported by water quality profiles, redox potential measurements, and the calculated stratification index (Figure 2.3 - Figure 2.11).

Holgerson et al. (2022) established a density gradient mixing threshold using a set of ponds across North America and Europe that had a range in density gradients from -0.5 – 6 kg m^{-3} m^{-1}, wherein ponds with water column density differences consistently above 0.287 kg m^{-3} m^{-1} were considered intermittently or rarely mixed. Considering the ponds in the Holgerson et al. study were sampled during their peak stratification from June to August, if we compare the mean stratification indexes for the four ponds in this study during that same time period (shallow & low salt: 1.06, shallow & high salt: 2.12, deep & low salt: 0.640, deep & high salt: 0.697), all four ponds are consistently above the mixing threshold (Figure 2.5). These results indicate that not only are the ponds considered intermittently or even rarely mixed, but that chronic road salt loading from an urban watershed can amplify density

driven separation beyond what is expected compared to other ponds of similar depth and size, even when both the engineered and naturalized ponds are in relatively well-connected flow through systems. Elevated road salt levels appear to inhibit complete vertical mixing in the deepest regions of the engineered shallow pond, even during periods of large water inputs associated with spring melt and during expected thermally-driven turnover. Contrastingly, while the naturalized deep pond with low salt do not reach full vertical mixing, elevated salt levels can further suppress mixing at depth (Figure 2.3 & Figure 2.4). Overall, the stratification index effectively identifies systems with extreme stratification, though it is less sensitive for distinguishing mild to moderate road salt driven stratification in engineered or naturalized SWMPs, as observed in the deep & high salt pond, relative to expectations for typical freshwater systems. The data also showed that the water column stratification had consequences that extend beyond physical layering. The bottom waters of engineered and naturalized high-salt ponds consistently exhibited lower DO concentrations, even when total depth was less than 1 m (Figure 2.3 & Figure 2.4) or when inflow and outflow provided regular water movement (Figure 2.7 – Figure 2.10). Additionally, not only are the DO levels lowered and replenishment limited, but the conditions demonstrated that increased salinity limits vertical mixing and drives the engineered and naturalized ponds into an overall lower-energy state, altering redox zonation throughout the water column (Figure 2.11).

As a result, the capacity of these engineered and naturalized systems to support biogeochemical processes such as balanced nutrient redistribution and removal can be severely hindered and diminished by the salinity stratified low oxygen levels (Craig & Zhu, 2018; Kinsman-Costello et al., 2023; Sibert et al., 2015). For example, instead of being retained and mineralized in pond cycling as they would in a natural aquatic ecosystem, the nitrogen managed under high salt conditions can be released through desorption, microbial-plant competition, plant stress, microbial cell lysis, and sulphide accumulation (Kinsman-Costello et al., 2023; Steele & Aitkenhead-Peterson, 2013). This shift in nitrogen cycling results in higher concentration within the pond's water column, as well as increased levels in the outflow into the natural and sensitive downstream ecosystems. In

addition to the effects of salt on nitrogen adsorption and biogeochemical cycling, high ambient salt concentrations can also lead to the release of previously absorbed heavy metals (Nelson et al., 2009; Schuler & Relyea, 2018). As SWMPs are often designed for water quality improvement through contaminated sediment and harmful particulate retention, the addition of high levels of road salt could displace the elements sorbed to the sediments and may lead to enhanced transport of metals into the downstream waterways and the surrounding areas ecosystems. Another significant aspect or potentially harmful effect of the hypoxic conditions in SWMPs from road salt induced stratification is P remobilization through ion displacement, iron sorption, plant stress, and cell lysis (Kinsman-Costello et al., 2023). This P remobilization could lead to eutrophication within the ponds themselves and potential export downstream during flushing events (Radosavljevic et al., 2022). Given the ongoing concerns regarding the eutrophication of the Great Lakes and the need to preserve and protect watershed water quality in southern Ontario, the mobilization of nitrogen, phosphorus, and heavy metals from engineered and naturalized SWMPs into our natural waterways represents an important issue. If these systems release the accumulated contaminants through baseflow or overflow events, it could undermine the regional and provincial efforts to preserve water quality (ECCC & Canda Water Agency, 2018).

The water quality effects of the low DO and high salinity are not the only negative impacts; another significant aspect of the road salt-induced hypoxic conditions is the effect to the GHG exchanges of the ponds. The downward shift in redox state creates low energy conditions that support CH_4 production in the sediment and the bottom layers of the water column (Davidson et al., 2024; Dupuis et al., 2019; Radosavljevic et al., 2022). The reduction of oxic conditions within the pond water column also leads to less efficient organic matter decomposition leading to faster buildup of organic material with higher than typical lability in the pond sediment (Kaushal, Mayer, et al., 2014; Neubauer & Megonigal, 2021; Price et al., 2023; Zhang & Furman, 2021). This build up creates the perfect breeding ground for GHG production and exchange, with the shallow water depths limiting the opportunity for impactful levels of denitrification and CH_4 oxidation (Davidson et al., 2024;

Gorsky et al., 2019; Malyan et al., 2016, 2022). This shift in both redox potential and organic matter accumulation has serious impacts on the GHG cycling of engineered and naturalized SWMPs, which should be considered if these systems are to be part of climate change mitigation and resilience strategies (Warren & Lulham, 2021).

These low oxygen and high salt conditions will also limit habitat use of the ponds. Although engineered SWMPs are not designed as habitat, loss of wetlands during urbanization (Birch et al., 2022) suggests that engineered SWMPs may be some of the only remaining aquatic habitat in urban areas, making their function as aquatic habitats a key consideration in their function. Firstly, the salt has serious effects on aquatic organisms by changing the osmotic balance between the organism and the surrounding environment, in particular on the early development stages of aquatic organisms (Findlay & Kelly, 2011; Keith et al., 2025). Secondly, as sodium concentrations increase, there is a tendency to displace previously adsorbed ions such as Ca, K, and Mg; heavy metals such as Pb; or organic molecules from charged binding sites on clay minerals, thus releasing important nutrients, metals, or other elements/compounds into the water column (Haq et al., 2018; Kinsman-Costello et al., 2023; Malyan et al., 2021; Nelson et al., 2009). Therefore, any soil process linked to these compounds or any organisms susceptible to toxic effects may be negatively affected.

These findings emphasize that the functional stability of engineered and naturalized SWMPs cannot be assumed under increasing anthropogenic stress. If SWMPs are to be treated as systems that improve water quality, provide urban aquatic habitat, and cycle carbon, their design and management must account for how these systems actually function under urban conditions rather than how they were originally intended to perform (Alikhani et al., 2021). Elevated salt concentrations fundamentally change the physical and chemical environment, altering microbial metabolism and reducing the engineered and naturalized ponds' intended abilities, such as sustaining natural ecological function, processing nutrients, or mitigating carbon release. This recognition prompts a broader question about the role and value of these systems: should stormwater ponds be viewed solely as engineered basins designed to contain contaminants and protect downstream

ecosystems, or as ecosystems themselves—worthy of conservation and restoration? Balancing these perspectives requires reconsidering how we define “nature” within urban environments and how we prioritize among water quality, carbon cycling, and habitat health. As climate change and urbanization continue to intensify, finding this balance—between containment and care, between designed performance and ecological integrity—will be central to building effective, sustainable stormwater management strategies.

2.5 Conclusion

The water quality variables, stratification indices, and redox sampling results collectively indicate that both engineered shallow and naturalized deep ponds are affected by the addition of road salt in urban SWMPs. Spatial and temporal analyses of temperature, specific conductivity and DO show that, while thermal stratification occurs naturally in low salinity systems, elevated salinity amplifies stratification, reducing overall mixing and disrupting key seasonal processes such as spring turnover in both engineered and natural high salinity systems. The stratification index further demonstrates that engineered shallow ponds in extremely high salinity systems exhibit markedly different physical layering compared to low salinity counterparts. Redox sampling results revealed that engineered shallow and naturalized deep low salt ponds experience redox stratification at depth that is sensitive to seasonal changes and external inputs, whereas engineered shallow and naturalized deep high salt ponds display pronounced vertical stratification of redox sensitive elements that is less responsive to seasonal variability, particularly in ponds with extremely high salt concentrations. This enhanced stratification leads to larger areas of permanently anoxic water and greater portions of the sediment residing under anoxic conditions, with significant consequences for aquatic ecosystem health and carbon cycling within both the water column and sediment layers.

Chapter 3: Greenhouse Gas Emissions from Salt Impacted Stormwater Management Ponds in Southern Ontario

3.1 Introduction

Wetlands are ecosystems where the primary factor controlling the system, including the plant and animal life, is water; they occur where the water table is at or near the surface of the land or where the land is at least partially or temporarily covered in water (Ramsar Convention Secretariat, 2016). The presence of water promotes systems that are low in oxygen, reducing organic matter decomposition rates and making them important systems for carbon storage. However, these low oxygen conditions also result in the production of the greenhouse gases (GHG) methane (CH_4), and when nitrogen is abundant, nitrous oxide (N_2O). Nonetheless, wetlands are often GHG sinks over the long term, storing carbon for decades to millennia, and have been identified as potential nature-based solutions to climate change (Alikhani et al., 2021; Neubauer & Megonigal, 2021; Ontario Ministry of the Environment, 2003; Ruane et al., 2025). Wetlands also store and filter the water that enters them through sedimentation and are key providers of biodiversity and habitat for a large range of plant and animal life (Hotte et al., 2011). They are vital ecosystems to the Canadian landscape and its watersheds, providing key ecohydrological, biogeochemical, and biodiversity services (Neubauer & Megonigal, 2021; Price et al., 2023; Ramsar Convention Secretariat, 2016). Despite these benefits, wetlands have been continuously lost in Canada, and in particular in southern Ontario where an estimated 68% of wetland area been lost due to agricultural drainage and removal during urban development (Byun et al., 2018; Penfound & Vaz, 2022). In many urban areas, these wetlands have been directly or indirectly replaced with stormwater management ponds (SWMPs) (Birch et al., 2022).

Replacing wetlands with ponds during urban development by be effective for flood mitigation but may have other environmental consequence. Water bodies > 10 ha, the size

that is considered a pond, make up 27% of terrestrial water bodies in the world, but are reported to be responsible for emitting 50% of carbon dioxide (CO_2) and 88% of CH_4 emitted by all terrestrial waterbodies (Holgerson & Raymond, 2016; Richardson et al., 2022). Ponds are influential GHG emitters despite their size, so by replacing pre-development wetlands with SWMPs, we are not only shifting the ratio of wetland types within an area, therefore impacting habitat availability (Birch et al., 2022; Keith et al., 2025), we are often replacing it with a naturally high GHG emitting system. When you also consider that artificial waterbodies and urban ecosystems have shown higher per-area emissions then natural waterbodies of the same size and type, we are potentially creating systems that are not performing the functions and services of the preexisting wetlands (Grinham et al., 2018). Urban wetlands and SWMPs are valuable systems, yet their carbon cycling and GHG exchanges relative to natural wetlands is still not well understood, particularly in Canadian SWM systems (Herrero Ortega et al., 2019; Peacock et al., 2019; Withanage, 2025). While urban wetlands and SWMPs share the same nutrient cycling processes as natural systems, the elevated nutrient and contaminant load they receive through their urban catchment stormwater alters key biogeochemical conditions. As a result, the governing reactions differ from those in natural systems, leading to changes in CH_4, CO_2, and N_2O emissions (Badiou et al., 2019; Grinham et al., 2018; Kinsman-Costello et al., 2023; Malyan et al., 2021, 2022; Peacock et al., 2019).

To begin to understand how the urban environment shifts ponds conditions and affects GHG exchange and carbon cycling, we need to consider the predominant contaminants within SWM ponds and what effect they may be having. In southern Ontario's temperate climate, road salt is often applied to roads and parking lots during winter to prevent ice-related accidents. In 2019, over 4.2 million tonnes of solid salt were used across Canada (ECCC, 2023b). While necessary for road safety in the winter, much of this salt is transported via runoff into SWMPs, where it can accumulate or discharge downstream (Kaushal et al., 2022; Snodgrass et al., 2017). Elevated salinity enhances density driven stratification (Loewen & Jackson, 2024), reducing vertical mixing and oxygen replenishment within a pond (Chapter 2). This promotes dissolved oxygen (DO) depletion

and creates zones of accelerated redox progression, maintaining low energy conditions and providing greater opportunities for CH_4 production and exchange (Dupuis et al., 2019).

To effectively use urban wetlands and ponds for stormwater management while also benefitting from other ecosystem services they could provide, we must quantify their GHG emissions and understand driving processes. This will allow us to strategically select wetland designs that perform well under different chemical inputs and minimize GHG emissions. With ongoing urban growth in southern Ontario, such knowledge is critical for sustainable and informed development (Audet et al., 2020; Birch et al., 2022).

With climate change driving more extreme weather, maintaining reliable and resilient SWM infrastructure has become increasingly critical. SWMPs not only protect water quality and reduce flooding but may also contribute maintaining urban wetland habitat and biodiversity within city ecosystems. However, there remains a significant gap in knowledge regarding the GHG controls in road salt impacted SWMPs. Therefore, this research aims to address that gap by understanding and identifying the biogeochemical and physicochemical controls of the GHG emissions from road salt impacted SWMPs in Southern Ontario. The specific objectives of this study are to: (1) determine if a high salt content impacts the GHG emissions from both shallow and deep SWMPs, (2) determine if the sample location within a pond impacts the measured GHG emissions and (3) determine environmental conditions that explain variation in GHG emissions within and among SWMPs of varying depth and salinity. These results can be used to advance smarter and more sustainable urban stormwater management design and maintenance.

3.2 Methods

3.2.1 Site Selection & Study Design

Research was conducted in SWMPs located in Kitchener (43° 27´ 11˝N, 80° 29´ 42˝W) and Waterloo (43° 29´N, 80° 31´W) Ontario, two cities undergoing continuous urban

growth and development. The study was conducted across four ponds: with low/high water salinity orthogonal to low/high water depth to ensure both variables, water depth and salinity and their interaction were considered. In May 2024, 24 ponds were selected based on descriptions provided by the municipalities and were visited to determine depth and electrical conductivity (EC). Ponds were chosen for the present study to minimize differences in depth and maximize difference EC within each depth category (Table 2.1). During the main sampling period in 2024 the shallow & low salt pond had a maximum specific conductivity of 730 µS/cm, the shallow & high salt pond had a maximum specific conductivity of 7500 µS/cm, the deep & low salt pond had a maximum specific conductivity of 970 µS/cm, and the deep & high salt pond had a maximum specific conductivity of 2750 µS/cm. The shallow ponds are highly designed and engineered systems with pipe inlets and outlet control structures, and the deep ponds consist of a re-naturalized open-water wetland connected to a creek during mid to high flow conditions, and a natural pond integrated into the city's stormwater network, representing the low-salinity and high-salinity ponds, respectively.

Within each pond two sampling transects were identified, one from the inlet to the outlet (flow transect), and another from the deepest point to the nearest shore (depth transect) (Figure 2.1). The transect following the pond's flow had three sampling locations, and the transect following the pond's depth had three to four sampling locations, depending on the size of the pond. The two transects shared one location, the deepest location for the depth transect and the middle or the outlet for the flow transect. The sampling locations were then categorized as inlet, outlet, shoreline, and the remaining locations as main pond for statistical analysis of within pond differences (Figure 3.1, Figure B.1 – B.3, Figure A.1 – A.3). The ponds underwent sampling throughout the ice-free period: twice a month from June to August (peak microbial activity), once a month from September to November (less microbial activity due to cooler temperatures), and finally three times in the spring (transition of microbial activity due to warming temperatures) for a total of 12 sampling rounds.

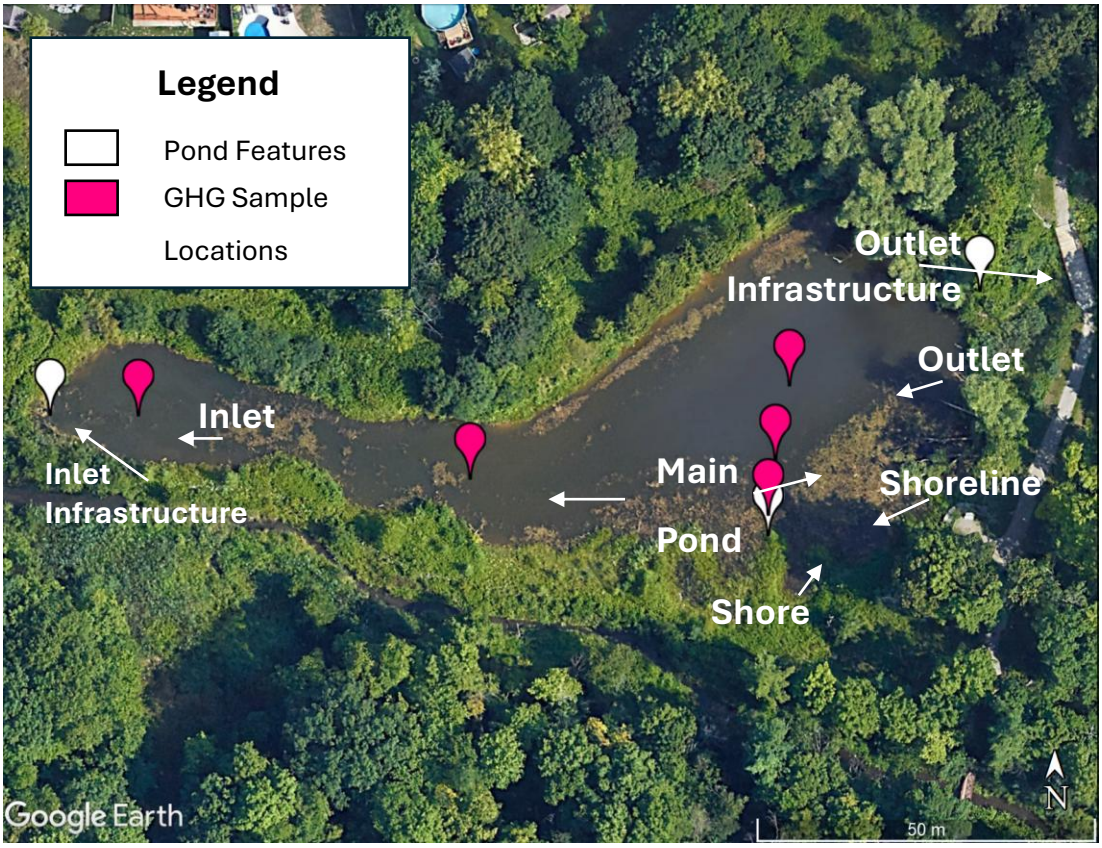


Figure 3.1. Site Selection - Deep & Low Salt Pond illustrating GHG emission sampling locations. No measurements were made at the pond features locations.

3.2.2 Pond Water Quality

Pond water quality was measured using a handheld ProQuatro YSI probe equipped with sensors for temperature, pH, conductivity/specific conductivity, and DO. These variables were measured at each sampling location on each measurement date at depths of 10 cm, 20 cm, 40 cm, 60 cm, 80 cm, 100 cm, 150 cm, 200 cm, 250 cm, 300 cm, 350 cm, and 10 cm above the sediment. At locations shallower than 350 cm, measurements were made from the surface following this depth pattern until 10 cm above the sediment was reached (Figure 2.2). Prior to each sampling campaign the YSI was calibrated according to manufacturer instructions (*606962-ProQuatro-User-Manual-English.Pdf*, n.d.).

3.2.3 Greenhouse Gas Fluxes

A closed dark floating chamber (Figure 3.2) was used to measure GHG fluxes (Gorsky et al., 2019). The chamber was constructed from an inverted plastic bucket, supported by styrofoam floats cut to fit flush to the bucket, and was equipped with two valves for the inlet and outlet tubes and a Type-K thermocouple to monitor chamber air temperature. The tubes were then connected to a portable greenhouse gas analyser (LICOR, LI7810 for CO_2 and CH_4, LI7820 for N_2O) to measure the GHG flux. Measurements were taken over a five-minute period at each of the sampling profile locations within each pond. The accumulated GHG concentrations over five minutes at each location was used to calculate the flux for each gas as shown in Equation 1.

Equation 3.1

$$F_E = \frac{\Delta C}{\Delta t} \times M \times \frac{1}{22.414} \times \frac{V}{A} \times T \times (86400) \times \frac{1}{10^3}$$

The equation converts the change in concentration of each gas into a mass per area per time. F_E is the GHG flux (mg/m^2/day), ΔC is the change in gas concentration from the start to the end of the quality controlled chamber closure period (ppm; µmol/mol), Δt is the time interval of the chamber closure, V is the temperature corrected volume of the chamber's headspace, A is the surface area of water enclosed by the chamber, T is the average chamber temperature during the flux measurement, and M is the molar mass of the considered gas (CO_2: 44 g/mol, CH_4: 16 g/mol, N_2O: 44 g/mol). The conversion factor of 86400 is used to convert seconds to days, 1/10^3 is used to convert µmol to mg, and 22.414 is the molar volume of an ideal gas at 1 atm of pressure at 0 °C.

Quality control of the concentration data collected during the GHG flux measurements was completed using the PEDRO software (Newton et al., 2025). The concentration data was trimmed to include the period when the chamber was sealed with the surface of the

water and the linear change in concentration was clearly visible. CH_4 ebullition was apparent as rapid shifts in concentration that varied from the steady increase in concentration during the chamber closure. Contribution of ebullition to GHG emissions within the flux was determined by calculating the flux accounting only for chamber sealing (i.e., the average slope determined from the concentration change from closure to end of chamber flux) and subtracting the flux calculated based on the slope of only the steady concentration increase. This provided us with what is thought of as the diffusive flux (steady slope only) as well as the ebullition flux for each sample. This method occasionally produced near zero or slightly negative values for the CH_4 ebullition emissions due to minor measurement variation and natural flux irregularities; however, these deviations were consistent across all flux calculations and are retained in the dataset.



Figure 3.2. The floating chamber used to measure the different GHG fluxes on the pond's water surface.

3.2.4 Dissolved Gas Concentration

Dissolved CH_4 and N_2O concentrations were measured at each sampling location and depth along the water column for the entire sampling period, with the exception of CH_4 in three ponds in late August 2024 and for N_2O in all ponds in late August 2024 and spring 2025, using the headspace equilibration method (Peacock et al., 2019). The water used for the headspace was collected with vinyl tubing connected to a manual syringe pump and a four-way stopcock. The tubing had an inner diameter of ¼", a length of 5 m (vol ~ 160 mL), and was attached to the outside of the YSI probe with one opening in line with the sensor

heads and the other connected to the four-way stopcock in the boat. 60 mL syringes were used to flush the tubing three times (vol ~ 180 mL) before each sample is taken to purge the tubing of the previous water and to rinse the tubing with the water at the current sample depth. The samples were then pulled up using the 60 mL syringes from the YSI water variable specified depths, excluding the intervals 10 cm below the surface and 10 cm above the sediment. The syringe was filled up to 30 mL with sample water and 30 mL of ambient air. The syringe was then vigorously shaken for 180 seconds, and the headspace was transferred to an appropriate cleaned and pre-evacuated glass vial (Exetainer, Labco Ltd., UK). Finally, the collected headspace gas samples were analysed by injecting a set volume, 10 mL, into a GHG analyser (LICOR, LI7810 for CH_4, LI7820 for N_2O) with the signal compared to a series of known standards (1, 5, 50, 1000 ppm and 0.0890, 1, 2 ppm, respectively) to measure the headspace GHG concentration. Quality control of the headspace concentration data was completed using the PEDRO software (Newton et al., 2025). The headspace concentration data was trimmed to the injection time and when the concentration peak is clearly visible. The PEDRO software then calculated the concentration of the injected samples by taking the area under the curve of the flux peaks and using the established volume, determined the CH_4 concentration of the headspace sample. Any concentrations that resulted in a headspace concentration less than zero were removed.

The dissolved CO_2 samples were excluded from this thesis because the gas analyser consistently assigned errors values to the CO_2 concentration of the injected samples due to interference from the high CH_4 concentration in the samples. As a result, the remaining valid dissolved CO_2 data was insufficient to provide meaningful insight into the pond conditions and was therefore excluded from the analysis.

3.2.5 Data Analysis

Prior to statistical analysis, the CH_4 fluxes were natural log transformed, ln for diffusive and total fluxes and ln + 0.05 for the ebullitive fluxes, to improve the normality of the samples.

The N_2O fluxes were also natural log transformed, ln + 5, to normalise the samples and account for negative values.

Differences in GHG emissions between ponds and the GHG sample location (i.e., inlet, outlet, main pond, shoreline) were determined using a linear mixed effects (LME) model using the package nlme (Pinheiro et al., 2025). For each GHG, the effect of pond identity (i.e., shallow & low salt, shallow & high salt, deep & low salt, deep & high salt) and general sample location within the pond and their interaction were included as fixed effects and specific sampling locations was included as a random effect to account for repeated measures throughout the sampling period.

To understand whether a high salt content stratified the water column within a pond and created a thicker anoxic section, the density gradient of each sample location for each sampling event was calculated based on the method in Holgerson et al. (2022) to determine if and how much the ponds and sample locations were physically stratifying themselves. Temperature, electrical conductivity (converted to salinity), and air pressure data from weather stations were used to calculate water density at each sampled depth. Salinity was determined using the gsw (*CRAN: Package Gsw*, n.d.) package in R, and density was calculated using the rLakeAnalyzer (Winslow et al., 2019) package. The density gradient (kg m^{-3} m^{-1}), also known as the stratification index, was computed as the difference between the top and bottom layer densities divided by the distance between them.

The effect of stratification indexes for explaining variation in GHG fluxes across the ponds was determined using the LME model (Pinheiro et al., 2025). For each GHG, the effect of pond identity, stratification index, and their interaction were included as fixed effects and the specific sampling locations was included as a random effect to account for repeated measures throughout the sampling period. If the interaction was significant ($p < 0.05$) then the trends of each pond were determined using the emmeans (Lenth, 2025) package, a pairwise comparison was then used to determine significant differences between slopes (R Core Team, 2023), and the regression line of each pond was plotted and its conditional

R^2 and marginal R^2 (R^2m) determined. If the interaction between pond and stratification index was not significant then the pond identity was removed as a fixed effect, and the LME was rerun. If the new model showed that stratification index was significant then the regression for the stratification index was plotted. The stratification index models were included because this metric is widely used as an indicator of mixing capacity (Holgerson et al., 2022; Chapter 2), making it useful for evaluating its influence both within the study design—where ponds were selected to span a gradient in specific conductivity associated with road salt—and on pond water columns more broadly.

The headspace gas concentrations measured using the GHG analyser described in the Section: 3.2.4 were converted to dissolved gas concentrations using the neonDissGas (Cawley, 2007) package in R. The dissolved gas concentrations measured along the water column for each pond had their dissolved CH_4 and N_2O concentrations averaged and summed, with the mean, standard deviation, minimum value, maximum value, and range determined. This was done to show the descriptive statistical values of the dissolved concentrations at each depth as well as the average integrated concentration along the water column in each pond.

In order to explore how water quality and physical variables within the ponds collectively affected GHG emissions a redundancy analysis (RDA) was conducted using the vegan package (Oksanen et al., 2025) in R. Environmental variables for the topmost water column layer and bottommost water layer were included alongside pond depth. For water variables, temperature, pH, DO, specific conductivity, sediment depth, dissolved CH_4, and dissolved N_2O were included. Response variables included CO_2 fluxes, diffusive CH_4 fluxes, ebullitive CH_4 fluxes, and N_2O fluxes. Prior to performing the RDA, all variables were standardized using the scales function (Wickham et al., 2025), and the dataset was cleaned so that any sample event missing data was removed. This resulted in the removal of sampling conducted in late August 2024 and spring 2025 due to missing dissolved CH_4 and dissolved N_2O values. The model was constructed with forward selection using the ordistep command in vegan and a p value of 0.05 to enter the model and 0.10 to be removed from the model.

3.3 Results

3.3.1 Environmental Conditions

The engineered and naturalized ponds differed in environmental variable values, as seen in the measured in-situ environmental descriptive statistics per pond across all sampling location for the top and bottom depths, with the mean shown in Table 3.1, with further site and statistical details found in Appendix B (Table B1).

Table 3.1. Summary mean of environmental variables at the top and bottom of the water columns across all sample locations of each pond.

		Shallow & Low Salt	Shallow & High Salt	Deep & Low Salt	Deep & High Salt
Parameter	Depth				
Water Column Depth (m)		0.89 (0.19)	0.96 (0.20)	2.06 (0.86)	2.12 (1.18)
Temperature (°C)	10 cm[a]	17.88 (6.59)	17.19 (6.44)	18.26 (5.87)	19.48 (5.89)
	10 cm as[a]	16.12 (4.85)	15.61 (4.78)	15.88 (5.13)	16.35 (5.85)
DO (mg/L)	10 cm	10.44 (4.21)	13.42 (3.73)	7.65 (2.51)	8.76 (2.6)
	10 cm as	7.34 (5.81)	7.03 (5.69)	5.53 (4.23)	4.59 (3.88)
pH	10 cm	8.62 (0.55)	8.15 (0.35)	8.1 (0.33)	8.41 (0.42)
	10 cm as	8.1 (0.56)	7.54 (0.52)	7.74 (0.35)	7.67 (0.59)
EC (us/cm)	10 cm	726.44 (175.71)	4208.46 (867.07)	849.85 (197.22)	1380.15 (267.11)
	10 cm as	771.25 (145.96)	5625.1 (2381.59)	876.18 (186.87)	1765.29 (745.86)
Dissolved CH_4 (µmol/L)	Shallow[b]	13.2 (2.69)	72.1 (56.5)	3.13 (0.155)	3.82 (2.73)
	Deep[b]	81.8 (127)	143 (145)	19.7 (41.4)	37.1 (63.4)
Dissolved N_2O (µmol/L)	Shallow	0.0139 (0.0297)	0.124 (0.0569)	1.81 (3.40)	0.0052 (0.00447)
	Deep	0.467 (2.24)	1.26 (4.12)	1.81 (3.40)	1.05 (3.63)
Stratification Index (kg m^{-3} m^{-1})		0.78 (1.23)	1.54 (1.70)	0.35 (0.36)	0.48 (0.40)

a "10 cm" refers to 10 cm below the water surface and "10 cm as" refers to 10 cm above the sediment layer.
b "Shallow" refers to the shallowest valid dissolved gas sample for the water column and "Deep" refers to the deepest valid dissolved gas sample for the water column.

3.3.2 Dissolved CH_4 and N_2O Concentrations

The total integrated CH_4 concentrations were highest in the shallow & low salt pond with a mean of 3230 µmol/L and lowest in the shallow & high salt pond with a mean of 833 µmol/L (Table 3.2). Average integrated CH_4 concentrations were an order of magnitude lower, with a mean of 4.13 µmol/L in the shallow & high salt pond to a mean of 30.7 µmol/L in the deep & low salt pond. Total N_2O concentrations were greatest in the shallow & high salt pond with a mean of 105 µmol/L and lowest in the deep & high salt pond with a mean of 22.3 µmol/L (Table 3.2). Average integrated N_2O concentrations were smaller, with the means ranging from 0.286 µmol/L in the deep & high salt pond to 0.559 µmol/L in the shallow & high salt pond.

Table 3.2. Water column integrated (Total) and sample depth (Average) dissolved CH_4 and N_2O concentration descriptive statistics (Standard Deviation: SD, Minimum: Min, Maximum: Max) across all locations per pond.

Porewater	Statistic	Shallow & Low Salt	Shallow & High Salt	Deep & Low Salt	Deep & High Salt
CH_4 µmol/L Total	Mean	3230	833	2930	681
	SD	5810	1140	3920	1340
	Min	5.09	20.5	22.7	53.3
	Max	24100	5130	18500	7090
	Range	24094.91	5109.5	18477.3	7036.7
CH_4 µmol/L Average	Mean	11.8	4.13	30.7	7.92
	SD	17.7	4.28	34.0	14.1
	Min	0.0848	0.341	0.473	0.834
	Max	74	20.3	137.5	70
	Range	73.92	20.26	136.53	70.07
N_2O µmol/L Total	Mean	68.4	105	34.7	22.3
	SD	242	323	94.1	70.6
	Min	0.0352	0.305	0.555	0.270
	Max	1260	1620	519	283
	Range	1259.96	1619.7	518.5	282.73
N_2O µmol/L Average	Mean	0.430	0.559	0.407	0.286
	SD	1.23	1.47	1.10	0.927
	Min	0.000705	0.00508	0.00965	0.00310
	Max	5.08	5.80	5.96	4.16
	Range	5.08	5.79	5.95	4.16

3.3.3 Greenhouse Gas Exchange

The summary statistics for the diffusive CH_4 fluxes, ebullitive CH_4 fluxes, total CH_4 fluxes, CO_2 fluxes, and N_2O fluxes measured from June 2024 to May 2025, with a pause in sampling over the 2025 Winter season, at every sample location per pond can be found in Table 3.3.

Table 3.3. Pond flux descriptive statistics (Standard Deviation: SD, Minimum: Min, Maximum: Max) across all locations per pond.

Flux	Statistic	Shallow & Low Salt	Shallow & High Salt	Deep & Low Salt	Deep & High Salt
CH_4 Diffusive Flux (mg $CH_4/m^2/d$)	Mean	101.3	200.8	33.7	59
	SD	156.5	684.1	40.5	75.3
	Min	6.5	7.7	2.8	0.8
	Max	1038.1	5193.4	267	348.6
	Range	1031.6	5185.6	264.2	347.8
CH_4 Ebullitive Flux (mg $CH_4/m^2/d$)	Mean	357.8	642.3	161.1	304.9
	SD	686.6	1444.5	588.3	802.3
	Min	-42	-4.3	-13.7	-6.5
	Max	3329.5	8927.5	2926.9	4792.5
	Range	3371.5	8931.8	2940.6	4799
CH_4 Total Flux (mg $CH_4/m^2/d$)	Mean	459.1	843	194.8	363.9
	SD	786.3	1658.3	608.4	825.2
	Min	8.9	8.3	3.2	1.4
	Max	4367.6	9098.4	3194	5108.8
	Range	4358.7	9090.2	3190.8	5107.4
CO_2 Flux (g $CO_2/m^2/d$)	Mean	0.0516	1.8724	3.4593	1.6981
	SD	3.1676	2.4882	2.8758	3.3463
	Min	-5.6450	-6.4310	0.1383	-2.0290
	Max	14.4736	10.6308	14.9813	11.9117
	Range	20.1185	17.0618	14.8430	13.9406
N_2O Flux (mg $N_2O/m^2/d$)	Mean	0.2381	1.5139	0.3956	-0.0816
	SD	0.3364	1.1524	0.6001	0.3028
	Min	-0.4561	0.1988	-1.0293	-1.9027
	Max	1.2090	6.0000	2.1793	0.5664
	Range	1.6651	5.8012	3.2086	2.4691

3.3.3.1 Methane

Both diffusive and ebullitive CH_4 fluxes were consistently higher in the engineered shallow ponds (Table 3.3). The shallow & high salt pond had the largest diffusive, followed by the shallow & low salt pond. The naturalized deep ponds had substantially lower diffusive fluxes in comparison. Ebullition fluxes showed the same pattern, with the shallow & high salt pond having the highest fluxes, the shallow & low salt pond being intermediate, and the deep ponds much lower values. This combination of diffusive and ebullitive fluxes resulted in the total CH_4 fluxes being greatest in the engineered shallow & high salt pond, moderate in the engineered shallow & low salt pond, and the lowest in the naturalized deep ponds. CH_4 fluxes varied widely across all ponds and sampling campaigns (Table 3.3), with ebullition accounting for 76% to 84% of total emissions (Table 3.4). For further information on the CH_4 flux patterns over the entire study period per pond, see Appendix B (Figure B.4).

Table 3.4. Sum of ebullition contribution to the sum of total pond CH_4 fluxes.

Flux	Shallow & Low Salt	Shallow & High Salt	Deep & Low Salt	Deep & High Salt
Ebullition CH_4 ($g\ CH_4\ m^{-2}\ d^{-1}$)	21	38	10	22
Total CH_4 ($g\ CH_4\ m^{-2}\ d^{-1}$)	28	50	12	26
Ebullition %	78	76	83	84

The LME model for the log transformed diffusive CH_4 fluxes revealed a significant effect of pond, indicating the fluxes differed primarily with pond depth and salinity (Figure 3.3a). There was no significant effect of sampling location or the interaction between pond and sampling location (Table 3.5). The engineered shallow ponds had higher fluxes than the naturalized deep ponds, and the high salt ponds emitted more CH_4 than their low salt counterparts, with a significant difference between the ponds (Figure 3.3). There was also a significant effect of pond for CH_4 emission via ebullition, with no effect of sampling location or its interaction with pond (Figure 3.3b, Table 3.5). Similar to the diffusive fluxes,

the shallow & high salt pond showed the highest emissions, indicating that sediment CH_4 production is influenced by both pond depth and salinity related stratification. Similar results were observed for total CH4 fluxes where only a significant effect of pond was observed (Figure 3.3c). The engineered shallow ponds consistently emitted more CH_4 than the naturalized deep ponds, and high salinity conditions amplified these emissions.

Table 3.5 LME model outputs for the GHG Fluxes ~ Pond x Sampling Location.

Diffusive CH4 Flux ~ Pond * Sampling Location				
	numDF	denDF	F-value	p-value
Intercept	1	230	901.6918	<0.0001
Pond	3	230	11.3217	<0.0001
Sampling Location	3	230	0.8686	0.4581
Pond x Sampling Location	9	230	1.0677	0.3876

Ebullitive CH4 Flux ~ Pond * Sampling Location				
	numDF	denDF	F-value	p-value
Intercept	1	230	277.3630	<0.0001
Pond	3	230	6.4206	0.0003
Sampling Location	3	230	0.7901	0.5005
Pond x Sampling Location	9	230	1.5528	0.1236

Total CH4 Flux ~ Pond * Sampling Location				
	numDF	denDF	F-value	p-value
Intercept	1	230	334.3945	<0.0001
Pond	3	230	11.0634	<0.0001
Sampling Location	3	230	1.8146	0.1452
Pond x Sampling Location	9	230	0.9378	0.4930

CO2 Flux ~ Pond * Sampling Location				
	numDF	denDF	F-value	p-value
Intercept	1	230	89.3786	<0.0001
Pond	3	230	13.2444	<0.0001
Sampling Location	3	230	3.0707	0.0286
Pond x Sampling Location	9	230	0.8581	0.5635

N2O Flux ~ Pond * Sampling Location				
	numDF	denDF	F-value	p-value
Intercept	1	230	27479.1420	<0.0001
Pond	3	230	70.9790	<0.0001
Sampling Location	3	230	0.5910	0.6213
Pond x Sampling Location	9	230	0.6350	0.7662

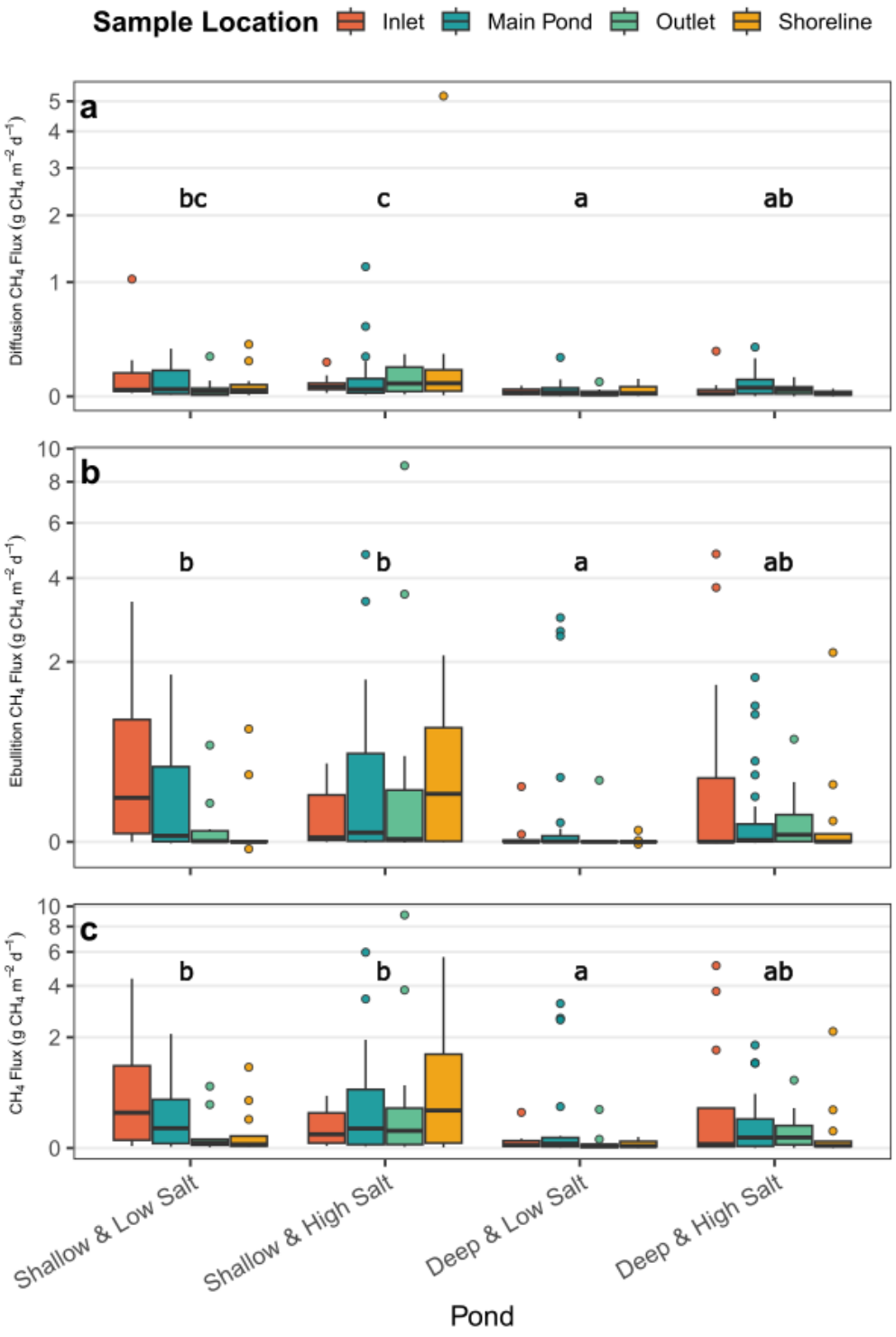


Figure 3.3 Boxplots depicting the diffusive CH_4 (a), ebullitive CH_4 (b), and total CH_4 (c) at the GHG exchange sample locations across the ponds. Ponds are significantly different from each other if they share no letters in common, Results from the LME model can be found in Table 3.5.

3.3.3.2 Carbon Dioxide

CO_2 fluxes were higher in the naturalized deep ponds, particularly in the deep & low salt pond, which showed the largest mean flux (Table 3.3). In contrast, the engineered shallow & low salt pond had the lowest mean flux, while the engineered shallow and deep high salt ponds displayed intermediate fluxes, respectively. The LME model for the CO_2 fluxes revealed a significant effect of pond and sample location, but not the interaction between them indicating that the effect of location was consistent across ponds (Figure 3.4) (Table 3.5). In general, CO_2 fluxes were highest at the inlet, declining in the main pond and outlet and were lowest near the shoreline. Although the overall effect of sample location was statistically significant, the pairwise comparison showed no significant differences between individual locations. This indicates that while variability among locations contributed to the model's overall variance structure, no single location had consistently higher or lower CO_2 fluxes that were statistically distinct after Tukey adjustment. Across the ponds CO_2 emissions were highest at the deep & low salt pond that was significantly higher than the shallow & high salt pond, which was significantly higher than the shallow & low salt pond, which was often a CO_2 sink; the deep & high salt pond had intermediate fluxes and was statistically similar to all other ponds (Figure 3.4). For further information on the CO_2 flux patterns over the entire study period per pond, see Appendix B (Figure B.5).

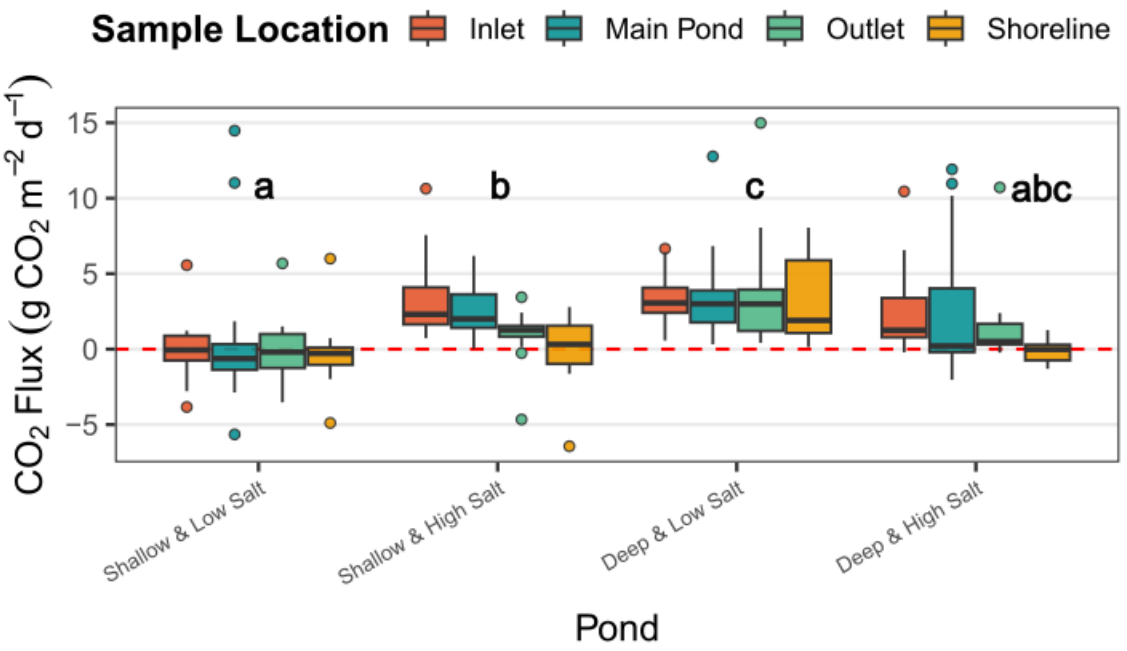


Figure 3.4 Boxplot depicting the CO_2 fluxes at the GHG exchange sample location across the ponds. Ponds are significantly different from each other if they share no letters in common. Results from the LME model can be found in Table 3.5.

3.3.3.3 Nitrous Oxide

N_2O fluxes were low and highly variable across the ponds (Table 3.3). The engineered shallow & high salt pond showed the highest mean flux, while the naturalized deep & high salt pond exhibited a slightly negative mean flux. The engineered shallow and naturalized deep low salt ponds had moderate positive mean fluxes. The LME model for the N_2O fluxes revealed a significant effect of pond with no effect of sampling location or its interaction with pond identity (Figure 3.5)(Table 3.5). The difference in N_2O fluxes do not appear to be directly related to salinity, as the deep & high salt pond exhibited the lowest N_2O emissions, while the shallow & high salt pond had the highest. For further information on the N_2O flux patterns over the entire study period per pond, see Appendix B (Figure B.6).

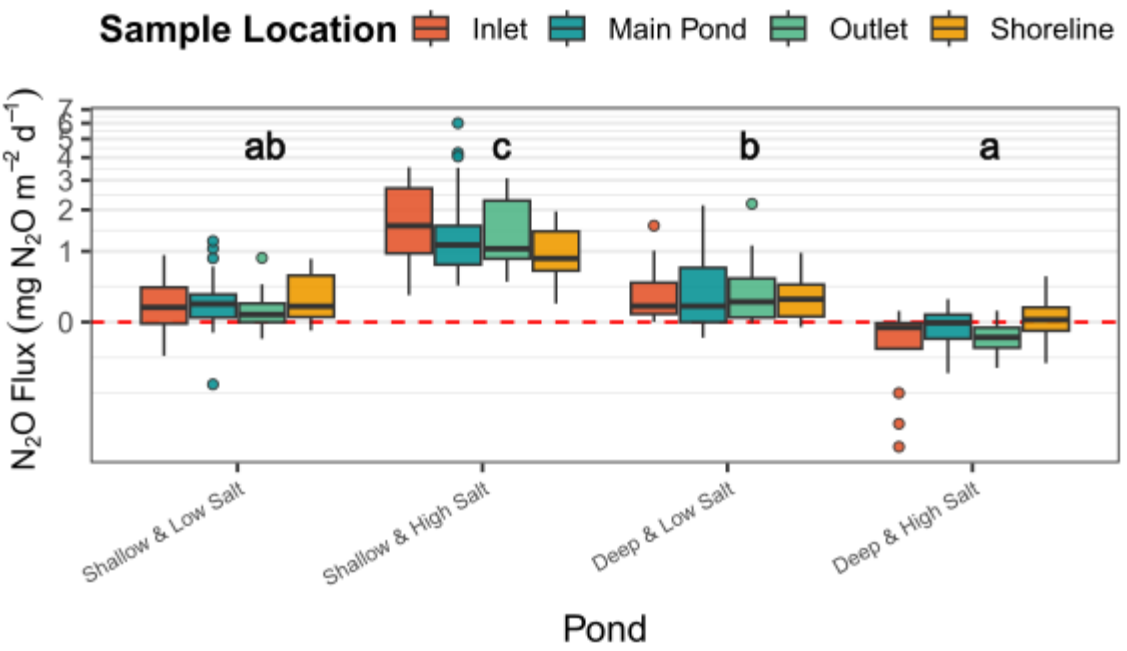


Figure 3.5 Boxplot depicting the N_2O fluxes at the GHG exchange sample location across the ponds. Ponds are significantly different from each other if they share no letters in common. Results from the LME model can be found in Table 3.5.

3.3.4 Environmental Controls on GHG Exchange

The effect of salinity induced stratification on GHG flux variation was evaluated using the stratification index for each flux measurement (Table 3.6). The LME model for the diffusive CH_4 fluxes revealed that the interaction of pond and stratification index was significant, with the deep & low salt pond the sole pond demonstrating explanatory power (Table 3.6)(Figure 3.6 a). Pairwise comparisons of the diffusive CH4 stratification slopes showed that only one pond differed significantly. The deep & low salt pond had a significantly different, steeper, trend compared to both shallow ponds ($p < 0.018$) and differed significantly from the deep & high salt pond ($p = 0.0357$). All other contrasts were non-significant ($p > 0.90$), indicating that most ponds exhibited similar diffusive CH_4 stratification relationships, with the primary differences driven by the deep & low salt pond.

The LME model for the ebullitive CH_4 fluxes when incorporating the fixed effect of pond identity, showed no significance for the stratification index, however when the fixed effect was removed the LME revealed that stratification index had a significant amount of the statistical power for total CH_4 fluxes across all ponds with little explanatory power (Table 3.6) (Figure 3.6b). Similarly, when the pond identity fixed effect is considered the stratification index showed no significance, but when it was removed the LME showed that stratification index had a significant amount of the statistical power for total CH_4 fluxes across all ponds with little explanatory power (Table 3.6) (Figure 3.6c). Therefore, for both ebullitive and total CH_4 fluxes the differences amongst the ponds explained greater variation than the stratification index, however the fluxes do appear to increase with stratification index.

Table 3.6 LME model outputs for GHG Flux ~ Pond * Stratification Index, with variance explained by the fixed effects (R^2m) and variance explained by fixed and random effects (R^2c). If stratification index was found not to be significant when pond identity was a fixed effect, then it was removed and GHG Flux ~ Stratification Index was run.

Diffusive CH_4 Flux ~ Pond * Stratification Index						
	numDF	denDF	F-value	p-value	*R^2m*	*R^2c*
Intercept	1	237	1210.7733	<0.0001		
Pond	3	237	11.1063	<0.0001		
Stratification Index	1	237	0.6128	0.4345		
Pond x Stratification Index	3	237	3.4011	0.0185		
Model					*0.149*	*0.1630*
Shallow & Low Salt					*0.0017*	*0.0085*
Shallow & High Salt					*0.009*	*0.009*
Deep & Low Salt					***0.214***	*0.293*
Deep & High Salt					*0.0013*	*0.11*

Ebullitive CH_4 Flux ~ Pond * Stratification Index						
	numDF	denDF	F-value	p-value	*R^2m*	*R^2c*
Intercept	1	237	337.8831	<0.0001		
Pond	3	237	6.0653	0.0005		
Stratification Index	1	237	2.7404	0.0992		
Pond x Stratification Index	3	237	0.2322	0.8739		

Model				*0.0783*	*0.0993*

Ebullitive CH_4 Flux ~ Stratification Index					
			t-value	p-value	R^2m	R^2c
Intercept			-19.4322	<0.0001		
Stratification Index			2.8912	0.0042	*0.0325*	*0.044*

Total CH_4 Flux ~ Pond * Stratification Index						
	numDF	denDF	F-value	p-value	R^2m	R^2c
Intercept	1	237	223.2540	<0.0001		
Pond	3	237	10.67698	<0.0001		
Stratification Index	1	237	2.4037	0.1224		
Pond x Stratification Index	3	237	1.0317	0.3792		
Model					*0.128*	*0.155*

Total CH_4 Flux ~ Stratification Index					
			t-value	p-value	R^2m	R^2c
Intercept			-19.0333	<0.0001		
Stratification Index			3.1155	0.0021	*0.0374*	*0.0383*

CO_2 Flux ~ Pond * Stratification Index						
	numDF	denDF	F-value	p-value	R^2m	R^2c
Intercept	1	237	42.7408	<0.0001		
Pond	3	237	14.08835	<0.0001		
Stratification Index	1	237	12.7208	0.0004		
Pond x Stratification Index	3	237	8.1007	<0.0001		
Model					*0.240*	*0.262*
Shallow & Low Salt					***0.142***	*0.142*
Shallow & High Salt					*0.0359*	*0.376*
Deep & Low Salt					*0.0382*	*0.0376*
Deep & High Salt					***0.216***	*0.265*

N_2O Flux ~ Pond * Stratification Index						
	numDF	denDF	F-value	p-value	R^2m	R^2c
Intercept	1	237	65798.92	<0.0001		
Pond	3	237	76.61	<0.0001		
Stratification Index	1	237	0.19	0.6661		
Pond x Stratification Index	3	237	2.08	0.1037		
Model					*0.486*	*0.486*

N_2O Flux ~ Stratification Index

	t-value	p-value	R^2m	R^2c
Intercept	85.5843	<0.0001		
Pond				
Stratification Index	4.0856	0.0001	*0.0595*	*0.142*

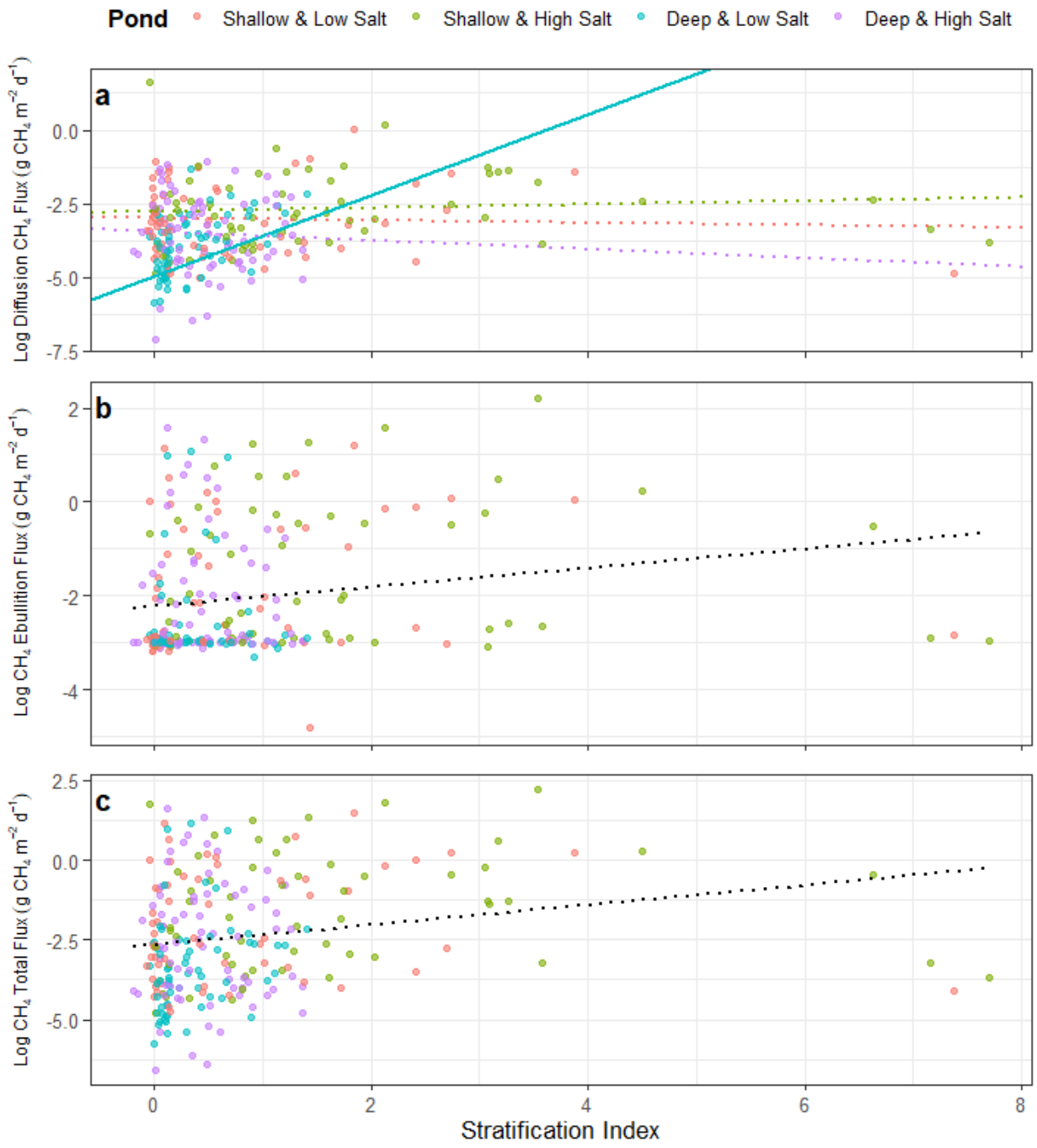


Figure 3.6 Scatterplot depicting the relationship between the water column stratification index & diffusive CH_4 (a), ebullitive CH_4 (b), and total CH_4 fluxes (c) across the ponds, with the solid lines showing significant relationships with strong explanatory power ($R^2m > 0.1$) and the dotted lines showing significant relationships with no explanatory power ($R^2m < 0.1$).

The LME model for the CO_2 flux revealed that the stratification index and the interaction between the pond and the stratification index was statistically significant (Figure 3.7) (Table 3.6). Pairwise comparison of slopes indicated that the deep & high salt pond (slope = -4.02 ± 0.85) exhibited the strongest negative relationship showing comparatively strong explanatory power and was significantly different compared to the other ponds ($p < 0.01$ for all). The shallow & low salt pond (slope = -0.93 ± 0.30) had a negative relationship with modest explanatory power, no significant difference between the shallow & high salt pond and a marginal ($p = 0.0503$) but not significant difference with the deep & low salt pond. The deep & low salt pond and the shallow and high salt pond had positive and negative slopes, respectively, and no explanatory power (Table 3.6).

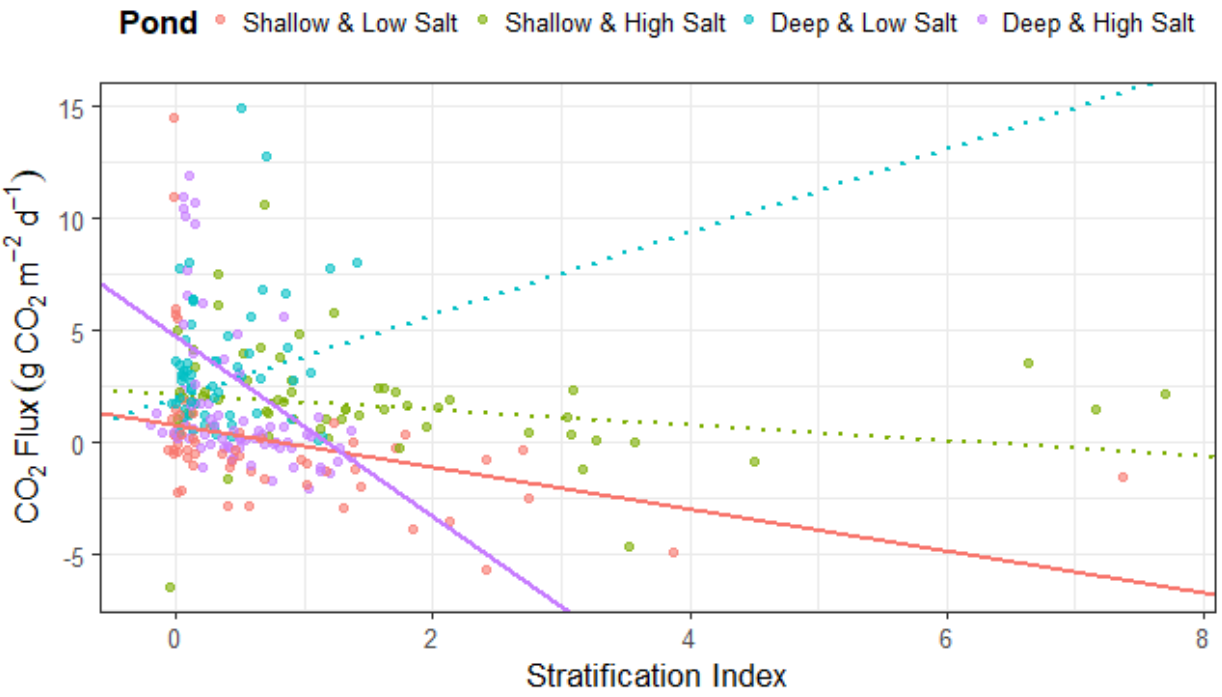


Figure 3.7. Scatterplot depicting the relationship between the water column stratification index and CO_2 fluxes across the ponds, with the solid lines showing significant relationships with strong explanatory power ($R^2m > 0.1$) and the dotted lines showing significant relationships with no explanatory power ($R^2m < 0.1$).

The LME model for the N_2O fluxes when incorporating the fixed effect of pond identity, showed no significance for the stratification index; however, when pond identity was removed the LME revealed that the stratification index explained a significant amount of the flux variation across all ponds but had little explanatory power (Table 3.6) (Figure 3.8). Therefore, for the N_2O fluxes the differences amongst the ponds explained greater variation than the stratification index, however the fluxes do appear to increase with stratification index.

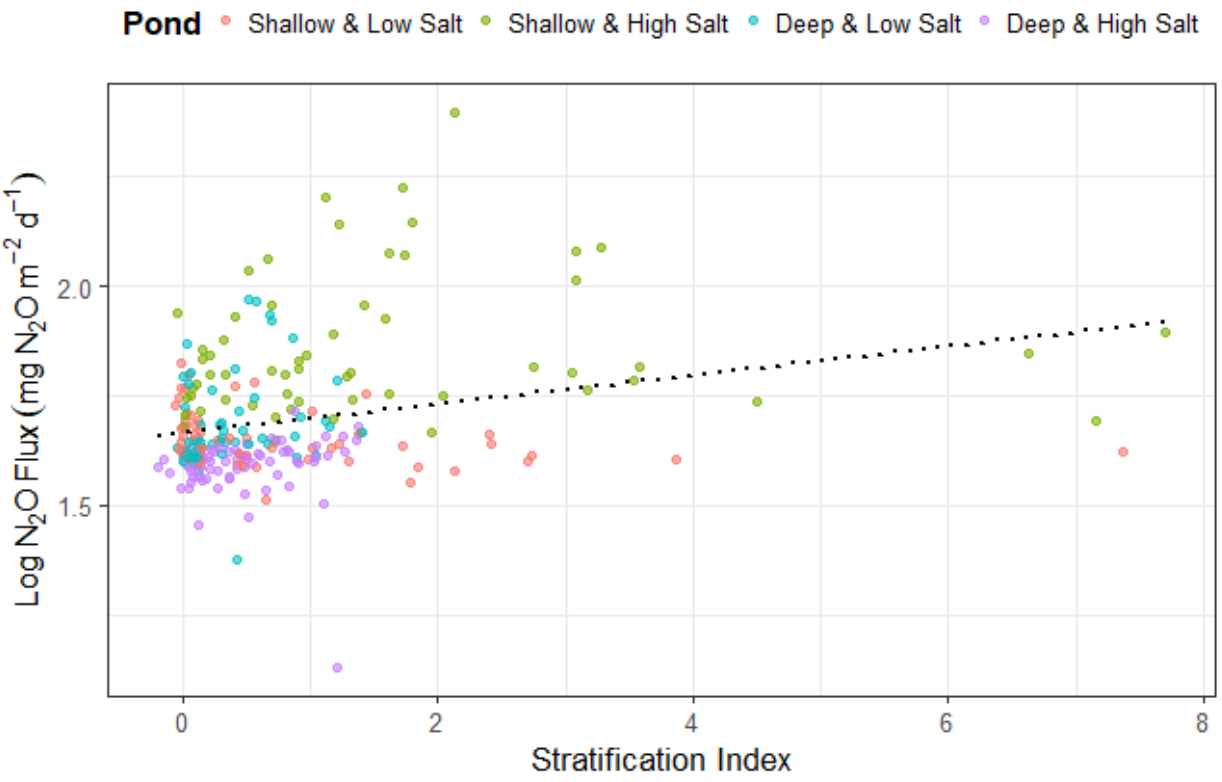


Figure 3.8 Scatterplot depicting the relationship between the water column stratification index & log N_2O Fluxes across the ponds, with the solid lines showing significant relationships with strong explanatory power ($R^2m > 0.1$) and the dotted lines showing significant relationships with no explanatory power ($R^2m < 0.1$).

A redundancy analysis was used to visualize the multivariate controls of water quality on measured GHG fluxes. Forward selection identified six significant environmental predictors of GHG dynamics: specific conductivity, temperature, pH, dissolved CH_4, DO, and pond depth (Figure 3.9). The majority of the predictors input as environmental variable were included in the final model, excluding the sediment depth and the dissolved N_2O concentration due to either being non-significant or adding little explanatory power to the model. The final RDA model explained 24% of total variation in GHG fluxes (adjusted R^2 = 0.24). RDA1 (61% of constrained variance) represented a conductivity–oxygen gradient, with high conductivity, low DO, and elevated dissolved CH_4 structuring CH_4 diffusion and N_2O flux patterns. RDA2 (35% of constrained variance) reflected a temperature–pH gradient, strongly influencing ebullitive CH_4. Higher CO_2 emissions were associated with deeper, cooler, low-conductivity conditions, whereas higher CH_4 diffusive and N_2O fluxes were associated with high-conductivity, low-oxygen waters. Ebullitive CH_4 emission aligned with warm, higher-pH environments. One thing to note, with the absence of denitrification relevant nutrient levels in the predictive model, the association of higher N_2O fluxes with high-conductivity, low-oxygen waters most likely is a correlation to a concurrent process that was not captured. Together, these results indicate that CH_4 is strongly driven by salinity and oxygen gradients, while CO_2 is more related to depth and temperature, and N_2O was not effectively captured.

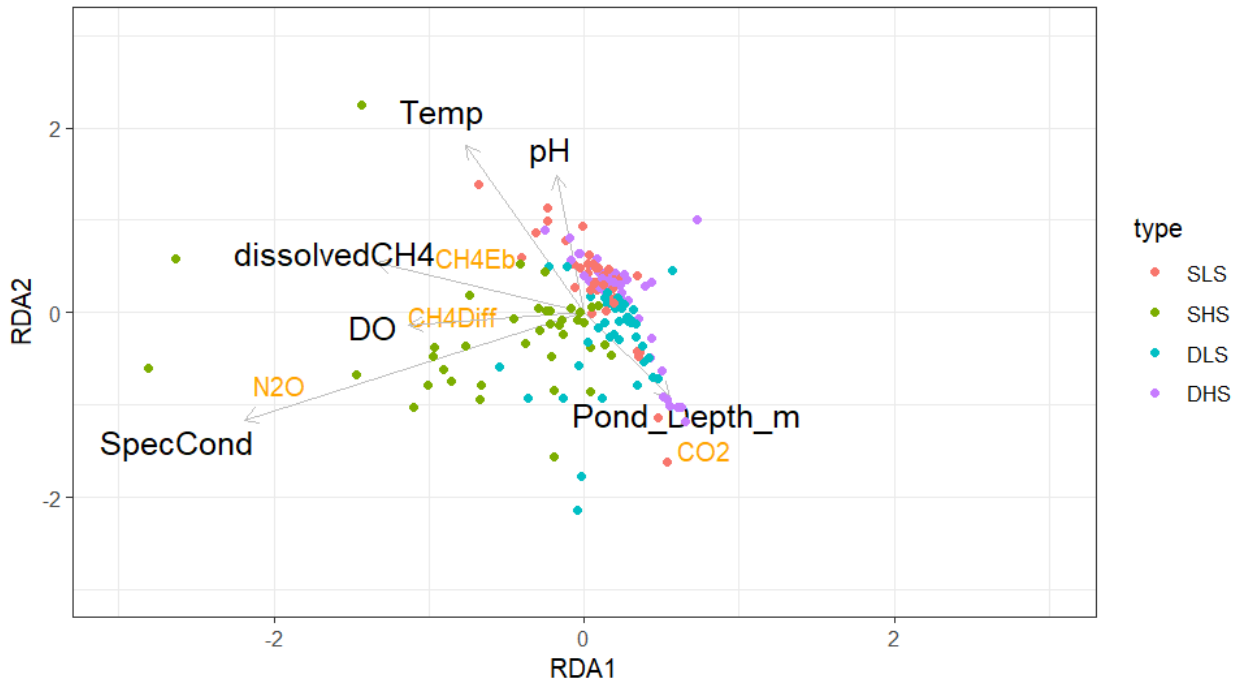


Figure 3.9. Redundancy analysis investigating environmental controls on GHG fluxes. RDA1 (61% of constrained variance) represented a conductivity–oxygen gradient, and RDA2 (35% of constrained variance) reflects a temperature–pH gradient. Pond identities (type) are abbreviated as shallow & low salt (SLS), shallow & high salt (SHS), deep & low salt (DLS), and deep & high salt (DHS). CH4Eb represents the ebullitive CH_4 fluxes, CH4Diff represents the diffusive CH_4 fluxes, N2O represents the N_2O fluxes, and CO2 represents the CO_2 fluxes. Temp represents water temperature, pH represents water pH, dissolvedCH4 represents the dissolved CH_4 concentrations, DO represents the dissolved oxygen concentration, SpecCond represents the specific conductivity concentration of the water, and Pond_Depth_m represents the pond depth where that sample is.

3.4 Discussion

Understanding the GHG dynamics of stormwater management ponds and the main environmental variables that explain variation in GHG emissions is essential for refining municipal GHG budgets and guiding the future design of healthier and more resilient SWMPs and urban blue-green infrastructure. These ponds are engineered or integrated into our systems to manage urban stormwater and protect urban infrastructure, but their GHG exchanges and the processes that guide them cannot be ignored as a major contributor to our cities' GHG budgets.

Within a single continuous urban area, the engineered and naturalized ponds in this study exhibited specific conductivity values spanning an order of magnitude, reflecting a gradient of road salt exposure and containment (Table 3.1). This variation provided an opportunity to evaluate how elevated salinity alters the environmental dynamics and GHG exchanges of SWMPs.

3.4.1 Methane Fluxes

The data showed that higher specific conductivity, linked to road salt contamination, promoted higher CH_4 emissions in similar SWMPs (i.e., comparing engineered shallow low salt to engineered shallow high salt and naturalized deep low salt to naturalized deep high salt) (Figure 3.3). The results suggest that restricted mixing in naturalized deeper ponds limits CH_4 oxidation typically seen in systems of similar depth and design, and increases the flux so that their emissions are comparable to shallower engineered ponds, systems that have been identified to be consistently higher CH_4 emitters (Bastviken et al., 2008; Malyan et al., 2016; Venetz et al., 2024). The difference among ponds varied for diffusive CH_4 fluxes compared to ebullitive CH_4 emissions (Figure 3.3), indicating that there are differences in the drivers between diffusion and ebullition within the study ponds as previously observed (Bastviken et al., 2008; Żygadłowska et al., 2024). This difference was also identified in the RDA, with the diffusive CH_4 fluxes strongly structured by RDA1, representing a conductivity–oxygen gradient, and the ebullitive CH_4 fluxes structured by RDA2, reflecting a temperature–pH gradient, showing us the major controls of the two pathways (Figure 3.9). These patterns indicate that diffusive CH_4 fluxes are primarily controlled by the capacity for CH_4 oxidation within the water column. Due to the slow speed of CH_4 diffusion in water, methanotrophs have substantial opportunity to oxidize CH_4 within the water column before it reaches the surface, provided that sufficient oxygen is available. Conversely, stratification decreases the depth of oxygenated water, limiting the zones in which oxidation can occur and weakening the effect of this control; nonetheless, physical stratification of the water column does not inherently indicate a lack

of oxygenation. The limited explanatory power of the CH_4 flux - stratification index relationships for most ponds (Figure 3.6), when considering that DO concentrations were not included in the stratification index calculation, underscores that DO is a critical control, particularly for diffusive CH4 fluxes, and cannot be overlooked (Davidson et al., 2024; Dupuis et al., 2019; Holgerson, 2015; Neubauer & Megonigal, 2021). In contrast, ebullitive CH_4 is less impacted by oxidation due to its greater volume to surface area ratio, resulting in the production rate as its primary controlling factor. As shown in other studies (Neubauer & Megonigal, 2021; Price et al., 2023), CH_4 production within wetland conditions increases with temperature, up to thresholds higher than those experienced in these ponds (Malyan et al., 2016), leading to warmer conditions driving ebullitive CH_4 fluxes.

Our results reveals differences in the controls between the diffusive CH_4 and the ebullitive CH_4 fluxes while Davidson et al. (2024) reported increases in both diffusive and ebullitive CH_4 with stratification. However, in that study stratification was intermittently thermally driven from early June to late August. In contrast, the ponds in this study experienced salinity driven stratification for the majority of the sampling period from June to November in the shallow & high salt pond and June to September in the deep & high salt pond. The differing drivers of stratification present in this study allowed for CH_4 fluxes to be measured across a broader temperatures range, enabling the distinction between the environmental controls of diffusion and ebullition that was not possible in Davidson et al. (2024).

Further, the present study showed that the drivers of diffusive CH_4 emissions differed from those reported in Dupuis et al. (2019), which reported that road salt induced stratification limited the diffusion of CH_4 to the surface. These differences may reflect the greater depths of the Dupuis et al. systems (12 – 14 m) compared to the ponds measured in this study (1.2 – 3.75 m on average), despite similar maximum bottom water dissolved CH_4 concentrations (400-600 µmol/L and 430-680 µmol/L, respectively). The greater depth in Dupuis et al. likely constrained diffusion rates, resulting in lower fluxes than those observed here. Additionally, the similarity between the ebullitive CH_4 and total CH_4 flux patterns in this study (Figure 3.3), along with the substantial contribution to total fluxes

(76% - 84%, Table 3.4), reflects the importance of capturing ebullition when measuring CH_4 emissions from shallow open water wetlands, and urban wetlands and SWMPs in particular (Davidson et al., 2024; Grinham et al., 2018; Żygadłowska et al., 2024). Overall, the CH_4 fluxes and exchange across the ponds showed that salinity driven stratification can result in greater CH_4 emissions with diffusive fluxes particularly amplified by the lack of mixing along the water column and the ebullitive fluxes amplified by warmer anoxic sediments.

3.4.2 Carbon Dioxide Fluxes

The data showed that the CO_2 fluxes differed significantly between the ponds, although these differences were not clearly driven by pond depth or salinity (Figure 3.4). The RDA indicated that higher CO_2 emissions were associated with cooler, deeper, and low-conductivity conditions, suggesting that fluxes are more strongly influenced by temperature and water column mixing. The stratification index-CO_2 flux relationship supports this interpretation of the results (Figure 3.7), as only negative correlations relationships have explanatory strength. The CO_2 fluxes measured in this study represent the net balance between CO_2 production by microbial and plant respiration (Filonchyk et al., 2024; Neubauer & Megonigal, 2021), as well as the uptake from microbial and plant processes, including photosynthesis (Gorsky et al., 2019; Holgerson, 2015; Neubauer & Megonigal, 2021). Consequently, interpretation of the measured CO_2 fluxes required consideration of both release and uptake processes. Within this framework, the CO_2 flux patterns observed under cooler temperatures, greater water column depths, and lower specific conductivity provide insights into the environmental conditions that control net CO_2 exchange. Cooler pond temperatures likely reflect non growing season conditions, which are generally associated with lower biological productivity and reduced CO_2 uptake by aquatic vegetation and microbes (Neubauer & Megonigal, 2021; Ray & Holgerson, 2023; Villa et al., 2020). Greater pond depth further limits CO_2 uptake by reducing light penetration through the water column, resulting in constrained photosynthetic activity or

excluding macrophytes altogether, both of which reduces the pond's overall biological uptake capacity (Gorsky et al., 2019; Holgerson et al., 2022; Malyan et al., 2022). Additionally, unstratified conditions facilitate vertical mixing, increasing nutrient availability throughout the water column but are also characteristic of cooler periods outside of the growing season (Figure 2.5). Under these conditions, productivity may be concentrated in the temperature extreme mediated sediments, while water column and plant mediated CO2 uptake remains limited, resulting in lower overall uptake despite (Filonchyk et al., 2024; Kumar et al., 2019; Malyan et al., 2022). These results align with previous work indicating that CO_2 production is primarily driven by sediment respiration and moderated by thermal reduction and stratification (Figure 3.9) (Holgerson, 2015; Malyan et al., 2022; Withanage, 2025). Although CO_2 emissions contribute to the overall GHG balance of the ponds, they do not appear to be driven by the key factors examined in this study.

3.4.3 Nitrous Oxide Fluxes

The results showed that the N_2O fluxes varied significantly among ponds, with the shallow & high salt pond having substantially higher emissions than the others (Figure 3.5). In contrast, the deep & high salt pond had the lowest fluxes, with a mean value below zero (Table 3.3). This pattern suggests that the elevated N_2O emissions in the shallow & high salt pond are not primarily driven by salinity or stratification, despite the association of N_2O with high conductivity, low oxygen conditions in the RDA. Instead, nitrate (NO_3^-) availability is likely the dominant control (Audet et al., 2020; Hefting et al., 2003; Neubauer & Megonigal, 2021). Supporting this interpretation, water quality data collected during the same sampling period (Withanage, 2025) indicate that the NO_3^- concentrations in the shallow & high salt pond were 4-9 times higher in summer and 14-250 times higher in fall relative to the other ponds. These results indicate that site specific nitrogen availability, rather than salinity, is the primary driver of N_2O flux conditions. As both salt and nutrients can be sourced from a ponds' watershed, salinity may be indirectly associated with higher

N_2O emissions in certain SWMPs. In contrast, the greater naturalized catchment conditions surrounding the deep and high salt pond may limit nitrogen inputs, contributing to lower N_2O fluxes, however more research is needed to fully understand how catchment characteristics contribute to SWMP N_2O emissions. The weak explanatory power of stratification for N_2O fluxes further suggests that nitrogen cycling in these systems is more strongly influenced by local redox and nutrient conditions than by mixing regimes.

3.4.4 Management Implications

Collectively, these findings emphasize that different GHGs respond to distinct environmental controls, underscoring the importance of considering multiple physiochemical pond characteristics when estimating regional or seasonal exchanges. Understanding these relationships not only improves predictive capacity for GHG balance but also provides practical insight and guidance for engineered and naturalized pond management. For instance, identifying shallow, highly engineered, or strongly stratified ponds, potential conditions associated with elevated CH_4 emissions and relevant to Canada's emission reduction goals (ECCC, 2023a; Warren & Lulham, 2021), can support targeted mitigation or restoration actions, such as designing ponds with continuous or bottom-drawn flow to limit the opportunity for stratification, implementing road salt programs within the catchment to reduce the salt load, and decreasing the intervals between dredging (Ontario Ministry of the Environment, 2003; Stone et al., 2010). Similarly, recognizing the environmental conditions that drive elevated N_2O or CO_2 fluxes can guide monitoring priorities and inform land-use or nutrient management strategies. Linking GHG fluxes to measurable pond attributes ultimately enables more informed strategies to minimize GHG contributions from necessary engineered and naturalized SWM systems urban settings.

3.5 Conclusion

This study highlights that greenhouse gas emissions from temperate engineered and natural SWM incorporated ponds are governed by distinct environmental controls for each gas. CH_4 fluxes were primarily influenced by pond depth, with salinity and the resulting stratification modulating emissions, while CO_2 fluxes were more strongly linked to temperature and water column mixing. N_2O fluxes exhibited site-specific variability, with stratification playing a minor role relative to other water chemistry factors. Multivariate analyses confirmed that specific conductivity, temperature, pH, dissolved CH_4, dissolved oxygen, and pond depth are key predictors of GHG dynamics. Overall, these findings demonstrate that pond morphometry and water chemistry jointly shape GHG emissions, emphasizing the need to consider both physical and biogeochemical gradients when assessing the role of ponds within our SWM systems as both flood mitigation and GHG sources. By linking environmental drivers to emission patterns, managers can make evidence-based decisions to target high emission systems and implement strategies, such as modifying water levels, dredging, or minimizing nutrient inputs, to minimize GHG outputs. This approach emphasizes the value of integrating ecological understanding into pond management and climate mitigation planning.

Chapter 4: Summary and Conclusion

This study was conducted with the main objectives to determine how the addition of road salt effects the water quality, stratification and GHG fluxes within and across ponds. Specifically the study aimed to: (1) determine if a high salt content stratifies the water column within a pond and create thicker anoxic sections, (2) assess if road salt interfere with the typical redox cascade in a pond, (3) determine how the addition of road salt effects the GHG emissions from the ponds, (4) determine if the location within a pond significantly affect GHG emissions. In the following sections, the main findings are summarized for the water quality and GHG studies separately and how those insights advance our understanding of the biogeochemical and physicochemical controls of the GHG emissions from road salt impacted engineered and naturalized SWMPs in southern Ontario.

4.1 Water Quality & Stratification

The water quality parameters, stratification indices, and redox sampling results indicated that both engineered shallow and naturalized deep ponds are affected by the addition of road salt in urban SWMPs. The spatial and temporal analyses of temperature, specific conductivity and dissolved oxygen show that, while thermal stratification occurs naturally in the low salinity systems, the introduction of excess road salt amplified stratification, reducing overall mixing and disrupting key seasonal processes in the high salinity systems. The stratification index further demonstrated that engineered shallow ponds in extremely high salinity systems exhibited markedly different physical layering compared to their low salinity counterparts. The redox sampling indicated that both the engineered shallow and naturalized deep low salt ponds developed redox stratification at depth, but this stratification shifted noticeable with seasonal changes and external inputs. In contrast, the engineered shallow and naturalized deep high salt ponds displayed pronounced vertical redox stratification that was less responsive to seasonal variability, particularly in depths or areas with extremely high salt concentrations. This enhanced stratification led to larger areas of

permanently anoxic water and greater portions of the sediment bed residing under anoxic conditions, which could have significant consequences for aquatic ecosystem health and carbon cycling within both the water column and sediment layers.

4.2 Greenhouse Gas Exchange

This study demonstrated that GHG emissions from temperate ponds are regulated by different environmental drivers for each gas. CH_4 fluxes were primarily influenced by pond depth, with salinity and stratification modulating emissions, while CO_2 fluxes were more strongly linked to temperature and water column mixing. N_2O fluxes exhibited site-specific nutrient availability variability. Multivariate analyses confirmed that specific conductivity, temperature, pH, dissolved CH_4, DO, and pond depth are key predictors of GHG dynamics. Overall, these findings demonstrate that pond geometry and water chemistry jointly shape GHG emissions, emphasizing the need to consider both physical and biogeochemical aspects when assessing the role of ponds within our SWM systems for both flood mitigation and GHG dynamics. By linking environmental drivers to emission patterns, this work enables decision makers to make evidence-based decisions to manage current and future high GHG emission SWMPs, and to implement strategies, such as modifying water levels through inlet and outlet design, maintaining consistent flow to encourage mixing, or reducing nutrient inputs, to minimize GHG outputs. This approach emphasizes the value of integrating environmental processes and biogeochemical understanding into pond management and climate change mitigation planning, beyond predictive modelling alone.

4.3 Limitations & Future Research Needs

4.3.1 Site Selection

While this study was concerned with how ponds react to high concentrations of road salt and specifically how it impacts pond stratification, biogeochemistry, and GHG emissions, there needed to be low salt level control groups as comparisons. We searched for a shallow and a deep urban stormwater pond within the study area with

healthy levels of specific conductivity for small freshwater systems in southern Ontario; however, we were unable to find any ponds lower than the two used in this study, which were above the target conductivity for freshwater systems for the majority of the sampling campaigns (500 µS/cm) (A Monitor's Guide to Water Quality, 2021). Consequently, within the scope of this study an unbiased comparison between currently functioning SWMPs impacted vs unimpacted by road salt in the same region could not be produced. A key research gap is the need to study SWMPs that remain largely unaffected by road salt in similar temperate climates, providing a true baseline for comparison. Another gap involves the different levels of engineering of the ponds within this study, as the shallow ponds were highly engineered systems and the deep ponds were natural or naturalized ponds that were incorporated into the SWM infrastructure. To ensure that the level of engineered design is considered in greater detail then this study could provide, the stratification processes and the GHG drivers of shallow and naturalized and deep and engineered ponds should also be studied.

4.3.2 Water Quality & Stratification

A key limitation of this study arises from the inherent design differences among the ponds, which influence hydrologic flow patterns independent of salt dynamics. Because the ponds were not constructed uniformly, they experience variable degrees of water movement and stagnation, ultimately affecting stratification patterns and biogeochemical conditions. For example, the deep & high salt pond remained consistently connected to the receiving system and maintained both inlet and outlet flow even under low-flow conditions, reducing the likelihood of prolonged stagnation. In contrast, the deep & low salt pond became hydrologically isolated during mid- to low-flow periods, with no inlet flow and with outlet flow ceasing once water levels fell below the engineered outflow height, resulting in extended stagnation. The shallow & low salt pond received water from multiple inlets, yet its outlet was positioned relatively high compared to the typical water level, and outflow was rarely observed, suggesting limited flushing. Meanwhile, the shallow & high salt pond featured a long forebay that the inflow needed to travel through before entering the main pond, and its outlet flow was consistently active. These structural differences in connectivity, inlet

configuration, and outlet positioning may influence thermal and chemical stratification independently of road salt inputs, complicating the ability to attribute observed stratification patterns solely to road salt concentrations. A key research gap is the need for controlled laboratory experiments using identical or replicated pond systems exposed to varying salt concentrations. By standardizing pond flow, connectivity, and physical structure, such experiments would isolate the sole influence of salinity on water-column stratification and water-quality dynamics. This would allow researchers to determine the true difference in stratification behaviour between natural, low-salt ponds and highly salt-impacted systems without the confounding effects present in natural stormwater ponds.

4.3.3 Greenhouse Gas Exchange

Several limitations were identified in this study that could influence the interpretation of the results. First, sampling immediately following storm events was not captured, which is particularly important for N_2O fluxes. Fresh inflows from stormwater can introduce pulses of nutrients, significantly influencing microbial processes and GHG emissions, especially N_2O, in the short term. Second, sediment characteristics at each sampling location were not included in the analysis of carbon dynamics. Given that a majority of CH_4 production occurs within sediments, this represents a potentially critical omission in understanding the drivers of CH_4 flux. Third, it is unclear whether the ponds received different types of road salt over their operational lifetimes, which may have influenced the composition of sediment microbial communities and, consequently, the type and magnitude of GHG emissions. Another key research gap is the lack of controlled studies examining the effects of road salt on pond systems. A microcosm or water column incubation study, in which different types and concentrations of road salt are applied, would allow for a detailed analysis of how pond sediment microbial communities respond to salinity and how GHG fluxes change over time. By isolating the influence of salt, such experiments could clarify the mechanisms driving alterations in water quality and stratification, providing a more precise understanding of how road salt impacts pond biogeochemistry and GHG production.

4.4 Implications

The findings of this study highlight the complex and dynamic nature of water quality and GHG fluxes in SWM facilities, while also revealing several areas where further research is needed to advance our understanding of these systems and improve SWMP design for both water quality and GHG emission management. Establishing this step in understanding the biogeochemical processes that shape water quality and GHG exchange dynamics allows us to understand the role ponds have in our urban environments. With clearer insight into how a common contaminant, such as road salt, impacts both shallow and deep ponds, decision makers can choose more appropriate SWM design and installations for areas that currently experience, or are to experience, high contaminant loads, for example those near major roads and parking lots that require winter road salt application in Southern Ontario. For example, SWM infrastructure such as grit separators can be used to capture solid rock salt particles from stormwater runoff, while vegetated buffer strips planted with salt tolerant species can intercept and assimilate dissolved salts, thereby reducing the salt load entering downstream naturalized SWM infrastructure (Ontario Ministry of the Environment, 2003, 2016a). For ponds and other end of pipe infrastructure, additional strategies are available. Ponds with accumulated road salt can be dredged to remove salt rich sediment that continuously contribute to elevated specific conductivity levels, while newly designed systems can incorporate shorter retention times and enhanced plant mediated treatment trains to limit salt accumulation.

This knowledge also helps clarify the total benefits provided by the different pond types, now that the processes governing GHG exchanges are more clearly understood. When combined with assessments of water volume capacity, biodiverse habitat value, and other key factors that are benefits, these insights support more informed evaluations of SWM infrastructure performance. As communities increasingly prioritize sustainable and resilient infrastructure in response to climate change, understanding the strengths, as well as the limitations of nature-based solutions, is essential for accurately assessing the long-term reliability and effectiveness of our system and resources.

References

606962-ProQuatro-User-Manual-English.pdf. (n.d.). Retrieved April 30, 2025, from https://www.ysi.com/File%20Library/Documents/Manuals/606962-ProQuatro-User-Manual-English.pdf?srsltid=AfmBOop_L7kTr0L3J7fjp-i2EUve72vEK_g8p4LSeAILAy0ADauGOkmv

Alikhani, S., Nummi, P., & Ojala, A. (2021). Urban Wetlands: A Review on Ecological and Cultural Values. *Water*, *13*(22), Article 22. https://doi.org/10.3390/w13223301

Armstrong, J., & Armstrong, W. (1991). A convective through-flow of gases in *Phragmites australis* (Cav.) Trin. Ex Steud. *Aquatic Botany*, *39*(1), 75–88. https://doi.org/10.1016/0304-3770(91)90023-X

Audet, J., Carstensen ,Mette Vodder, Hoffmann ,Carl C., Lavaux ,Lucile, Thiemer ,Kirstine, & and Davidson, T. A. (2020). Greenhouse gas emissions from urban ponds in Denmark. *Inland Waters*, *10*(3), 373–385. https://doi.org/10.1080/20442041.2020.1730680

Badiou, P., Page, B., & Ross, L. (2019). A comparison of water quality and greenhouse gas emissions in constructed wetlands and conventional retention basins with and without submerged macrophyte management for storm water regulation. *Ecological Engineering*, *127*, 292–301. https://doi.org/10.1016/j.ecoleng.2018.11.028

Bastviken, D., Cole, J. J., Pace, M. L., & Van de Bogert, M. C. (2008). Fates of methane from different lake habitats: Connecting whole-lake budgets and CH4 emissions. *Journal of Geophysical Research: Biogeosciences*, *113*(G2). https://doi.org/10.1029/2007JG000608

Birch, W. S., Drescher, M., Pittman, J., & Rooney, R. C. (2022). Trends and predictors of wetland conversion in urbanizing environments. *Journal of Environmental Management*, *310*, 114723. https://doi.org/10.1016/j.jenvman.2022.114723

Byun, E., Finkelstein, S. A., Cowling, S. A., & Badiou, P. (2018). Potential carbon loss associated with post-settlement wetland conversion in southern Ontario, Canada. *Carbon Balance and Management*, *13*, 6. https://doi.org/10.1186/s13021-018-0094-4

Calvin, K., Dasgupta, D., Krinner, G., Mukherji, A., Thorne, P. W., Trisos, C., Romero, J., Aldunce, P., Barrett, K., Blanco, G., Cheung, W. W. L., Connors, S., Denton, F., Diongue-Niang, A., Dodman, D., Garschagen, M., Geden, O., Hayward, B., Jones, C., … Péan, C. (2023). *IPCC, 2023: Climate Change 2023: Synthesis Report. Contribution of Working Groups I, II and III to the Sixth Assessment Report of the Intergovernmental Panel on Climate Change [Core Writing Team, H. Lee and J. Romero (eds.)]. IPCC, Geneva, Switzerland*. (First). Intergovernmental Panel on Climate Change (IPCC). https://doi.org/10.59327/IPCC/AR6-9789291691647

Canadian Council of Ministers of the Environment. (2011). *Protocols Manual for Water Quality Sampling in Canada*.

Cawley, K. (2007). *neonDissGas: Calculates Dissolved CO2, CH4, and N2O Concentrations in Surface Water* (Version 0.0.0.9002) [R (>= 3.3.2)]. https://github.com/NEONScience/NEON-dissolved-gas/blob/master/neonDissGas/R/def.calc.sdg.conc.R

Climate Risk Institute. (2023). *Ontario Provincial Climate Change Impact Assessment*.

Cornwell, J. C., Kemp, W. M., & Kana, T. M. (1999). Denitrification in coastal ecosystems: Methods, environmental controls, and ecosystem level controls, a review. *Aquatic Ecology*, *33*(1), 41–54. https://doi.org/10.1023/A:1009921414151

Craig, S., & Zhu, W. (2018). Impacts of Deicing Salt and Nitrogen Addition on Soil Nitrogen and Carbon Cycling in a Roadside Ecosystem. *Water, Air, & Soil Pollution*, *229*(6), 187. https://doi.org/10.1007/s11270-018-3838-6

CRAN: Package gsw. (n.d.). Retrieved September 30, 2025, from https://cloud.r-project.org/web/packages/gsw/index.html

D'Acunha, B., & Johnson, M. S. (2019). Water quality and greenhouse gas fluxes for stormwater detained in a constructed wetland. *Journal of Environmental Management*, *231*, 1232–1240. https://doi.org/10.1016/j.jenvman.2018.10.106

Davidson, E., Keller, M., Erickson, H. E., Verchot, L. V., & Veldkamp, E. (2000). Testing a Conceptual Model of Soil Emissions of Nitrous and Nitric Oxides: Using two functions based on soil nitrogen availability and soil water content, the hole-in-the-pipe model characterizes a large fraction of the observed variation of nitric oxide and nitrous oxide emissions from soils. *BioScience*, *50*(8), 667–680. https://doi.org/10.1641/0006-3568(2000)050%255B0667:TACMOS%255D2.0.CO;2

Davidson, Søndergaard, M., Audet, J., Levi, E., Esposito, C., Bucak, T., & Nielsen, A. (2024). Temporary stratification promotes large greenhouse gas emissions in a shallow eutrophic lake. *Biogeosciences*, *21*(1), 93–107. https://doi.org/10.5194/bg-21-93-2024

Dupuis, D., Sprague, E., Docherty, K. M., & Koretsky, C. M. (2019). The influence of road salt on seasonal mixing, redox stratification and methane concentrations in urban kettle lakes. *Science of The Total Environment*, *661*, 514–521. https://doi.org/10.1016/j.scitotenv.2019.01.191

ECCC. (2023a). *National Inventory Report 1990 – 2021*. Environment and Climate Change Canada.

ECCC. (2023b, June 29). *Review of Progress: Code of Practice for the Environmental Management of Road Salts 2014 to 2019*. https://www.canada.ca/en/environment-climate-change/services/pollutants/road-salts/road-salts-final-five-year-review-progress.html

ECCC & Canda Water Agency. (2018). *Partnering on Achieving Phosphorus Loading Reductions to Lake Erie from Canadian Sources*. ECCC and the Ontario Ministry of the Environement and Climate Change. https://www.canada.ca/en/canada-water-agency/freshwater-ecosystem-initiatives/great-lakes/great-lakes-protection/action-plan-reduce-phosphorus-lake-erie.html

ECCC & NAVCAN. (2024). *Kitchener/Waterloo Ontario—Climate Station* (Climate Station No. 48569). https://climate.weather.gc.ca/

Fan, M., Zhang, W., Wu, J., & Zhou, J. (2022). Agricultural land use and pond management influence spatial-temporal variation of CH4 and N2O emission fluxes in ponds in a subtropical agricultural headstream watershed. *Frontiers in Environmental Science*, *10*. https://doi.org/10.3389/fenvs.2022.1029334

Filonchyk, M., Peterson, M. P., Zhang, L., Hurynovich, V., & He, Y. (2024). Greenhouse gases emissions and global climate change: Examining the influence of CO2, CH4, and N2O. *Science of The Total Environment*, *935*, 173359. https://doi.org/10.1016/j.scitotenv.2024.173359

Findlay, S. E. G., & Kelly, V. R. (2011). Emerging indirect and long-term road salt effects on ecosystems. *Annals of the New York Academy of Sciences*, *1223*(1), 58–68. https://doi.org/10.1111/j.1749-6632.2010.05942.x

Golden Software, LLC. (n.d.). *Surfer®* (Version 26) [Computer software]. www.goldensoftware.com

Gorsky, A. L., Racanelli, G. A., Belvin, A. C., & Chambers, R. M. (2019). Greenhouse gas flux from stormwater ponds in southeastern Virginia (USA). *Anthropocene*, *28*, 100218. https://doi.org/10.1016/j.ancene.2019.100218

Grinham, A., Albert, S., Deering, N., Dunbabin, M., Bastviken, D., Sherman, B., Lovelock, C. E., & Evans, C. D. (2018). The importance of small artificial water bodies as sources of methane emissions in Queensland, Australia. *Hydrology and Earth System Sciences*, *22*(10), 5281–5298. https://doi.org/10.5194/hess-22-5281-2018

Haq, S., Kaushal, S. S., & Duan, S. (2018). Episodic salinization and freshwater salinization syndrome mobilize base cations, carbon, and nutrients to streams across urban regions. *Biogeochemistry*, *141*(3), 463–486.

Hefting, M. M., Bobbink, R., & de Caluwe, H. (2003). Nitrous Oxide Emission and Denitrification in Chronically Nitrate-Loaded Riparian Buffer Zones. *Journal of Environmental Quality*, *32*(4), 1194–1203. https://doi.org/10.2134/jeq2003.1194

Herrero Ortega, S., Romero González-Quijano, C., Casper, P., Singer, G. A., & Gessner, M. O. (2019). Methane emissions from contrasting urban freshwaters: Rates, drivers, and a whole-city footprint. *Global Change Biology*, *25*(12), 4234–4243. https://doi.org/10.1111/gcb.14799

Holgerson, M. A. (2015). Drivers of carbon dioxide and methane supersaturation in small, temporary ponds. *Biogeochemistry*, *124*(1), 305–318. https://doi.org/10.1007/s10533-015-0099-y

Holgerson, M. A., & Raymond, P. A. (2016). Large contribution to inland water CO2 and CH4 emissions from very small ponds. *Nature Geoscience*, *9*(3), 222–226. https://doi.org/10.1038/ngeo2654

Holgerson, M. A., Richardson, D. C., Roith, J., Bortolotti, L. E., Finlay, K., Hornbach, D. J., Gurung, K., Ness, A., Andersen, M. R., Bansal, S., Finlay, J. C., Cianci-Gaskill, J. A., Hahn, S., Janke, B. D., McDonald, C., Mesman, J. P., North, R. L., Roberts, C. O., Sweetman, J. N., & Webb, J. R. (2022). Classifying Mixing Regimes in Ponds and Shallow Lakes. *Water Resources Research*, *58*(7), e2022WR032522. https://doi.org/10.1029/2022WR032522

Hotte, N., Kennedy, M., & Lantz, V. (2011). *Valuing wetlands in southern Ontario's Credit River watershed*. Pembina Institute & Credit Valley Conservation. https://books.scholarsportal.info/en/read?id=/ebooks/ebooks0/gibson_cppc/2011-11-18/1/10497703#page=12

Joye, S. B., & Hollibaugh, J. T. (1995). Influence of Sulfide Inhibition of Nitrification on Nitrogen Regeneration in Sediments. *Science*, *270*(5236), 623–625.

Kati, V., & Jari, N. (2016). Bottom-up thinking—Identifying socio-cultural values of ecosystem services in local blue–green infrastructure planning in Helsinki, Finland. *Land Use Policy*, *50*, 537–547. https://doi.org/10.1016/j.landusepol.2015.09.031

Kaushal, S., Mayer, P., Vidon, P., Smith, R., Pennino, M., Newcomer Johnson, T., Duan, S., Welty, C., & Belt, K. (2014). Land Use and Climate Variability Amplify Carbon, Nutrient, and Contaminant Pulses: A Review with Management Implications. *JAWRA Journal of the American Water Resources Association*, *50*. https://doi.org/10.1111/jawr.12204

Kaushal, S., McDowell, W. H., & Wollheim, W. M. (2014). Tracking evolution of urban biogeochemical cycles: Past, present, and future. *Biogeochemistry*, *121*, 1–21.

Kaushal, S., Reimer, J. E., Mayer, P. M., Shatkay, R. R., Maas, C. M., Nguyen, W. D., Boger, W. L., Yaculak, A. M., Doody, T. R., Pennino, M. J., Bailey, N. W., Galella, J. G., Weingrad, A., Collison, D. C., Wood, K. L., Haq, S., Newcomer-Johnson, T. A., Duan, S., & Belt, K. T. (2022). Freshwater salinization syndrome alters retention and release of chemical cocktails along flowpaths: From stormwater management to urban streams. *Freshwater Science*, *41*(3), 420–441. https://doi.org/10.1086/721469

Keith, K. M., Potvin, M. K., Saad, S. R., & Surasinghe, T. D. (2025). Temporal Shifts in Biological Community Structure in Response to Wetland Restoration: Implications for Wetland Biodiversity Conservation and Management. *Diversity*, *17*(3), 198. https://doi.org/10.3390/d17030198

Kim, S., & Koretsky, C. (2013). Effects of road salt deicers on sediment biogeochemistry. *Biogeochemistry*, *112*(1), 343–358. https://doi.org/10.1007/s10533-012-9728-x

Kinsman-Costello, L., Bean, E., Goeckner, A., Matthews, J. W., O'Driscoll, M., Palta, M. M., Peralta, A. L., Reisinger, A. J., Reyes, G. J., Smyth, A. R., & Stofan, M. (2023). Mud in the city: Effects of freshwater salinization on inland urban wetland nitrogen and phosphorus

availability and export. *Limnology and Oceanography Letters*, *8*(1), 112–130. https://doi.org/10.1002/lol2.10273

Koop-Jakobsen, K., & Gutbrod, M. S. (2019). Shallow Salt Marsh Tidal Ponds–An Environment With Extreme Oxygen Dynamics. *Frontiers in Environmental Science*, *7*. https://doi.org/10.3389/fenvs.2019.00137

Kumar, A., Yang, T., & Sharma, M. P. (2019). Greenhouse gas measurement from Chinese freshwater bodies: A review. *Journal of Cleaner Production*, *233*, 368–378. https://doi.org/10.1016/j.jclepro.2019.06.052

Lehner, B., Anand, M., Fluet-Chouinard, E., Tan, F., Aires, F., Allen, G. H., Bousquet, P., Canadell, J. G., Davidson, N., Finlayson, C. M., Gumbricht, T., Hilarides, L., Hugelius, G., Jackson, R. B., Korver, M. C., McIntyre, P. B., Nagy, S., Olefeldt, D., Pavelsky, T. M., … Thieme, M. (2024). *Mapping the world's inland surface waters: An update to the Global Lakes and Wetlands Database (GLWD v2)*. ESSD – Land/Hydrology. https://doi.org/10.5194/essd-2024-204

Lenth, R. V. (2025). *emmeans: Estimated Marginal Means, aka Least-Squares Means* (Version R package version 1.11.2-8) [Computer software]. https://CRAN.R-project.org/package=emmeans

Li, Y., Tian, H., Yao, Y., Shi, H., Bian, Z., Shi, Y., Wang, S., Maavara, T., Lauerwald, R., & Pan, S. (2024). Increased nitrous oxide emissions from global lakes and reservoirs since the pre-industrial era. *Nature Communications*, *15*(1), 942. https://doi.org/10.1038/s41467-024-45061-0

Loewen, C. J. G., & Jackson, D. A. (2024). Salinization, warming, and loss of water clarity inhibit vertical mixing of small urban ponds. *Limnology and Oceanography Letters*, *9*(2), 155–164. https://doi.org/10.1002/lol2.10367

Lunau, M., Voss, M., Erickson, M., Dziallas, C., Casciotti, K., & Ducklow, H. (2013). Excess nitrate loads to coastal waters reduces nitrate removal efficiency: Mechanism and implications for coastal eutrophication. *Environmental Microbiology*, *15*(5), 1492–1504. https://doi.org/10.1111/j.1462-2920.2012.02773.x

Lyu, Z., Shao, N., Akinyemi, T., & Whitman, W. B. (2018). Methanogenesis. *Current Biology*, *28*(13), R727–R732. https://doi.org/10.1016/j.cub.2018.05.021

Malyan, S. K., Bhatia, A., Kumar, A., Gupta, D. K., Singh, R., Kumar, S. S., Tomer, R., Kumar, O., & Jain, N. (2016). Methane production, oxidation and mitigation: A mechanistic understanding and comprehensive evaluation of influencing factors. *Science of The Total Environment*, *572*, 874–896. https://doi.org/10.1016/j.scitotenv.2016.07.182

Malyan, S. K., Singh, O., Kumar, A., Anand, G., Singh, R., Singh, S., Yu, Z., Kumar, J., Fagodiya, R. K., & Kumar, A. (2022). Greenhouse Gases Trade-Off from Ponds: An Overview of Emission Process and Their Driving Factors. *Water*, *14*(6), Article 6. https://doi.org/10.3390/w14060970

Malyan, S. K., Yadav, S., Sonkar, V., Goyal, V. C., Singh, O., & Singh, R. (2021). Mechanistic understanding of the pollutant removal and transformation processes in the constructed wetland system. *Water Environment Research*, *93*(10), 1882–1909. https://doi.org/10.1002/wer.1599

Marques, P., Illyes, E., McCauley, S., Jackson, D. A., Michalakos, D., Ferzoco, I. M. C., Timms, L., Murray, R. L., MacFarlane, Z. S., Duval, T. P., Dolson, R., Din, S., Pebesma, D., Kirkwood, A. E., Turner, N. A., Clayton, J., Horton, K., Boston, C. M., Sapozhnikova, E., … Mandrak, N. E. (2024). Ecosystem functions and services in urban stormwater ponds: Co-producing knowledge for better management. *Ecological Solutions and Evidence*, *5*(3), e12366. https://doi.org/10.1002/2688-8319.12366

Masson-Delmotte, V. & Intergovernmental Panel on Climate Change (Eds.). (2023). *Climate change 2021: The physical science basis: Working Group I contribution to the Sixth*

Assessment Report of the Intergovernmental Panel on Climate Change. Cambridge University Press.

Megonigal, J. P., Hines, M. E., & Visscher, P. T. (2014). 10.8 - Anaerobic Metabolism: Linkages to Trace Gases and Aerobic Processes. In H. D. Holland & K. K. Turekian (Eds.), *Treatise on Geochemistry (Second Edition)* (pp. 273–359). Elsevier. https://doi.org/10.1016/B978-0-08-095975-7.00808-1

Moseman-Valtierra, S., Gonzalez, R., Kroeger, K. D., Tang, J., Chao, W. C., Crusius, J., Bratton, J., Green, A., & Shelton, J. (2011). Short-term nitrogen additions can shift a coastal wetland from a sink to a source of N2O. *Atmospheric Environment*, *45*(26), 4390–4397. https://doi.org/10.1016/j.atmosenv.2011.05.046

Nelson, S. S., Yonge, D. R., & Barber, M. E. (2009). Effects of Road Salts on Heavy Metal Mobility in Two Eastern Washington Soils. *Journal of Environmental Engineering*, *135*(7), 505–510. https://doi.org/10.1061/(ASCE)0733-9372(2009)135:7(505)

Neubauer, S. C., & Megonigal, J. P. (2021). Biogeochemistry of Wetland Carbon Preservation and Flux. In *Wetland Carbon and Environmental Management* (pp. 33–71). American Geophysical Union (AGU). https://doi.org/10.1002/9781119639305.ch3

Newton, B., Hunter, E., & Hunter, M. (2025). *PEDRO - Peatland Equipment Data Re-organizer* (Version 1.2.0) [Computer software]. https://github.com/BrianNewton/PEDRO

Oksanen, J., Simpson, G. L., Blanchet, F. G., Kindt, R., Legendre, P., Minchin, P. R., O'Hara, R. B., Solymos, P., Stevens, M. H. H., Szoecs, E., Wagner, H., Barbour, M., Bedward, M., Bolker, B., Borcard, D., Borman, T., Carvalho, G., Chirico, M., Caceres, M. D., … Weedon, J. (2025). *vegan: Community Ecology Package* (Version 2.7-2) [Computer software]. https://cran.r-project.org/web/packages/vegan/index.html

Ontario Ministry of the Environment. (2003). *Stormwater Management Planning and Design Manual* (Nos. 0-7794-2969–9). Ontario Ministry of the Environment. https://www.ontario.ca/document/stormwater-management-planning-and-design-manual-0

Ontario Ministry of the Environment. (2016a, April 5). *Policy Review of Municipal Stormwater Management in the Light of Climate Change*. http://www.ontario.ca/page/policy-review-municipal-stormwater-management-light-climate-change

Ontario Ministry of the Environment. (2016b, May 6). *Understanding Stormwater Management: An Introduction to Stormwater Management Planning and Design*. http://www.ontario.ca/page/understanding-stormwater-management-introduction-stormwater-management-planning-and-design

Peacock, M., Audet, J., Jordan, S., Smeds, J., & Wallin, M. B. (2019). Greenhouse gas emissions from urban ponds are driven by nutrient status and hydrology. *Ecosphere*, *10*(3), e02643. https://doi.org/10.1002/ecs2.2643

Penfound, E., & Vaz, E. (2022). Analysis of 200 years of change in ontario wetland systems. *Applied Geography*, *138*, 102625. https://doi.org/10.1016/j.apgeog.2021.102625

Pinheiro, J., Bates, D., Saikat DebRoy, Sarkar, D., Heisterkamp, S., Ranke, J., & R Core Team. (2025). *nlme: Linear and Nonlinear Mixed Effects Models* (Version 3.1-168) [Computer software]. https://cran.r-project.org/web/packages/nlme/index.html

Pollock, J. & The Conversation. (2019, February 12). *Salt Doesn't Melt Ice-Here's How It Makes Winter Streets Safer*. Scientific American. https://www.scientificamerican.com/article/salt-doesnt-melt-ice-heres-how-it-makes-winter-streets-safer/

Prentice, I. C., Farquhar, G. D., Fasham, M. J. R., Goulden, M. L., Heimann, M., Jaramillo, V. J., Kheshgi, H. S., Quéré, C. L., Scholes, R. J., Wallace, D. W. R., Archer, D., Ashmore, M. R., Aumont, O., Baker, D., Battle, M., Bender, M., Bopp, L., Bousquet, P., Caldeira, K., … Yool, A. (2021). The carbon cycle and atmospheric carbon dioxide. *Climate Change*

2001: The Scientific Basis, Intergovernmental Panel on Climate Change, *74*(1). https://hal.science/hal-03333974v1

Price, J. S., Sutton, O. F., McCarter, C. P. R., Quinton, W. L., Waddington, J. M., Whittington, P. N., Strack, M., & Petrone, R. M. (2023). Advances in wetland hydrology: The Canadian contribution over 75 years. *Canadian Water Resources Journal / Revue Canadienne Des Ressources Hydriques*, *48*(4), 379–427. https://doi.org/10.1080/07011784.2023.2269137

Qiao, Z., Sun, R., Wu, Y., Hu, S., Liu, X., Chan, J., & Mi, X. (2020). Characteristics and metabolic pathway of the bacteria for heterotrophic nitrification and aerobic denitrification in aquatic ecosystems. *Environmental Research*, *191*, 110069. https://doi.org/10.1016/j.envres.2020.110069

R Core Team. (2023). *R: A Language and Environment for Statistical Computing* (Version R version 4.3.2 (2023-10-31 ucrt)) [Computer software]. R Foundation for Statistical Computing. https://www.R-project.org/

Radosavljevic, J., Slowinski, S., Shafii, M., Akbarzadeh, Z., Rezanezhad, F., Parsons, C. T., Withers, W., & Van Cappellen, P. (2022). Salinization as a driver of eutrophication symptoms in an urban lake (Lake Wilcox, Ontario, Canada). *Science of The Total Environment*, *846*, 157336. https://doi.org/10.1016/j.scitotenv.2022.157336

Ramsar Convention Secretariat. (2016). *An Introduction to the Convenetion on Wetlands* (No. 5th Edition; Ramsar Handbooks). https://www.ramsar.org/sites/default/files/documents/library/handbook1_5ed_introductiontoconvention_final_e.pdf

Ravishankara, A. R., Daniel, J. S., & Portmann, R. W. (2009). Nitrous Oxide (N_20): The Dominant Ozone-Depleting Substance Emitted in the 21st Century. *Science*, *326*(5949), 123–125.

Ray, N. E., & Holgerson, M. A. (2023). High Intra-Seasonal Variability in Greenhouse Gas Emissions From Temperate Constructed Ponds. *Geophysical Research Letters*, *50*(18). https://doi.org/10.1029/2023GL104235

Residential Development Impact Scorecard for the Environment. (2023). https://uwaterloo.ca/residential-development-impact-scorecard-environment/about-rise

Richardson, D. C., Holgerson, M. A., Farragher, M. J., Hoffman, K. K., King, K. B. S., Alfonso, M. B., Andersen, M. R., Cheruveil, K. S., Coleman, K. A., Farruggia, M. J., Fernandez, R. L., Hondula, K. L., López Moreira Mazacotte, G. A., Paul, K., Peierls, B. L., Rabaey, J. S., Sadro, S., Sánchez, M. L., Smyth, R. L., & Sweetman, J. N. (2022). A functional definition to distinguish ponds from lakes and wetlands. *Scientific Reports*, *12*(1), 10472. https://doi.org/10.1038/s41598-022-14569-0

Robertson, H., Hilton, G., Job, N., Kumar, R., Simpson, M., Aggestam, F., Aldred, M., Chacón, A., Costanza, R., Davidson, N., Field, C., Finlayson, C. M., Gandra, F., Gillis, L. G., Hernández-Blanco, M., Moritsch, M., Thornton, S., Wood, K., & Van 'T Hoff, V. (2025). *Global Wetland Outlook 2025: Valuing, conserving, restoring and financing wetlands* (First Edition). Convention on Wetlands. https://doi.org/10.69556/GWO-2025-eng

Ruane, D., Martin, J., Brooker, M., Bernal, B., Anderson, C., Nairn, R., & Mitsch, W. J. (2025). 29 years of carbon sequestration in two constructed riverine wetlands. *Ecological Engineering*, *210*, 107435. https://doi.org/10.1016/j.ecoleng.2024.107435

Schuler, M. S., & Relyea, R. A. (2018). A Review of the Combined Threats of Road Salts and Heavy Metals to Freshwater Systems. *BioScience*, *68*(5), 327–335.

Sibert, R. J., Koretsky, C. M., & Wyman, D. A. (2015). Cultural meromixis: Effects of road salt on the chemical stratification of an urban kettle lake. *Chemical Geology*, *395*, 126–137. https://doi.org/10.1016/j.chemgeo.2014.12.010

Snodgrass, J. W., Moore, J., Lev, S. M., Casey, R. E., Ownby, D. R., Flora, R. F., & Izzo, G. (2017). Influence of Modern Stormwater Management Practices on Transport of Road Salt to

Surface Waters. *Environmental Science & Technology*, *51*(8), 4165–4172. https://doi.org/10.1021/acs.est.6b03107

Sorrell, B. K., & Boon, P. I. (1994). Convective gas flow in *Eleocharis sphacelata* R. Br.: Methane transport and release from wetlands. *Aquatic Botany*, *47*(3), 197–212. https://doi.org/10.1016/0304-3770(94)90053-1

Steele, M. K., & Aitkenhead-Peterson, J. A. (2013). Salt impacts on organic carbon and nitrogen leaching from senesced vegetation. *Biogeochemistry*, *112*, 245–259.

Stone, M., Emelko, M., Marsalek, Pricce, J., Rudolph, D., Saini, & Tighe. (2010). *Assessing the Efficacy of Current Road Salt Management Programs*. University of Waterloo, National Water Research Institute.

Szklarek, S., Górecka, A., & Wojtal-Frankiewicz, A. (2022). The effects of road salt on freshwater ecosystems and solutions for mitigating chloride pollution—A review. *Science of The Total Environment*, *805*, 150289. https://doi.org/10.1016/j.scitotenv.2021.150289

Thirimanne, H. D. T. D. (2025). *Erosion Risk Modelling: An Improved Screening Tool for Urban Watershed Management* [Univeristy of Waterloo]. https://hdl.handle.net/10012/21296

U.S. Geological Survey. (2021, July 22). *Brackish Groundwater Assessment | U.S. Geological Survey*. https://www.usgs.gov/mission-areas/water-resources/science/brackish-groundwater-assessment

Venetz, J., Żygadłowska, O. M., Dotsios, N., Wallenius, A. J., van Helmond, N. A. G. M., Lenstra, W. K., Klomp, R., Slomp, C. P., Jetten, M. S. M., & Veraart, A. J. (2024). Seasonal dynamics of the microbial methane filter in the water column of a eutrophic coastal basin. *FEMS Microbiology Ecology*, *100*(3). Scopus. https://doi.org/10.1093/femsec/fiae007

Villa, J. A., Ju, Y., Stephen, T., Rey-Sanchez, C., Wrighton, K. C., & Bohrer, G. (2020). Plant-mediated methane transport in emergent and floating-leaved species of a temperate freshwater mineral-soil wetland. *Limnology and Oceanography*, *65*(7), 1635–1650. https://doi.org/10.1002/lno.11467

Warren, F. J., & Lulham, N. (Eds.). (2021). *Canada in a Changing Climate: National Issues Report*. Government of Canada.

Wickham, H., Pedersen, T. L., & Seidel, D. (2025). *scales: Scale Functions for Visualization* (Version R package version 1.4.0) [Computer software]. https://scales.r-lib.org/

Winslow, L., Read, J., Woolway, R., Brentrup, J., Leach, T., Zwart, J., Albers, S., & Collinge, D. (2019). *rLakeAnalyzer: Lake Physics Tools* (Version 1.11.4.1) [Computer software]. https://cran.r-project.org/web/packages/rLakeAnalyzer/index.html

Withanage, A. (2025). *Greenhouse gas fluxes from stormwater ponds and urban wetlands in southern Ontario* [Manuscript, Univeristy of Waterloo]. https://dspacemainprd01.lib.uwaterloo.ca/server/api/core/bitstreams/e601d570-6864-45ef-809f-a46b972bc879/content

YSI Environmental. (2005). *Environmental Dissolved Oxygen Values Above 100% Air Saturation*.

Zhang, Z., & Furman, A. (2021). Soil redox dynamics under dynamic hydrologic regimes—A review. *Science of The Total Environment*, *763*, 143026. https://doi.org/10.1016/j.scitotenv.2020.143026

Żygadłowska, O. M., Venetz, J., Lenstra, W. K., van Helmond, N. A. G. M., Klomp, R., Röckmann, T., Veraart, A. J., Jetten, M. S. M., & Slomp, C. P. (2024). Ebullition drives high methane emissions from a eutrophic coastal basin. *Geochimica et Cosmochimica Acta*, *384*, 1–13. https://doi.org/10.1016/j.gca.2024.08.028

Appendix A: Chapter 2 Supplemental Figures & Tables

Figures

Site Maps

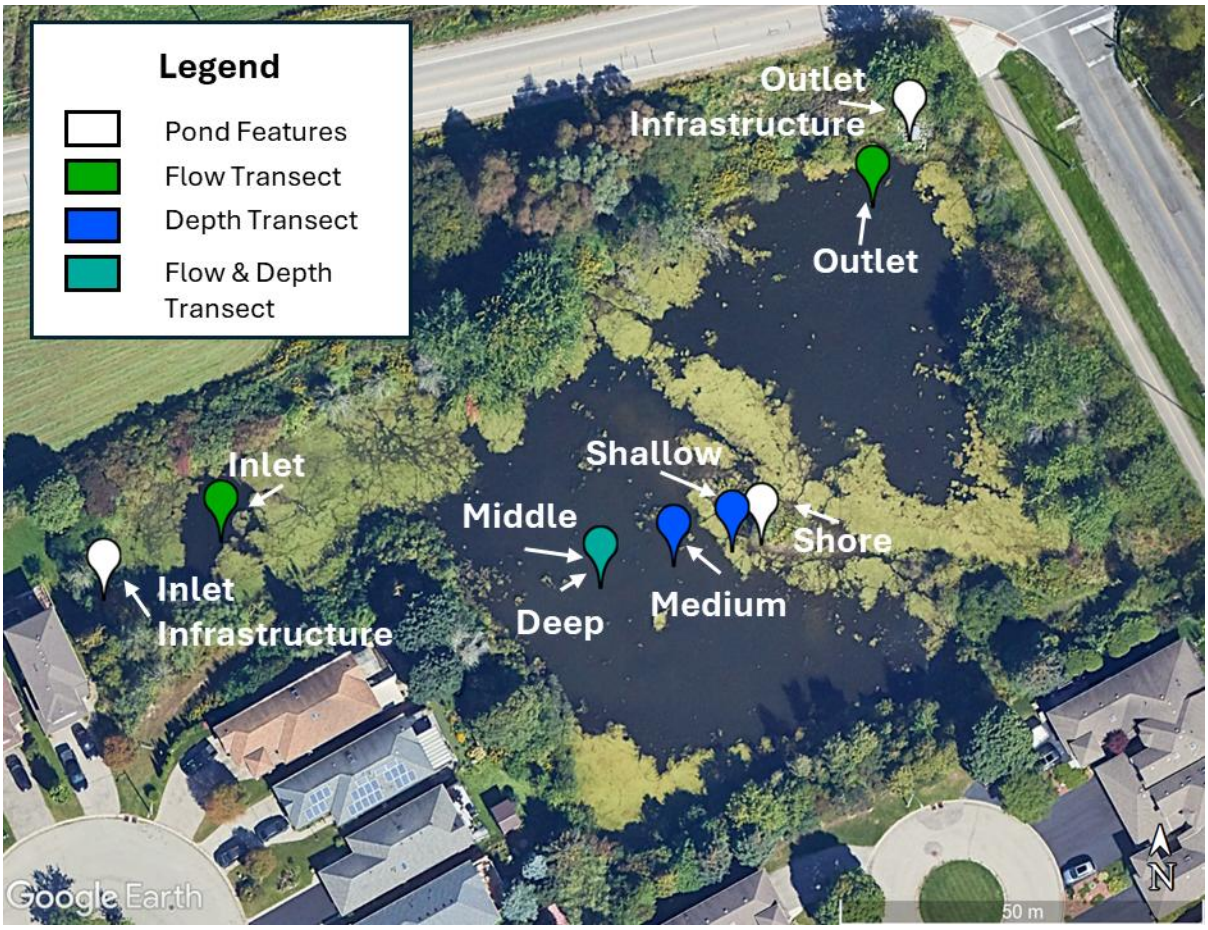


Figure A.1 Site Selection – Shallow & Low Salt Pond: Water Quality Sampling Locations

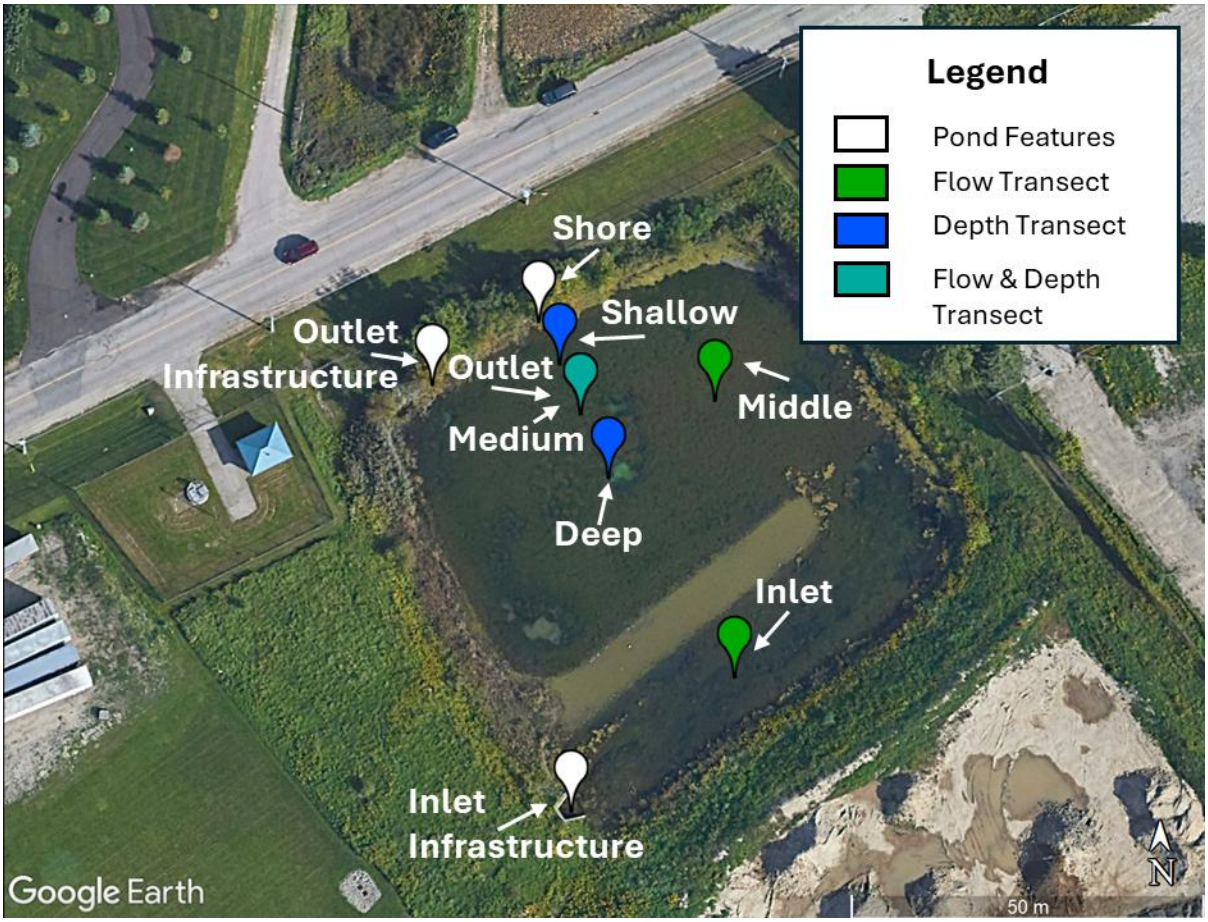


Figure A.2 Site Selection - Shallow & High Salt Pond: Water Quality Sampling Locations

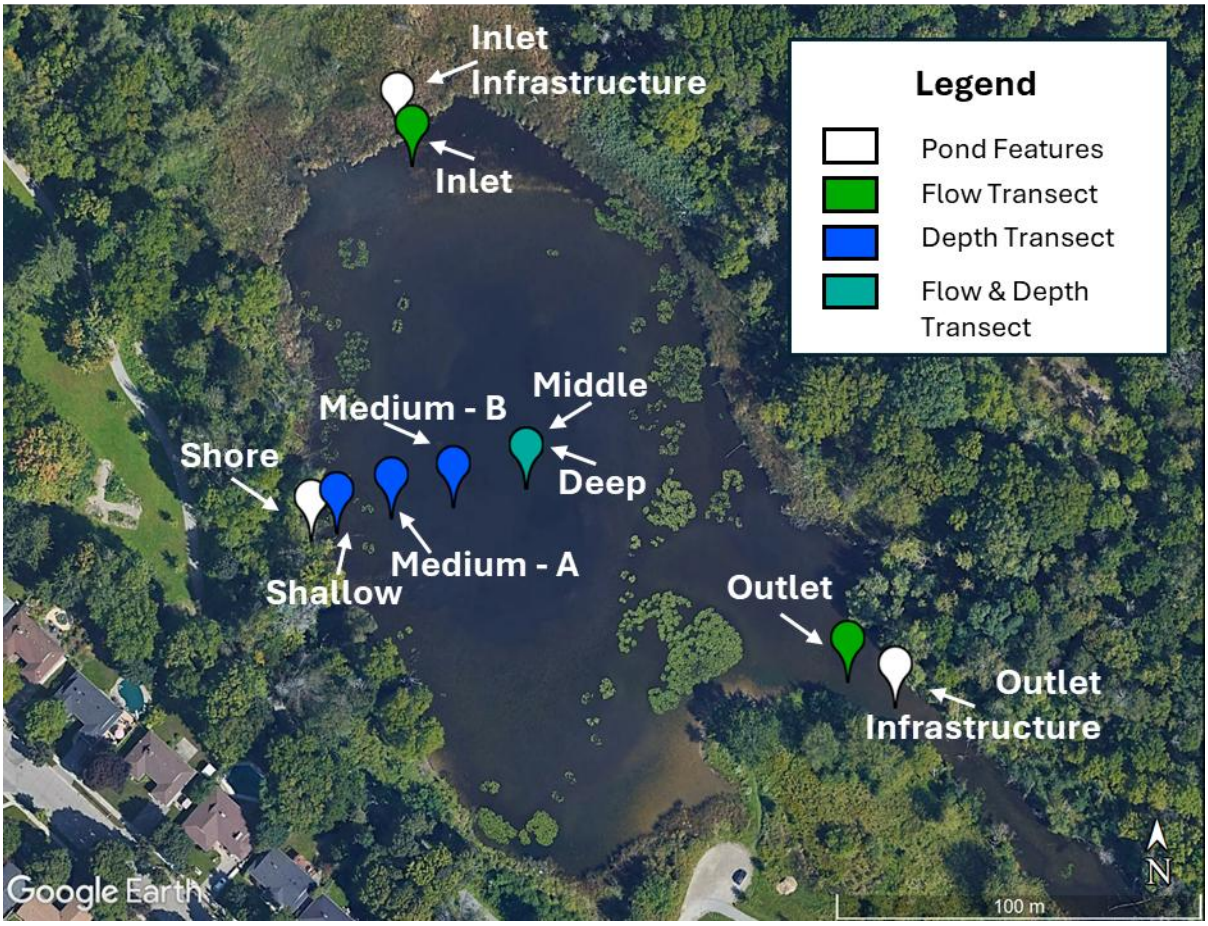


Figure A.3 Site Selection - Deep & High Salt Pond: Water Quality Sampling Locations

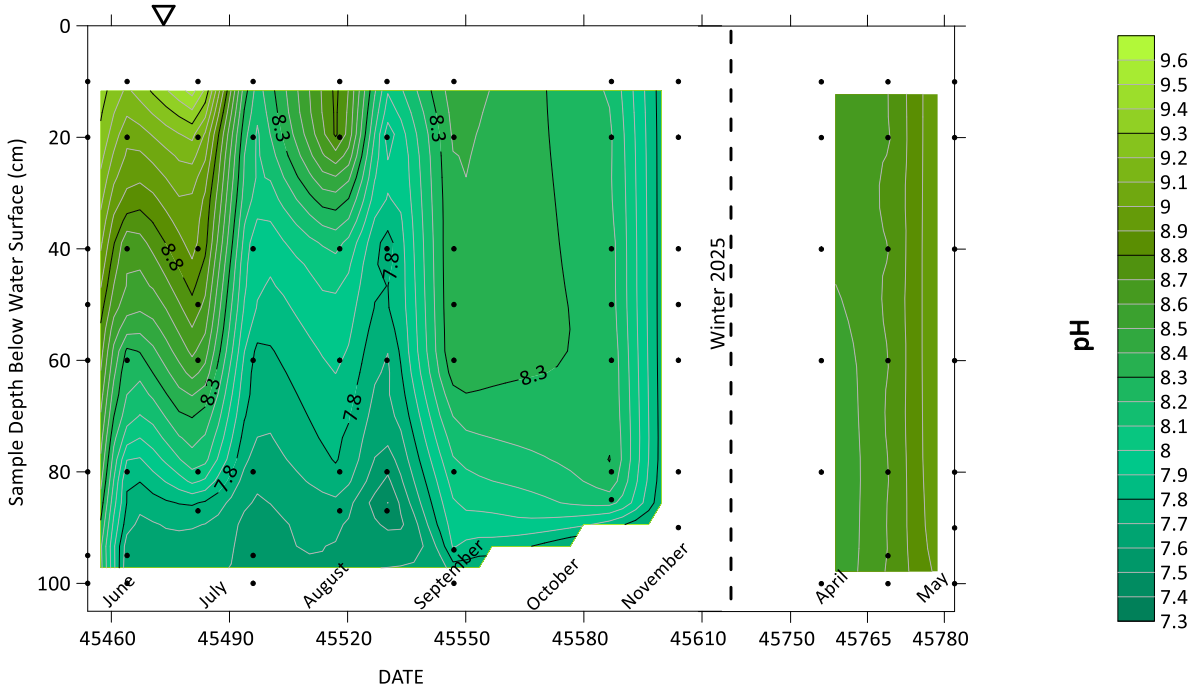


Figure A.4 Shallow & Low Salt – Deepest Location Time Series pH

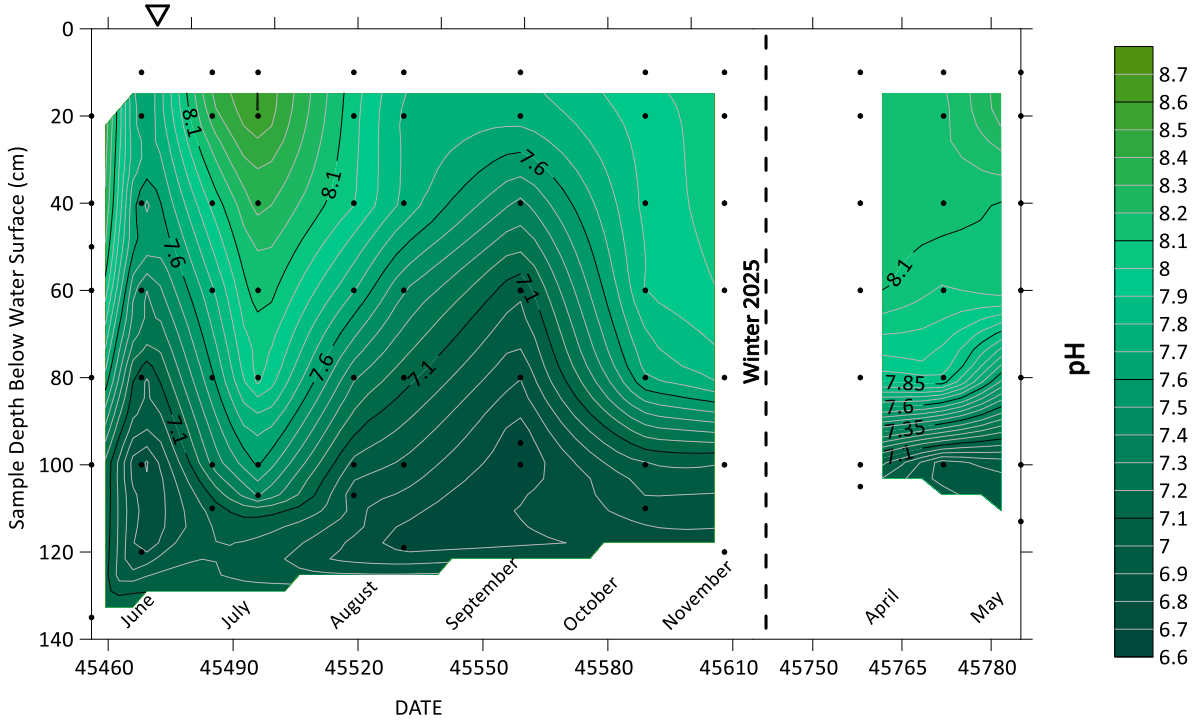


Figure A.5 Shallow & High Salt – Deepest Location Time Series pH

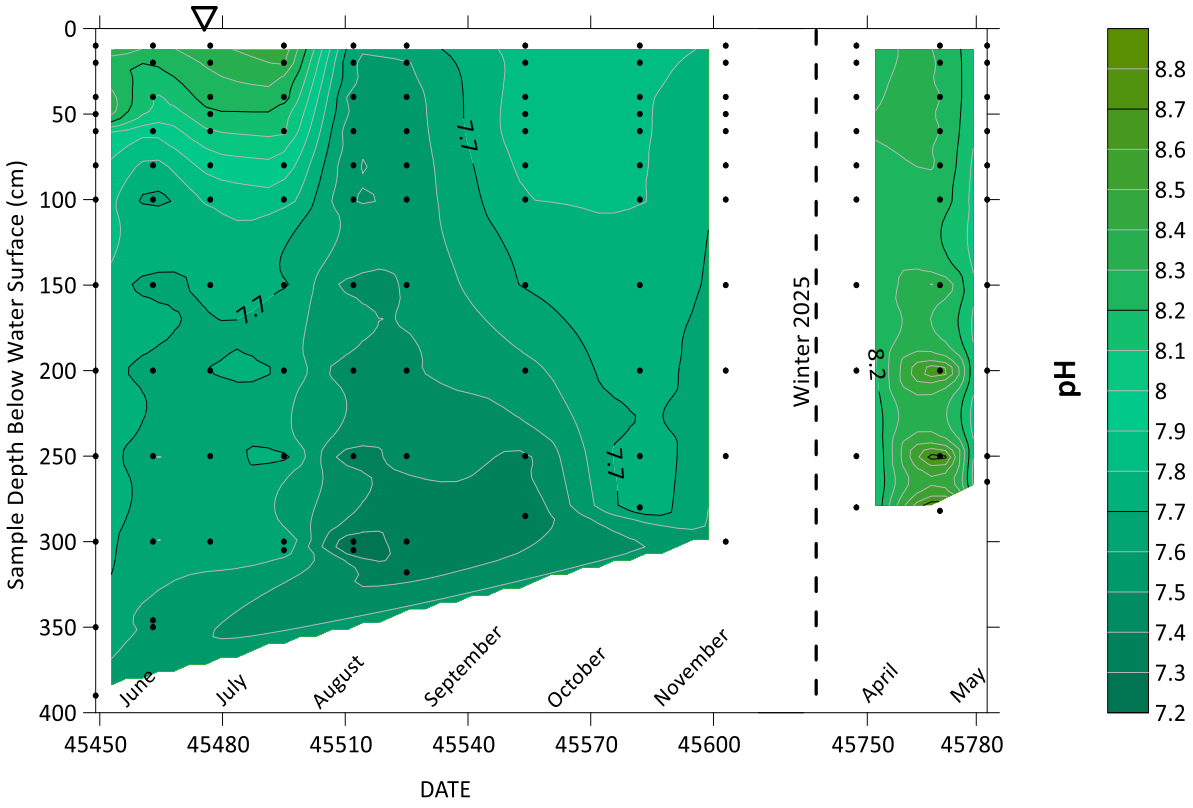


Figure A.6 Deep & Low Salt – Deepest Location Time Series pH

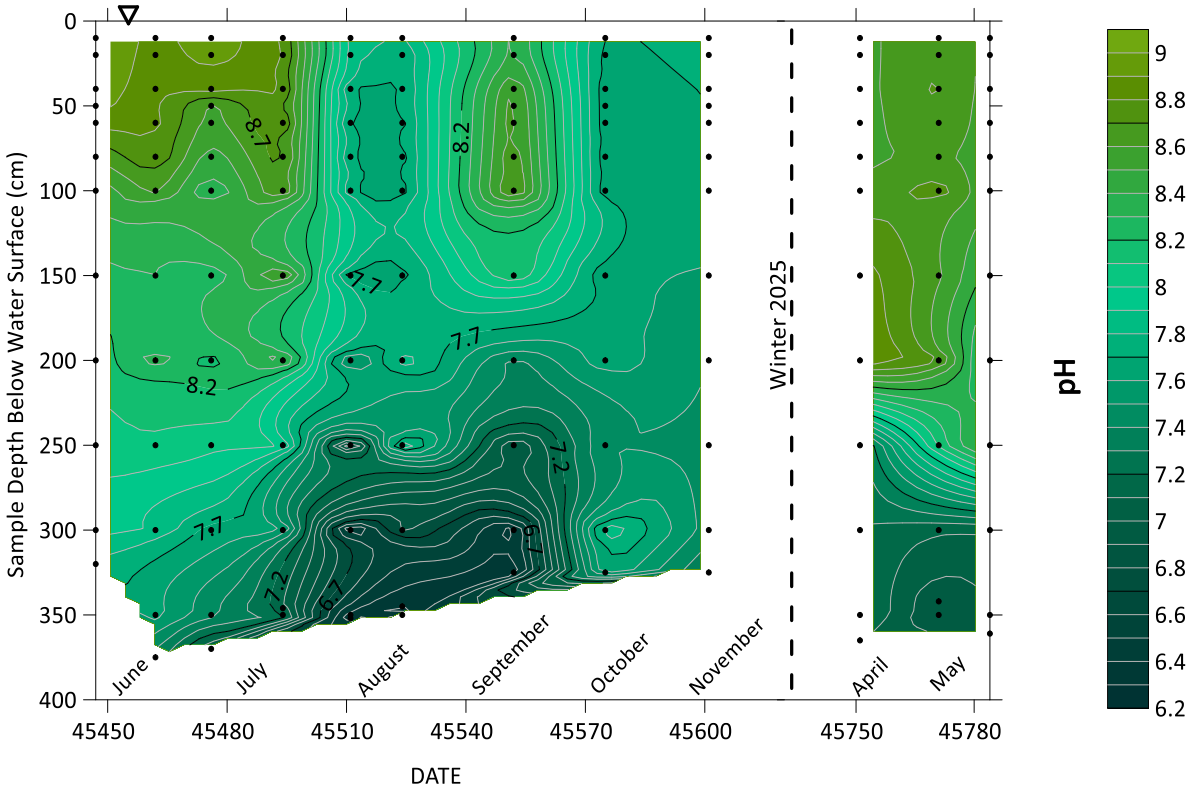
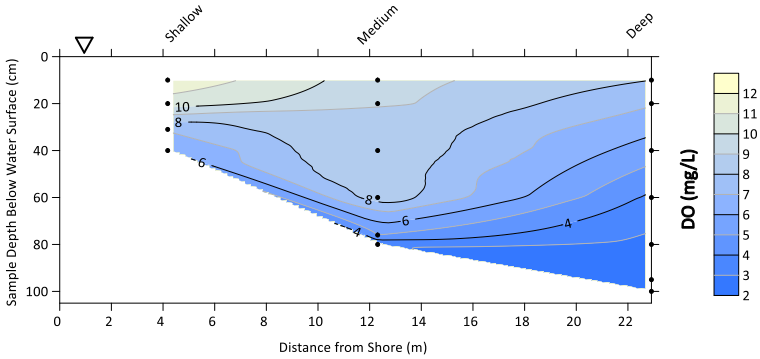


Figure A.7 Deep & High Salt - Deepest Location Time Series pH



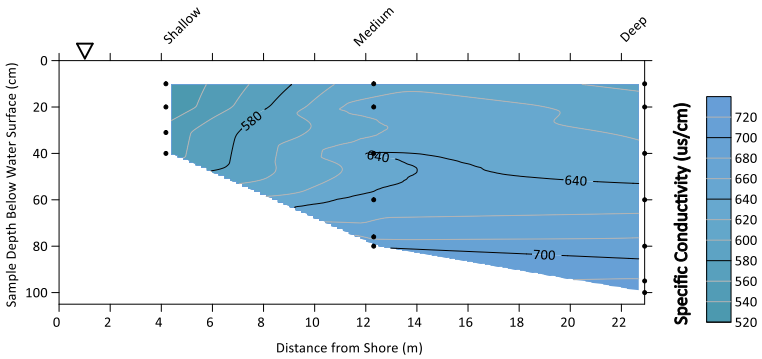
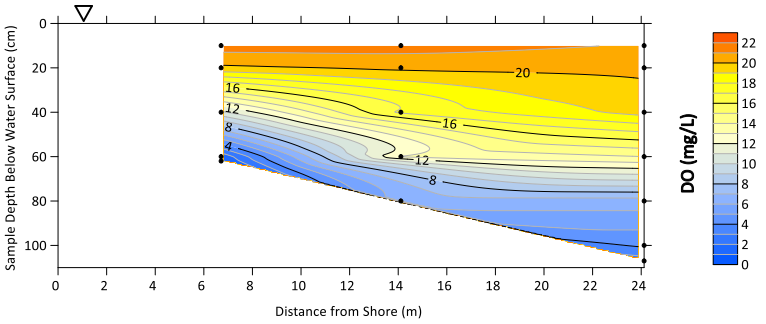


Figure A.8 Shallow & Low Salt Pond



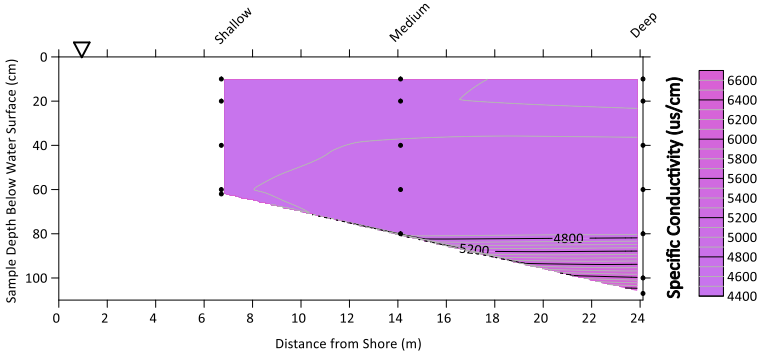
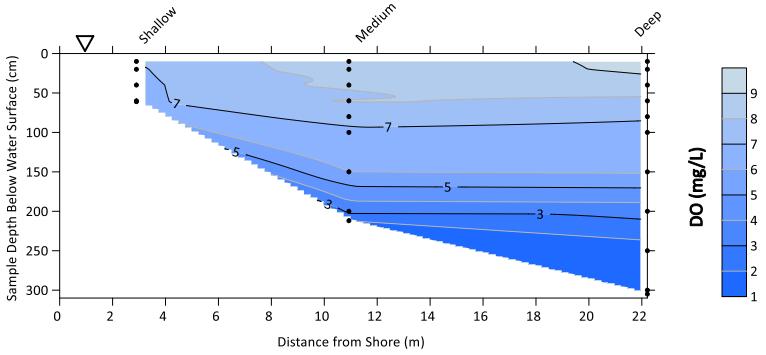


Figure A.9 Shallow & High Salt Pond



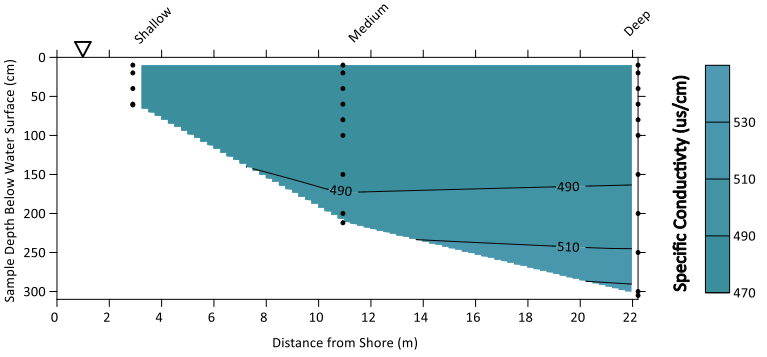
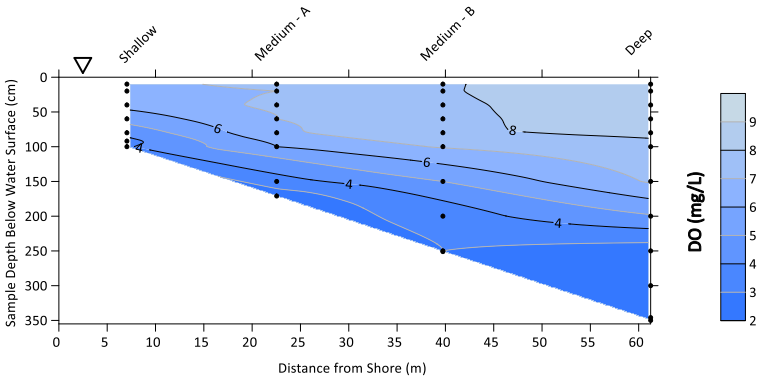


Figure A.10 Deep & Low Salt Pond



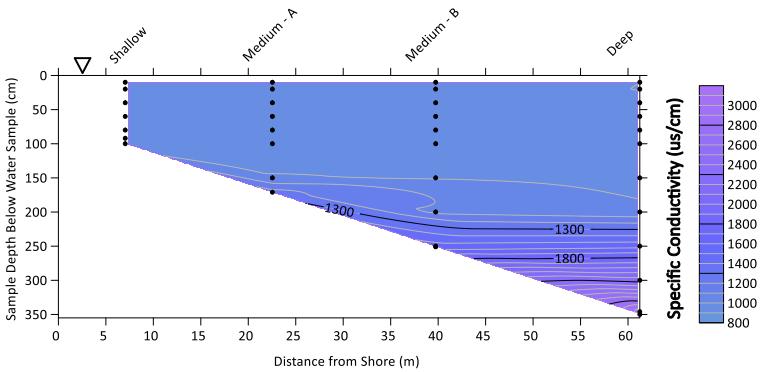
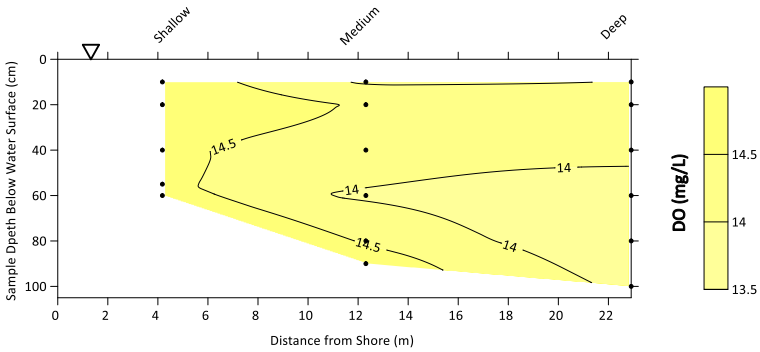


Figure A.11 Deep & High Salt Pond



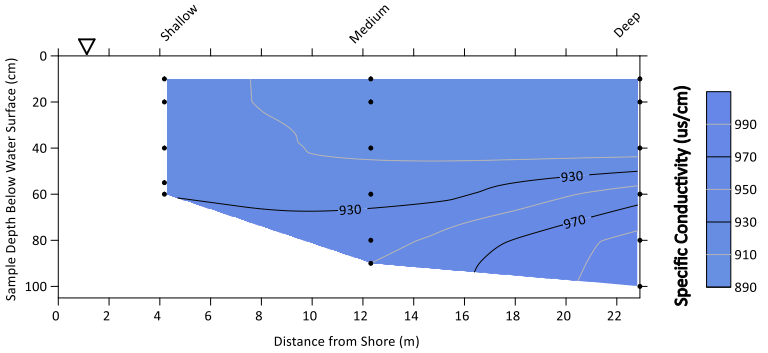
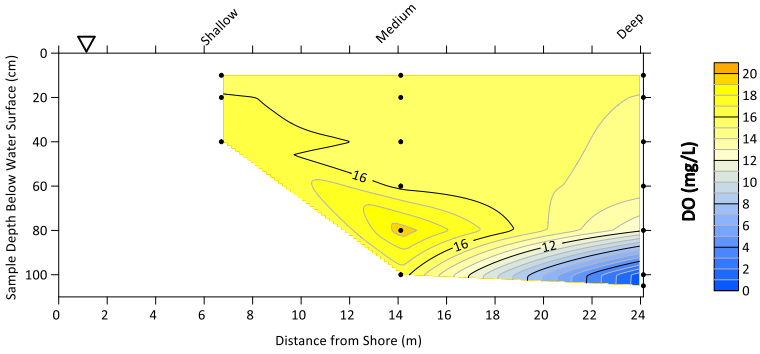


Figure A.12 Shallow & Low Salt Pond



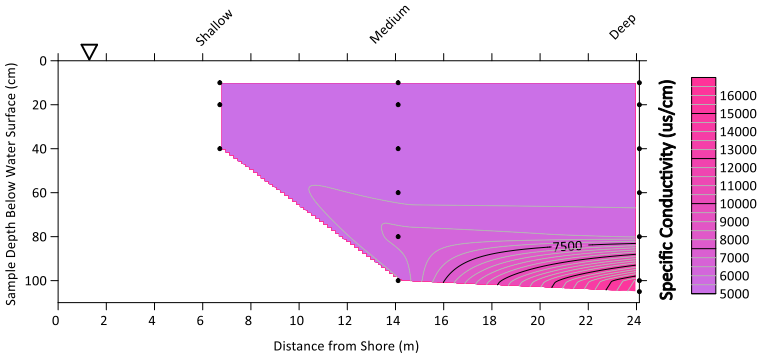
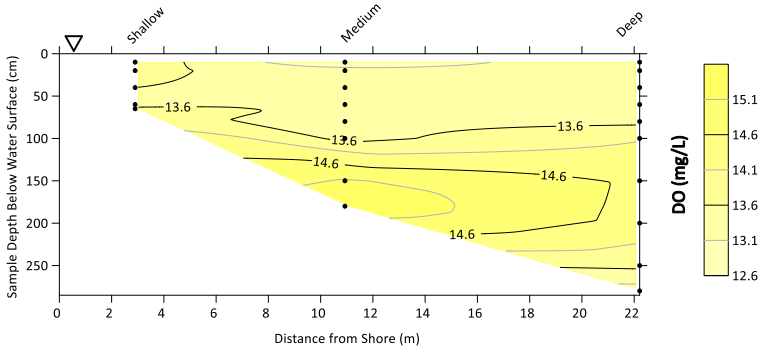


Figure A.13 Shallow & High Salt Pond



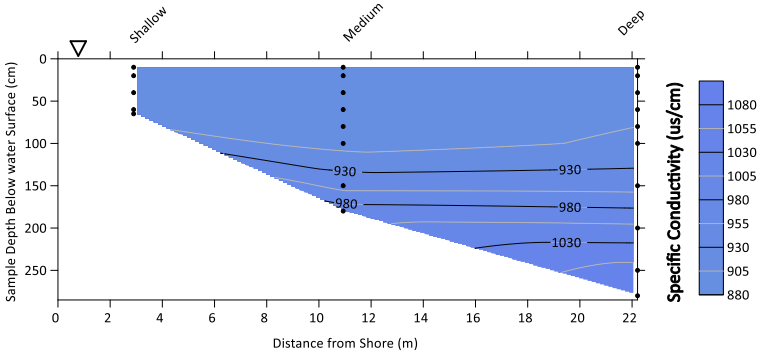
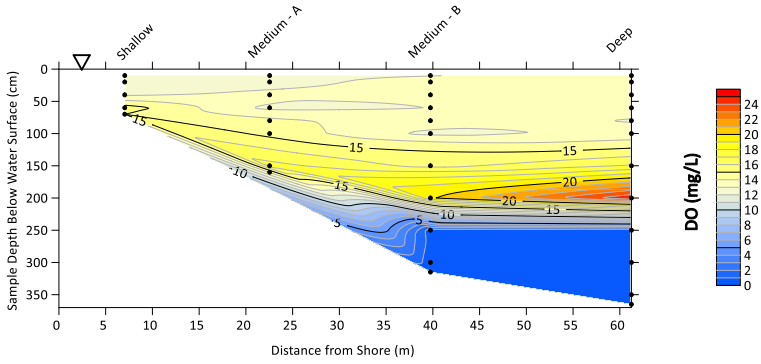


Figure A.14 Deep & Low Salt Pond



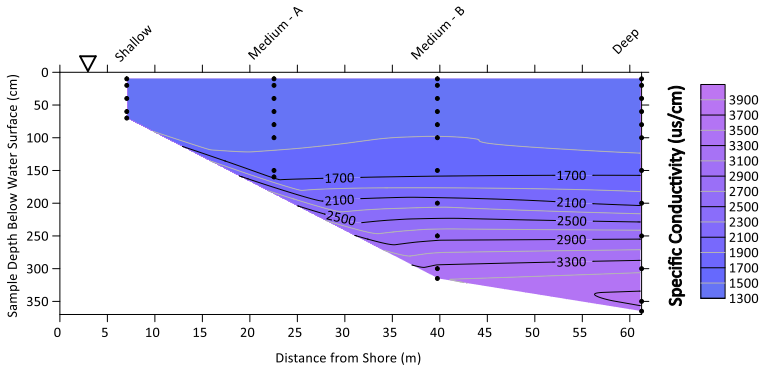


Figure A.15 Deep & High Salt Pond

Tables

Table A.1 Water quality sampling depths for the GS and NGS sampling events

Water Quality Parameter	Growing Season				Non - Growing Season			
	Shallow & Low Salt	Shallow & High Salt	Deep & Low Salt	Deep & High Salt	Shallow & Low Salt	Shallow & High Salt	Deep & Low Salt	Deep & High Salt
Temp	20, 40, 60, 10a	20, 40, 60, 10a	20, 40, 60, 80, 100, 150, 200, 250, 10a	20, 40, 60, 80, 100, 150, 200, 250, 300, 10a	20, 40, 60, 10a	20, 40, 60, 10a	20, 40, 60, 80, 100, 150, 200, 250, 10a	20, 40, 60, 80, 100, 150, 200, 250, 300, 10a
pH	20, 40, 60, 10a	20, 40, 60, 10a	20, 40, 60, 80, 100, 150, 200, 250, 10a	20, 40, 60, 80, 100, 150, 200, 250, 300, 10a	20, 40, 60, 10a	20, 40, 60, 10a	20, 40, 60, 80, 100, 150, 200, 250, 10a	20, 40, 60, 80, 100, 150, 200, 250, 300, 10a
DO	20, 40, 60, 10a	20, 40, 60, 10a	20, 40, 60, 80, 100, 150, 200, 250, 10a	20, 40, 60, 80, 100, 150, 200, 250, 300, 10a	20, 40, 60, 10a	20, 40, 60, 10a	20, 40, 60, 80, 100, 150, 200, 250, 10a	20, 40, 60, 80, 100, 150, 200, 250, 300, 10a
Cond	20, 40, 60, 10a	20, 40, 60, 10a	20, 40, 60, 80, 100, 150, 200, 250, 10a	20, 40, 60, 80, 100, 150, 200, 250, 300, 10a	20, 40, 60, 10a	20, 40, 60, 10a	20, 40, 60, 80, 100, 150, 200, 250, 10a	20, 40, 60, 80, 100, 150, 200, 250, 300, 10a
Fluoride mg/L	NA	NA	NA	NA	20, 40, 60, 10a	20, 40, 60, 10a	20, 40, 60, 80, 100, 150, 200, 250, 10a	20, 40, 60, 80, 100, 150, 200, 250, 300, 10a
Chloride mg/L	20, 40, 60, 10a	20, 40, 60, 10a	20, 40, 60, 80, 100, 150, 200, 250, 10a	20, 40, 60, 80, 100, 150, 200, 250, 300, 10a	20, 40, 60, 10a	20, 40, 60, 10a	20, 40, 60, 80, 100, 150, 200, 250, 10a	20, 40, 60, 80, 100, 150, 200, 250, 300, 10a
Nitrite mg/L	20, 40, 60, 10a	20, 40, 60, 10a	20, 40, 60, 80, 100, 150, 200, 250, 10a	20, 40, 60, 80, 100, 150, 200, 250, 300, 10a	20, 40, 60, 10a	20, 40, 60, 10a	20, 40, 60, 80, 100, 150, 200, 250, 10a	20, 40, 60, 80, 100, 150, 200, 250, 300, 10a
Bromide mg/L	20, 40, 60, 10a	20, 40, 60, 10a	20, 40, 60, 80, 100, 150, 200, 250, 10a	20, 40, 60, 80, 100, 150, 200, 250, 300, 10a	20, 40, 60, 10a	20, 40, 60, 10a	20, 40, 60, 80, 100, 150, 200, 250, 10a	20, 40, 60, 80, 100, 150, 200, 250, 300, 10a
Nitrate mg/L	20, 40, 60, 10a	20, 40, 60, 10a	20, 40, 60, 80, 100, 150, 200, 250, 10a	20, 40, 60, 80, 100, 150, 200, 250, 300, 10a	20, 40, 60, 10a	20, 40, 60, 10a	20, 40, 60, 80, 100, 150, 200, 250, 10a	20, 40, 60, 80, 100, 150, 200, 250, 300, 10a
Sulphate mg/L	20, 40, 60, 10a	20, 40, 60, 10a	20, 40, 60, 80, 100, 150, 200, 250, 10a	20, 40, 60, 80, 100, 150, 200, 250, 300, 10a	20, 40, 60, 10a	20, 40, 60, 10a	20, 40, 60, 80, 100, 150, 200, 250, 10a	20, 40, 60, 80, 100, 150, 200, 250, 300, 10a
Phosphate mg/L	20, 40, 60, 10a	20, 40, 60, 10a	20, 40, 60, 80, 100, 150, 200, 250, 10a	20, 40, 60, 80, 100, 150, 200, 250, 300, 10a	20, 40, 60, 10a	20, 40, 60, 10a	20, 40, 60, 80, 100, 150, 200, 250, 10a	20, 40, 60, 80, 100, 150, 200, 250, 300, 10a
Aluminum mg/L	NA	NA	NA	NA	20, 40, 10a	20, 40, 10a	40, 100, 200, 10a	40, 100, 200, 300, 10a
Calcium mg/L	40, 10a	40, 10a	40, 10a	40, 10a	20, 40, 10a	20, 40, 10a	40, 100, 200, 10a	40, 100, 200, 300, 10a
Iron mg/L	40, 10a	40, 10a	40, 10a	40, 10a	20, 40, 10a	20, 40, 10a	40, 100, 200, 10a	40, 100, 200, 300, 10a
Potassium mg/L	NA	NA	NA	NA	20, 40, 10a	20, 40, 10a	40, 100, 200, 10a	40, 100, 200, 300, 10a
Magnesium mg/L	NA	NA	NA	NA	20, 40, 10a	20, 40, 10a	40, 100, 200, 10a	40, 100, 200, 300, 10a
Manganese mg/L	40, 10a	40, 10a	40, 10a	40, 10a	20, 40, 10a	20, 40, 10a	40, 100, 200, 10a	40, 100, 200, 300, 10a
Sodium mg/L	40, 10a	40, 10a	40, 10a	40, 10a	20, 40, 10a	20, 40, 10a	40, 100, 200, 10a	40, 100, 200, 300, 10a
Phosphorus mg/L	NA	NA	NA	NA	20, 40, 10a	20, 40, 10a	40, 100, 200, 10a	40, 100, 200, 300, 10a
Sulfur mg/L	40, 10a	40, 10a	40, 10a	40, 10a	20, 40, 10a	20, 40, 10a	40, 100, 200, 10a	40, 100, 200, 300, 10a

Silicon mg/L	NA	NA	NA	NA	20, 40, 10a	20, 40, 10a	40, 100, 200, 10a	40, 100, 200, 300, 10a
NH4 ug N/L	NA	NA	NA	NA	20, 40, 60, 10a	20, 40, 60, 10a	40, 100, 200, 10a	40, 100, 200, 300, 10a
Fe (II) (umol/L)	20, 40, 60, 10a	20, 40, 60, 10a	20, 40, 60, 80, 100, 150, 200, 250, 10a	20, 40, 60, 80, 100, 150, 200, 250, 300, 10a	20, 40, 60, 10a	20, 40, 60, 10a	40, 100, 200, 10a	40, 100, 200, 300, 10a
Dissolved CH4 mol/L	20, 40, 60, 10a	20, 40, 60, 10a	20, 40, 60, 80, 100, 150, 200, 250, 10a	20, 40, 60, 80, 100, 150, 200, 250, 300, 10a	20, 40, 60, 10a	20, 40, 60, 10a	20, 40, 60, 80, 100, 150, 200, 250, 10a	20, 40, 60, 80, 100, 150, 200, 250, 300, 10a

Table A.2 MDL of Water Quality Sampling Analysis

Fluoride mg/L	Chloride mg/L	Nitrite mg/L	Bromide mg/L	Nitrate mg/L	Sulphate mg/L	Phosphate mg/L	Aluminium mg/L	Calcium mg/L	Iron mg/L
0.011	0.046	0.052	0.093	0.091	0.64	0.077	0.0057	0.009	0.0062
0.0055	0.023	0.026	0.0465	0.0455	0.32	0.0385	0.00285	0.0045	0.0031

Potassium mg/L	Magnesium mg/L	Manganese mg/L	Sodium mg/L	Phosphorus mg/L	Sulfur mg/L	Silicon mg/L	NH4 ug N/L	Fe (II) (umol/L)
0.6059	0.0067	0.0017	0.0907	0.0033	0.0389	0.01	1.083	0.028
0.30295	0.00335	0.00085	0.04535	0.00165	0.01945	0.005	0.5415	0.014

Table A.3 Environmental conditions in the ponds at the flow and depth transects

Parameter	Depth	Deep & Low Salt			Deep & Low Salt			Deep & Low Salt			Deep & Low Salt			Deep & Low Salt		
		Inlet			Middle			Outlet			Medium			Shallow		
		Min Value	Max Value	Mean (SD) Value	Min Value	Max Value	Mean (SD) Value	Min Value	Max Value	Mean (SD) Value	Min Value	Max Value	Mean (SD) Value	Min Value	Max Value	Mean (SD) Value
Water Column Depth (m)		1.37	2.30	1.82 (0.21)	1.02	2.40	1.37 (0.43)	2.75	4.00	3.17 (0.34)	1.70	2.90	2.19 (0.32)	0.49	1.25	0.76 (0.2)
Temperature (°C)	10 cm	5.80	23.20	17.18 (6.03)	6.00	23.90	17.89 (6.06)	6.60	24.20	18.28 (5.95)	6.70	25.20	18.83 (6.05)	6.90	24.80	19.13 (6.1)
	10 cm as	6.50	17.80	13.83 (3.77)	5.50	22.70	16.61 (5.63)	6.20	21.60	15.23 (5.23)	6.20	22.70	16.13 (5.35)	6.70	23.50	17.63 (5.52)
DO (mg/L)	10 cm	5.20	13.80	7.51 (2.67)	4.70	13.48	7.41 (2.49)	4.50	13.60	7.85 (2.76)	4.00	12.61	7.71 (2.41)	4.70	13.90	7.76 (2.64)
	10 cm as	0.00	8.47	2.45 (2.73)	3.70	13.34	6.57 (2.97)	0.30	19.55	4.61 (5.8)	2.00	15.47	6.37 (4.25)	4.30	13.71	7.67 (3.1)
pH	10 cm	7.63	8.64	8.15 (0.37)	7.53	8.52	8.04 (0.3)	7.62	8.54	8.09 (0.33)	7.53	8.66	8.11 (0.35)	7.60	8.55	8.12 (0.34)
	10 cm as	7.19	8.00	7.53 (0.25)	7.46	8.28	7.73 (0.26)	7.16	9.00	7.68 (0.46)	7.38	8.66	7.77 (0.35)	7.50	8.40	7.98 (0.31)
EC (us/cm)	10 cm	541.00	1127.00	852.17 (186.78)	501.00	1137.00	848.17 (202.15)	476.10	1137.00	845.84 (206.33)	483.90	1142.00	847.41 (206.8)	490.10	1205.00	855.68 (217.85)
	10 cm as	755.00	1154.00	952.17 (106.48)	515.60	1152.00	857.72 (197.63)	537.00	1139.00	871.92 (205.74)	502.10	1140.00	854.76 (207.99)	477.20	1146.00	844.35 (207.42)

Parameter	Depth	Shallow & High Salt			Shallow & High Salt			Shallow & High Salt			Shallow & High Salt			Shallow & High Salt		
		Inlet			Middle			Outlet			Medium			Shallow		
		Min Value	Max Value	Mean (SD) Value	Min Value	Max Value	Mean (SD) Value	Min Value	Max Value	Mean (SD) Value	Min Value	Max Value	Mean (SD) Value	Min Value	Max Value	Mean (SD) Value
Water Column Depth (m)		0.90	1.05	0.97 (0.04)	0.80	1.15	0.89 (0.1)	1.05	1.45	1.22 (0.1)	0.70	1.15	0.93 (0.14)	0.50	0.78	0.64 (0.1)
Temperature (°C)	10 cm	5.80	22.70	15.34 (5.44)	5.80	26.80	17.07 (6.64)	6.50	27.60	17.45 (6.72)	6.80	28.20	17.95 (6.87)	7.40	28.80	18.23 (7.21)
	10 cm as	5.70	17.60	13.49 (4.1)	6.70	20.80	15.18 (4.82)	9.40	20.80	16.14 (3.9)	7.10	20.60	16.08 (4.65)	7.20	23.90	17.32 (6.2)
DO (mg/L)	10 cm	3.90	17.40	10.83 (3.74)	8.70	20.60	13.74 (3.77)	8.30	20.90	13.74 (3.72)	9.40	21.50	14.07 (3.4)	10.00	21.50	14.83 (3.26)
	10 cm as	0.00	18.55	7.1 (5.95)	1.20	15.82	7.57 (4.74)	0.00	8.09	2.34 (2.24)	1.10	16.74	6.97 (5.58)	0.80	20.78	11.56 (5.91)
pH	10 cm	7.51	8.54	7.99 (0.32)	7.68	8.76	8.13 (0.36)	7.51	8.67	8.13 (0.35)	7.63	8.69	8.17 (0.33)	7.59	8.99	8.35 (0.38)
	10 cm as	6.80	8.33	7.67 (0.46)	6.92	8.29	7.6 (0.43)	6.63	7.41	6.91 (0.24)	6.93	8.14	7.54 (0.41)	7.51	8.60	7.99 (0.36)
EC (us/cm)	10 cm	1850.00	5244.00	4212.75 (961.56)	2040.00	5246.00	4243.58 (872.1)	1852.00	5222.00	4178.25 (904.3)	1994.00	5218.00	4169.33 (879.9)	1985.00	5216.00	4241.09 (866.04)
	10 cm as	4758.00	5657.00	5031.5 (273.46)	3916.00	5495.00	4836.25 (378.18)	5488.00	16540.00	8673.83 (4042.88)	4559.00	6456.00	4981.83 (537.11)	3725.00	5230.00	4509.09 (413.74)

Parameter	Depth	Shallow & Low Salt			Shallow & Low Salt			Shallow & Low Salt			Shallow & Low Salt			Shallow & Low Salt		
		Inlet			Middle			Outlet			Medium			Shallow		
		Min Value	Max Value	Mean (SD) Value	Min Value	Max Value	Mean (SD) Value	Min Value	Max Value	Mean (SD) Value	Min Value	Max Value	Mean (SD) Value	Min Value	Max Value	Mean (SD) Value
Water Column Depth (m)		0.73	0.90	0.81 (0.05)	0.95	1.10	1.02 (0.04)	0.98	1.25	1.06 (0.07)	0.78	1.00	0.88 (0.06)	0.34	0.65	0.49 (0.09)
Temperature (°C)	10 cm	7.20	25.70	17.32 (5.95)	4.90	28.20	18.17 (7.24)	4.30	27.60	17.22 (6.72)	5.30	27.60	18.13 (6.91)	5.90	29.80	18.58 (7.1)
	10 cm as	6.80	22.40	16.18 (4.95)	6.00	20.80	15.92 (4.77)	4.30	20.20	15.53 (4.89)	6.00	21.80	16.17 (4.96)	6.20	24.20	16.83 (5.42)
DO (mg/L)	10 cm	2.50	18.25	8.33 (5.08)	4.70	17.15	11.19 (3.9)	4.90	16.29	10.5 (3.71)	5.00	17.28	10.88 (3.91)	5.70	18.32	11.3 (4.27)
	10 cm as	0.90	19.11	6.29 (6.04)	0.50	17.36	7 (5.78)	0.90	20.49	6.95 (6.56)	0.80	17.20	7.47 (5.99)	2.70	18.23	8.99 (5.25)
pH	10 cm	7.56	8.85	8.39 (0.44)	7.61	9.64	8.66 (0.61)	7.64	10.17	8.71 (0.74)	7.63	9.33	8.67 (0.5)	7.65	9.20	8.65 (0.41)
	10 cm as	7.31	8.82	7.89 (0.5)	7.36	8.98	8.01 (0.55)	7.28	8.97	8.11 (0.59)	7.43	9.19	8.11 (0.59)	7.63	9.20	8.4 (0.52)
EC (us/cm)	10 cm	249.20	995.00	725.73 (213.89)	521.00	967.00	747.33 (148.69)	224.00	958.00	682.65 (207.58)	453.80	965.00	740.65 (158.02)	484.20	956.00	735.85 (163.67)
	10 cm as	401.10	1029.00	763.49 (185.49)	720.00	1002.00	830.83 (94.85)	460.90	955.00	720.55 (161.17)	624.00	962.00	791.08 (115.9)	504.80	953.00	750.27 (154.29)

Parameter	Depth	Deep & High Salt			Deep & High Salt			Deep & High Salt			Deep & High Salt			Deep & High Salt		
		Inlet			Middle			Outlet			Medium - B			Medium - A		
		Min Value	Max Value	Mean (SD) Value	Min Value	Max Value	Mean (SD) Value	Min Value	Max Value	Mean (SD) Value	Min Value	Max Value	Mean (SD) Value	Min Value	Max Value	Mean (SD) Value
Water Column Depth (m)		0.20	0.62	0.51 (0.1)	3.30	3.85	3.56 (0.18)	0.50	0.95	0.81 (0.12)	2.00	3.40	2.8 (0.37)	1.30	1.81	1.6 (0.15)
Temperature (°C)	10 cm	6.30	25.70	17.86 (6.32)	7.00	27.80	19.44 (6.32)	6.70	26.00	18.23 (6.17)	8.50	27.20	19.91 (5.86)	9.30	27.00	20.29 (5.66)
	10 cm as	6.80	25.60	17.49 (5.88)	4.30	17.00	12.07 (4.37)	6.60	26.20	17.76 (6.01)	4.30	21.20	14.56 (5.74)	5.10	22.90	17.31 (5.78)
DO (mg/L)	10 cm	3.40	11.85	7.18 (2.17)	5.20	13.27	9.07 (2.75)	3.10	11.93	7.72 (2.63)	5.50	13.10	9.27 (2.71)	6.30	12.85	8.89 (2.1)
	10 cm as	0.90	10.65	4.99 (3.06)	0.00	5.90	1.51 (1.87)	0.20	7.89	4.79 (2.68)	0.11	14.76	3.37 (3.94)	1.00	16.03	5.34 (4.98)
pH	10 cm	7.67	8.98	8.23 (0.4)	7.67	9.01	8.42 (0.51)	7.72	8.80	8.35 (0.33)	7.71	9.01	8.38 (0.45)	7.69	8.78	8.39 (0.36)
	10 cm as	6.95	8.42	7.84 (0.46)	6.27	7.77	7.02 (0.52)	7.03	8.33	7.93 (0.45)	6.46	7.83	7.27 (0.37)	7.06	8.66	7.73 (0.51)
EC (us/cm)	10 cm	994.00	1745.00	1421.42 (254.13)	900.00	1712.00	1375.75 (279.37)	869.00	1718.00	1360.42 (290.21)	919.00	1713.00	1373.42 (274.88)	912.00	1716.00	1377.67 (279.2)
	10 cm as	1020.00	1785.00	1467 (249.85)	1292.00	3641.00	2820.83 (868.11)	907.00	1713.00	1374.5 (286.06)	1154.00	3487.00	2092.17 (825.6)	1081.00	1812.00	1456.33 (272.5)

Parameter	Depth	Deep & High Salt		
		Shallow		
		Min Value	Max Value	Mean (SD) Value
Water Column Depth (m)		0.55	1.15	0.88 (0.17)
Temperature (°C)	10 cm	10.90	26.90	21.18 (5.55)
	10 cm as	8.20	26.10	18.92 (5.43)
DO (mg/L)	10 cm	6.70	14.50	10.41 (2.31)
	10 cm as	1.50	15.00	7.57 (3.81)
pH	10 cm	8.03	9.31	8.69 (0.36)
	10 cm as	7.57	8.82	8.21 (0.37)
EC (us/cm)	10 cm	924.00	1722.00	1372.25 (278.82)
	10 cm as	925.00	1723.00	1380.92 (275.69)

Table A.4 Water quality sampling results for the GS and NGS sampling events

Date	Site	Sample Depth (cm)	Pond Depth	Temp	pH	DO	Cond	Fluoride mg/L	Chloride mg/L	Nitrite mg/L	Bromide mg/L	Nitrate mg/L	Sulphate mg/L	Phosphate mg/L	Aluminum mg/L	Calcium mg/L	Iron mg/L	Potassium mg/L	Magnesium mg/L	Manganese mg/L	Sodium mg/L	Phosphorus mg/L	Sulfur mg/L	Silicon mg/L	NH4 ug N/L	Fe (II) (umol/L)	Dissolved CH4 mol/L	Sample Event
2024-07-21	Deep & High Salt	20	3.56	25.6	8.83	8.9	905	NA	200	0	0.338	0.17	3.36	0	NA	NA	NA	NA	NA	NA	NA	NA	NA	NA	NA	2.15	7.70E-06	GS
2024-07-21	Deep & High Salt	40	3.56	25.2	8.82	8.7	907	NA	201	0	0	0.235	2.76	0	NA	28	0.027	NA	NA	0.00237	131.9	NA	1.64	NA	NA	1.2	3.40E-06	GS
2024-07-21	Deep & High Salt	60	3.56	24.6	8.82	8.5	904	NA	200	0	0.423	0	2.78	0	NA	NA	NA	NA	NA	NA	NA	NA	NA	NA	NA	1.41	2.54E-06	GS
2024-07-21	Deep & High Salt	100	3.56	23.8	8.71	7.7	919	NA	206	0	0	0.422	2.47	0	NA	NA	NA	NA	NA	NA	NA	NA	NA	NA	NA	3.64	4.03E-06	GS
2024-07-21	Deep & High Salt	150	3.56	23.2	8.63	7.1	928	NA	212	0	0.34	0.217	2.29	0	NA	NA	NA	NA	NA	NA	NA	NA	NA	NA	NA	3.17	1.05E-06	GS
2024-07-21	Deep & High Salt	200	3.56	22.5	8.47	4.9	969	NA	235	0	0.322	0.2	2.78	0	NA	NA	NA	NA	NA	NA	NA	NA	NA	NA	NA	0.959	8.09E-05	GS
2024-07-21	Deep & High Salt	250	3.56	20.8	8.01	2.4	1439	NA	387	0	0.428	0.182	3.23	0	NA	NA	NA	NA	NA	NA	NA	NA	NA	NA	NA	2.63	0.00023	GS
2024-07-21	Deep & High Salt	300	3.56	18.9	7.62	2.1	1980	NA	581	0	0.565	0.17	0.32	0	NA	NA	NA	NA	NA	NA	NA	NA	NA	NA	NA	55.6	4.91E-05	GS
2024-07-21	Deep & High Salt	346	3.56	15.7	7.12	2.1	2528	NA	753	0	0.394	0.299	0.32	0.667	0.00285	92.815	5.5645	5.7795	16.117	12.0465	483.585	0.3725	0.01945	5.318	NA	140	0.000164	GS
2024-07-22	Deep & Low Salt	20	3.15	23	8.42	9.1	460.9	NA	56.8	0.026	0	0.218	9.56	0	NA	NA	NA	NA	NA	NA	NA	NA	NA	NA	NA	1.28	3.67E-06	GS
2024-07-22	Deep & Low Salt	40	3.15	22.4	8.26	8.8	457.6	NA	58.1	0.026	0.335	0.367	9.76	0	NA	47.4	0.026	NA	NA	0.0178	36.9	NA	3.54	NA	NA	2.25	2.08E-06	GS
2024-07-22	Deep & Low Salt	60	3.15	22.2	8.13	7.7	449.2	NA	55.7	0.026	0.349	0.188	9.16	0	NA	NA	NA	NA	NA	NA	NA	NA	NA	NA	NA	1.71	1.33E-06	GS
2024-07-22	Deep & Low Salt	100	3.15	21.8	7.87	6.4	444.5	NA	55.4	0.026	0.341	0.287	8.99	0	NA	NA	NA	NA	NA	NA	NA	NA	NA	NA	NA	0.746	6.71E-06	GS
2024-07-22	Deep & Low Salt	150	3.15	21.1	7.72	6.1	451.3	NA	56	0.026	0.329	0.26	9.27	0	NA	NA	NA	NA	NA	NA	NA	NA	NA	NA	NA	1.136	3.82E-07	GS
2024-07-22	Deep & Low Salt	200	3.15	20.5	7.7	3.4	452.6	NA	58.6	0.026	0.362	0.809	9.77	0	NA	NA	NA	NA	NA	NA	NA	NA	NA	NA	NA	1.152	1.14E-06	GS
2024-07-22	Deep & Low Salt	250	3.15	19.9	7.74	1.5	460.5	NA	61.4	0.026	0.33	0.56	10.1	0	NA	NA	NA	NA	NA	NA	NA	NA	NA	NA	NA	12.8	2.93E-06	GS
2024-07-22	Deep & Low Salt	305	3.15	19.2	7.66	1.1	476.7	NA	65.6	0	0.337	0.291	9.06	0	NA	53	0.309	NA	NA	0.464	41.4	NA	3.34	NA	NA	1.57	9.91E-05	GS
2024-07-23	Shallow & High Salt	20	1.17	27.5	8.61	20.2	4687	NA	1296	0	0.408	3.4	40.4	0	NA	NA	NA	NA	NA	NA	NA	NA	NA	NA	NA	0.634	3.66E-05	GS
2024-07-23	Shallow & High Salt	40	1.17	25.6	8.35	19.4	4568	NA	1308	0	0.402	5.86	42	0	0.07745	110.438	0.1872	6.3887	33.07	0.00085	975.38	0.158	12.03	1.1836	NA	0.1038	9.12E-06	GS
2024-07-23	Shallow & High Salt	60	1.17	20.9	8.19	14	4258	NA	1300	0.086	0.317	4.22	39	0	NA	NA	NA	NA	NA	NA	NA	NA	NA	NA	NA	0.474	6.12E-05	GS
2024-07-23	Shallow & High Salt	107	1.17	20.8	7.41	2.5	6056	NA	1860	0	0.486	0.471	33.9	0	0.00285	174.224	0.3132	6.8515	37.13	0.0282	1456.04	0.00165	9.692	16.267	NA	7.43	4.55E-05	GS
2024-07-23	Shallow & Low Salt	20	1.05	22.2	8.04	7.1	572	NA	85.7	0.026	0.374	0.603	9.15	0	NA	NA	NA	NA	NA	NA	NA	NA	NA	NA	NA	0.83	2.71E-05	GS
2024-07-23	Shallow & Low Salt	40	1.05	21.5	7.89	5.5	581	NA	90	0.059	0.406	2.39	9.69	0	NA	45.7	0.0289	NA	NA	0.0157	56.5	NA	3.54	NA	NA	0.55	4.49E-06	GS
2024-07-23	Shallow & Low Salt	60	1.05	21.2	7.74	3.8	600	NA	93.7	0.079	0.325	1.11	9.98	0	NA	NA	NA	NA	NA	NA	NA	NA	NA	NA	NA	0.308	2.97E-06	GS
2024-07-23	Shallow & Low Salt	95	1.05	20.8	7.51	2	662	NA	104	0.104	0.315	2.03	10.8	0	NA	56.9	0.0464	NA	NA	0.0402	67.1	NA	4.02	NA	NA	0.513	9.79E-06	GS
2024-10-10	Deep & High Salt	20	3.35	13.9	7.65	5.9	1025	0.133	277.2	0	0.514	0.0455	7.01	0	NA	NA	NA	NA	NA	NA	NA	NA	NA	NA	NA	NA	1.50E-05	NGS
2024-10-10	Deep & High Salt	40	3.35	13.9	7.62	5.8	1024	0.298	273.8	0	0.514	0.0455	4.98	0	0.0705	48.397	0.0957	0.30295	11.576	0.1781	237.11	0.00165	0.748	0.4109	108	2.45974	1.28E-05	NGS
2024-10-10	Deep & High Salt	60	3.35	13.9	7.62	5.7	1025	0.129	274.2	0.026	0.515	0.0455	7.56	0	NA	NA	NA	NA	NA	NA	NA	NA	NA	NA	NA	NA	3.61E-06	NGS
2024-10-10	Deep & High Salt	100	3.35	13.9	7.62	5.9	1024	0.249	274.4	0.026	0.516	0.0455	5.87	0	0.00285	48.624	0.1231	0.30295	12.067	0.1605	249.28	0.00165	1.577	0.3712	159	2.15094	8.75E-06	NGS
2024-10-10	Deep & High Salt	150	3.35	13.9	7.62	5.7	1024	0.124	271.9	0	0.515	0.0455	3.69	0	NA	NA	NA	NA	NA	NA	NA	NA	NA	NA	NA	NA	9.08E-06	NGS
2024-10-10	Deep & High Salt	200	3.35	13.5	7.66	5.4	1011	0.12	273.1	0	0.514	0.0455	5.93	0	0.00285	47.615	0.0696	0.30295	12.212	0.0647	252.35	0.00165	1.588	0.3594	151	2.15976	6.37E-06	NGS
2024-10-10	Deep & High Salt	250	3.35	13.3	7.49	4.8	1011	0.127	276.2	0.026	0.515	0.0455	4.33	0	NA	NA	NA	NA	NA	NA	NA	NA	NA	NA	NA	NA	2.74E-05	NGS
2024-10-10	Deep & High Salt	300	3.35	12.7	7.89	6.4	988	0.119	273.2	0.026	0.513	0.0455	4.4	0	0.00285	45.788	0.0842	0.30295	11.935	0.0238	248.26	0.00165	1.697	0.1701	86	2.62085	4.95E-06	NGS
2024-10-10	Deep & High Salt	325	3.35	12.3	7.7	5.9	979	0.128	271	0	0.513	0.0455	8.924	0	0.00285	42.338	0.0709	0.30295	11.135	0.00085	232.48	0.00165	2.824	0.005	98	2.5075	4.95E-06	NGS
2024-10-17	Deep & Low Salt	20	2.9	11.3	7.83	5.9	560	0.138	94	0.026	0.51	0.0455	20.3	0	NA	NA	NA	NA	NA	NA	NA	NA	NA	NA	NA	NA	1.39E-06	NGS
2024-10-17	Deep & Low Salt	40	2.9	11	7.81	5.5	555	0.145	98.6	0.026	0.511	0.095	24.08	0	0.00285	66.71	0.0031	0.30295	22.355	0.00085	71.958	0.00165	8.454	5.2356	109	2.08401	1.48E-06	NGS
2024-10-17	Deep & Low Salt	60	2.9	10.9	7.81	5.2	554	0.133	95.6	0.026	0.509	0.13	25.06	0	NA	NA	NA	NA	NA	NA	NA	NA	NA	NA	NA	NA	2.43E-06	NGS
2024-10-17	Deep & Low Salt	100	2.9	10.9	7.81	5.3	553	0.137	94	0.026	0.522	0.11	20.1	0	0.00285	60.341	0.0031	0.30295	22.065	0.00085	70.321	0.00165	6.643	6.1701	95	1.53119	2.32E-06	NGS
2024-10-17	Deep & Low Salt	150	2.9	10.8	7.8	5.3	552	0.153	98	0	0.51	0.09	26.4	0	NA	NA	NA	NA	NA	NA	NA	NA	NA	NA	NA	NA	1.21E-06	NGS
2024-10-17	Deep & Low Salt	200	2.9	10.7	7.79	5.1	551	0.14	94	0.026	0.521	0.1	21.4	0	0.00285	58.333	0.0704	0.30295	21.24	0.00085	67.184	0.00165	11.38	6.5068	116	1.50149	1.30E-06	NGS
2024-10-17	Deep & Low Salt	250	2.9	10.6	7.8	5.1	550	0.151	94	0.026	0.51	0.0455	23.2	0	NA	NA	NA	NA	NA	NA	NA	NA	NA	NA	NA	NA	1.31E-06	NGS
2024-10-17	Deep & Low Salt	280	2.9	10.6	7.79	4.9	552	0.142	94.3	0	0.511	0.123	21.94	0	0.00285	71.971	0.0738	0.30295	22.066	0.0254	70.059	0.00165	8.022	5.9947	106	2.85517	1.31E-06	NGS
2024-10-22	Shallow & Low Salt	20	0.95	13	8.22	8.4	724	0.134	146	0.026	0.515	0.542	13.72	0	0.0717	47.161	0.0721	0.30295	18.026	0.0222	134.25	0.00165	3.302	4.6364	331	2.04006	2.00E-05	NGS
2024-10-22	Shallow & Low Salt	40	0.95	12.9	8.25	8.7	718	0.134	144	0.026	0.515	0.498	24.28	0	0.00285	70.592	0.0899	0.30295	15.387	0.0788	110.79	0.036	19.82	4.3941	589	1.49932	1.29E-05	NGS
2024-10-22	Shallow & Low Salt	60	0.95	12.8	8.28	9.1	714	0.139	147	0.026	0.515	0.509	19.54	0	NA	NA	NA	NA	NA	NA	NA	NA	NA	NA	375	0.98631	1.79E-05	NGS
2024-10-22	Shallow & Low Salt	85	0.95	12.8	8.17	8.6	716	0.14	144	0.026	0.515	0.478	35.3	0	0.00285	53.41	0.0907	0.30295	14.062	0.0613	100.34	0.038	10.76	3.4558	303	1.66313	8.98E-06	NGS
2024-10-24	Shallow & High Salt	20	1.2	12.6	7.94	8.4	3610	0.725	1221	0.062	0.574	4.543	40.79	0	0.00285	92.964	0.1598	0.30295	33.906	0.00085	991.38	0.00165	13.418	0.9652	102	0.31461	5.98E-06	NGS
2024-10-24	Shallow & High Salt	40	1.2	12.4	7.93	9.6	3610	0.207	1209	0	0.573	4.188	37.35	0	0.00285	79.156	0.0031	0.30295	29.224	0.00085	862.68	0.00165	10.454	0.664	121	0.33198	5.69E-06	NGS
2024-10-24	Shallow & High Salt	60	1.2	12.2	7.91	9.4	3596	0.268	1198	0.053	0.573	3.994	39.671	0	NA	NA	NA	NA	NA	NA	NA	NA	NA	NA	196	0.50232	1.03E-05	NGS
2024-10-24	Shallow & High Salt	110	1.2	14	6.87	2.7	4605	0.228	1462	0	0.626	0.0455	25.26	0	0.00285	149.434	0.1764	6.3887	39.11	0.0346	1266.5	0.00165	9.656	21.192	9550	6.29967	0.00014	NGS

Appendix B: Chapter 3 Supplemental Figures & Tables

Figures

Site Maps

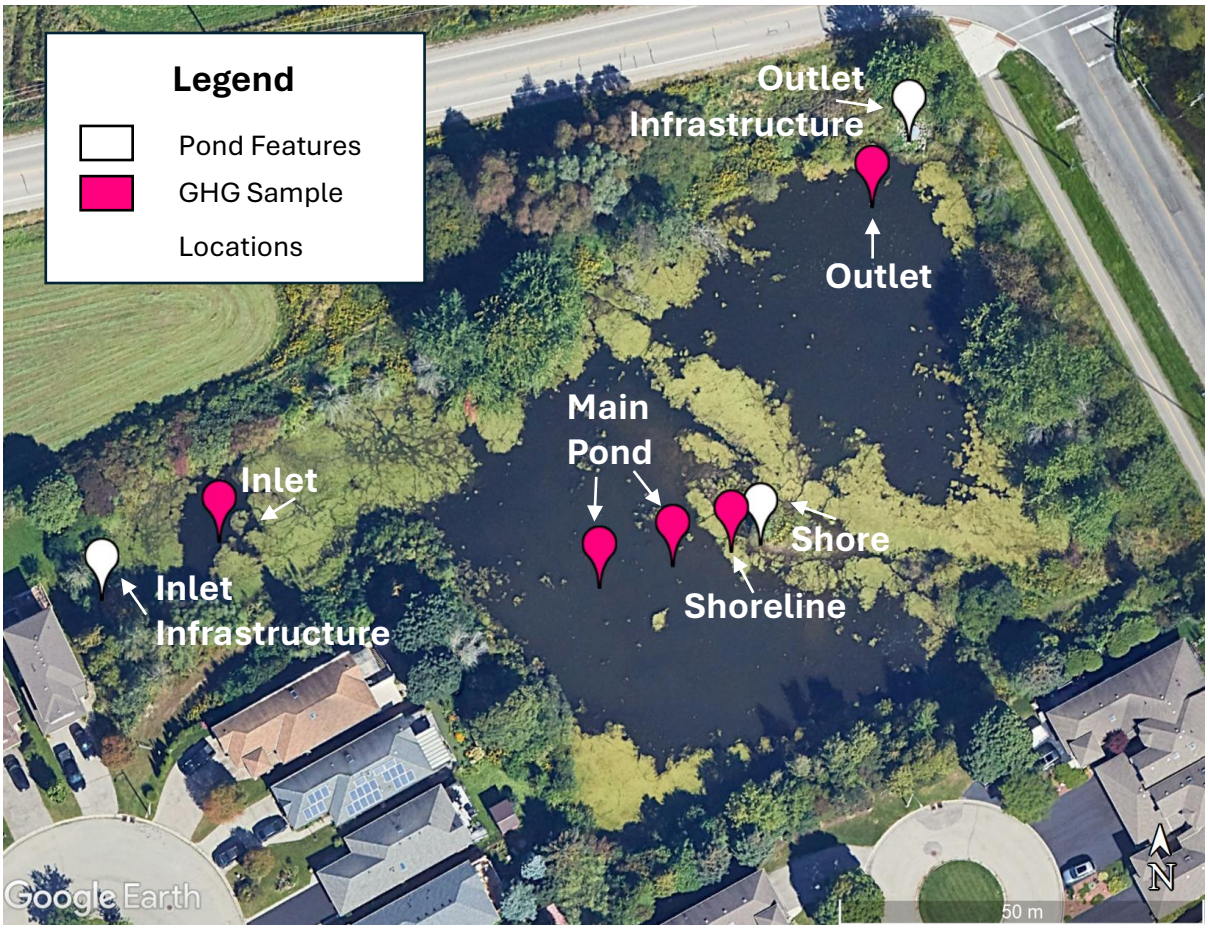


Figure B.1 Site Selection - Shallow & Low Salt Pond: GHG Sampling Locations

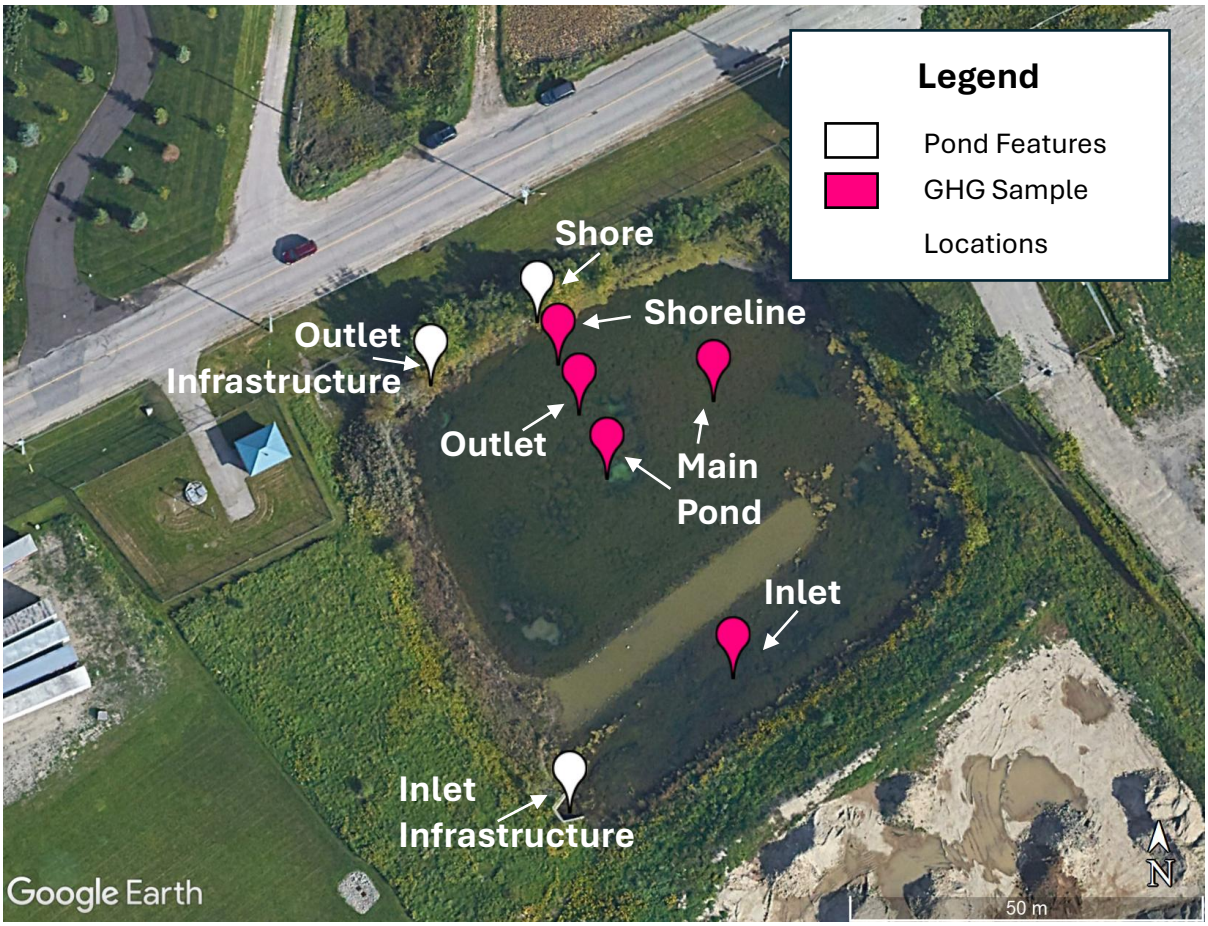


Figure B.2 Site Selection - Shallow & High Salt Pond: GHG Sampling Locations

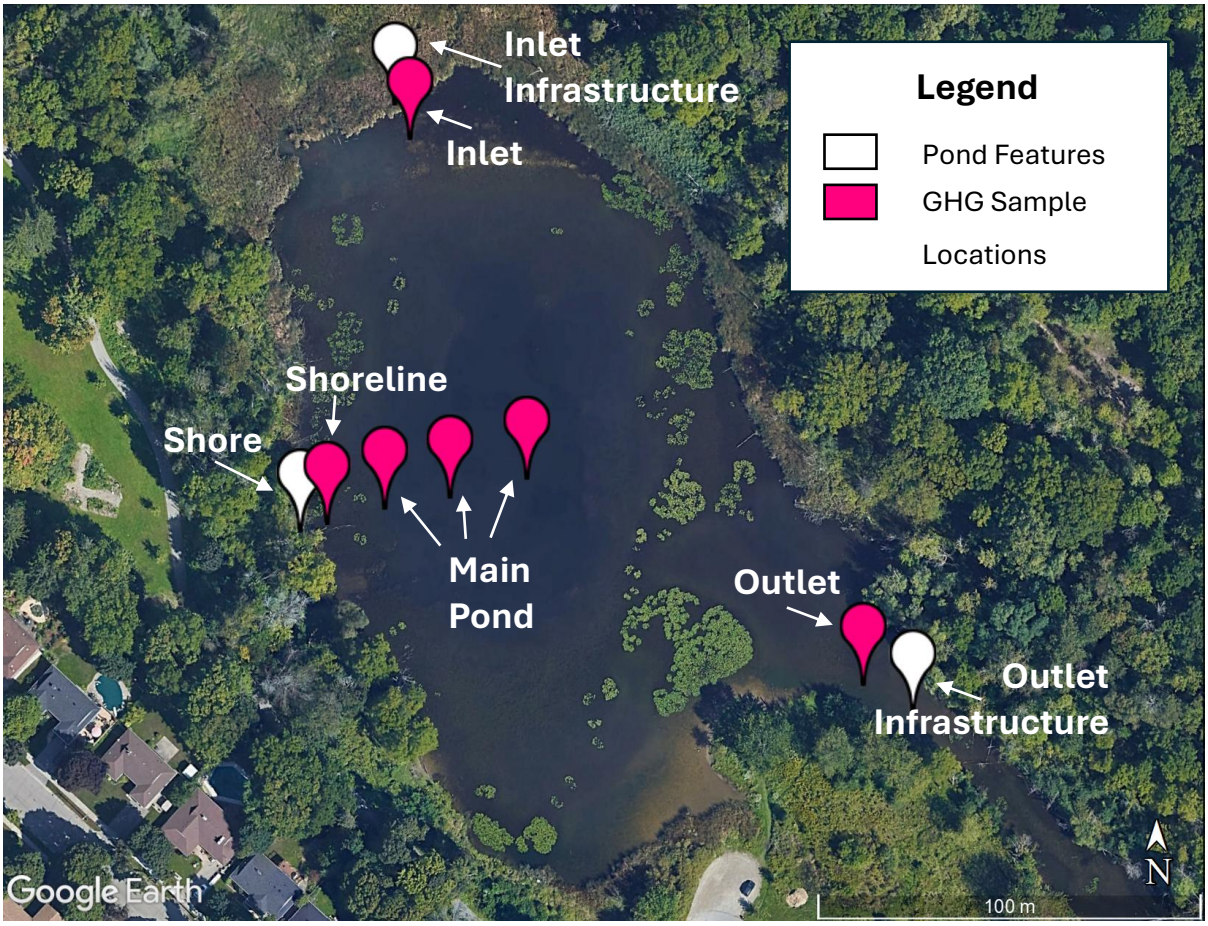


Figure B.3 Site Selection - Deep & High Salt Pond: GHG Sampling Locations

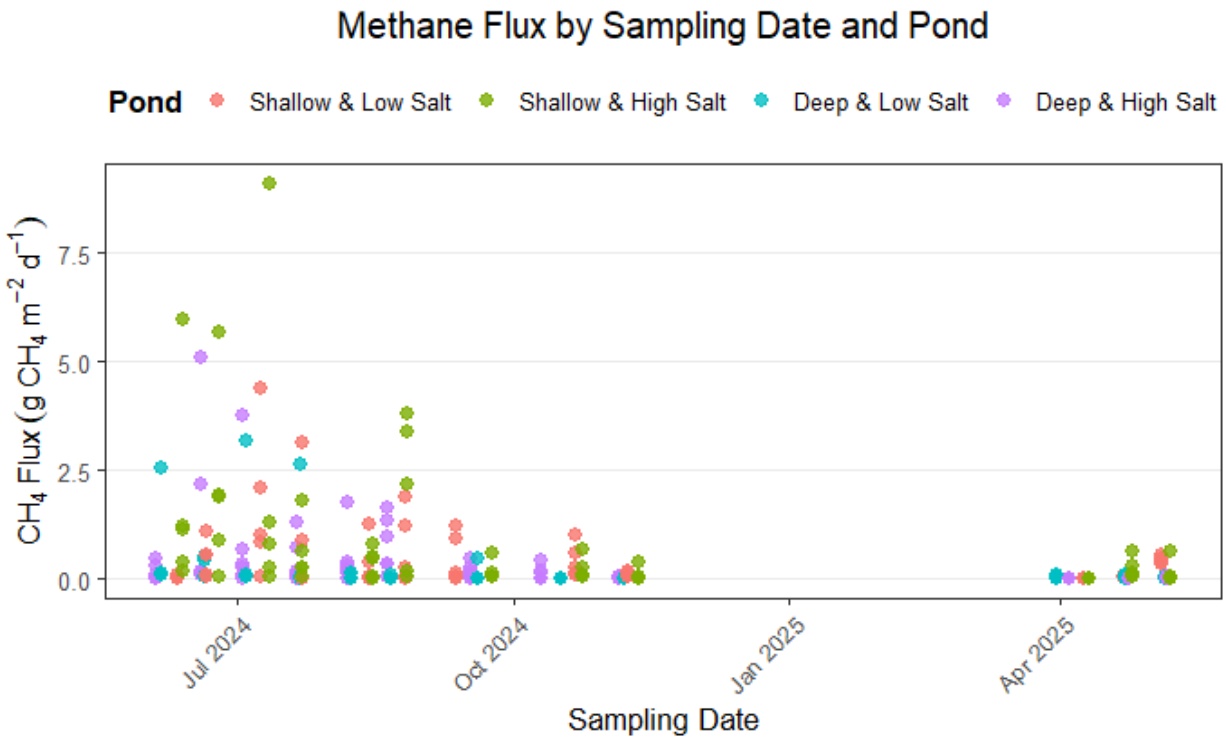


Figure B.4 Total CH_4 fluxes by pond and sampling date

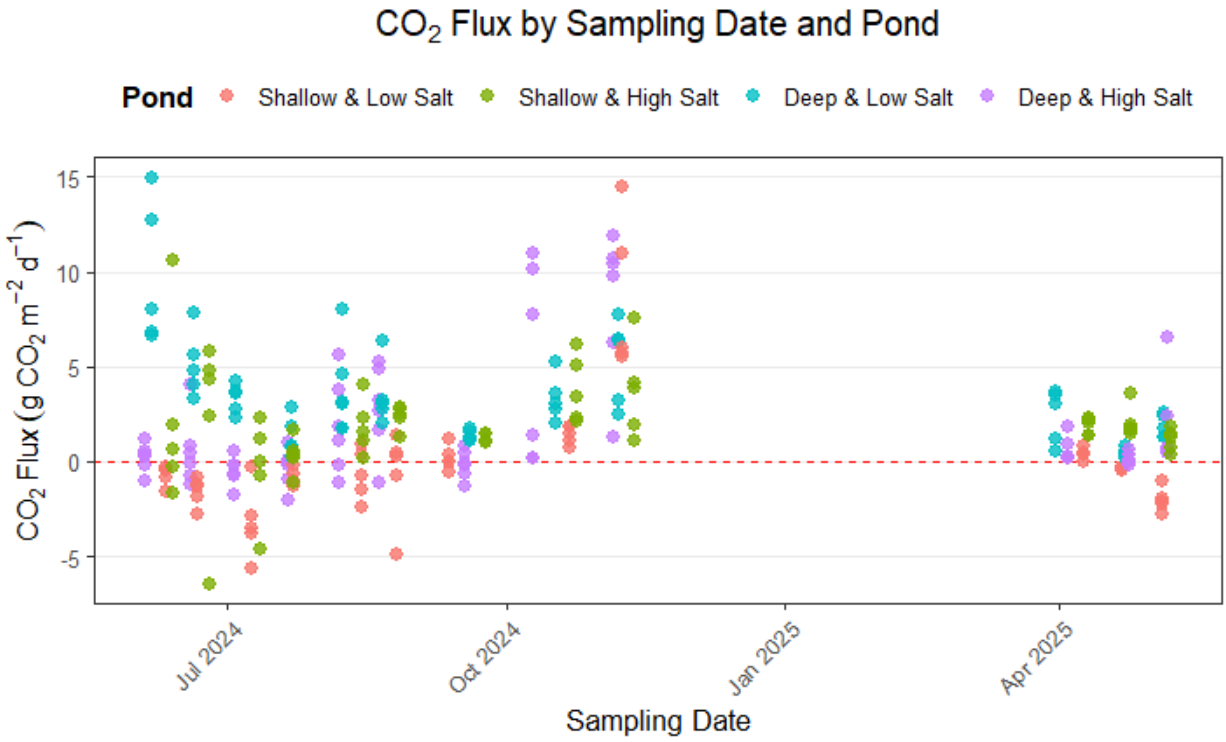


Figure B.5 CO_2 fluxes by pond and sampling date. Samples below 0 indicate uptake.

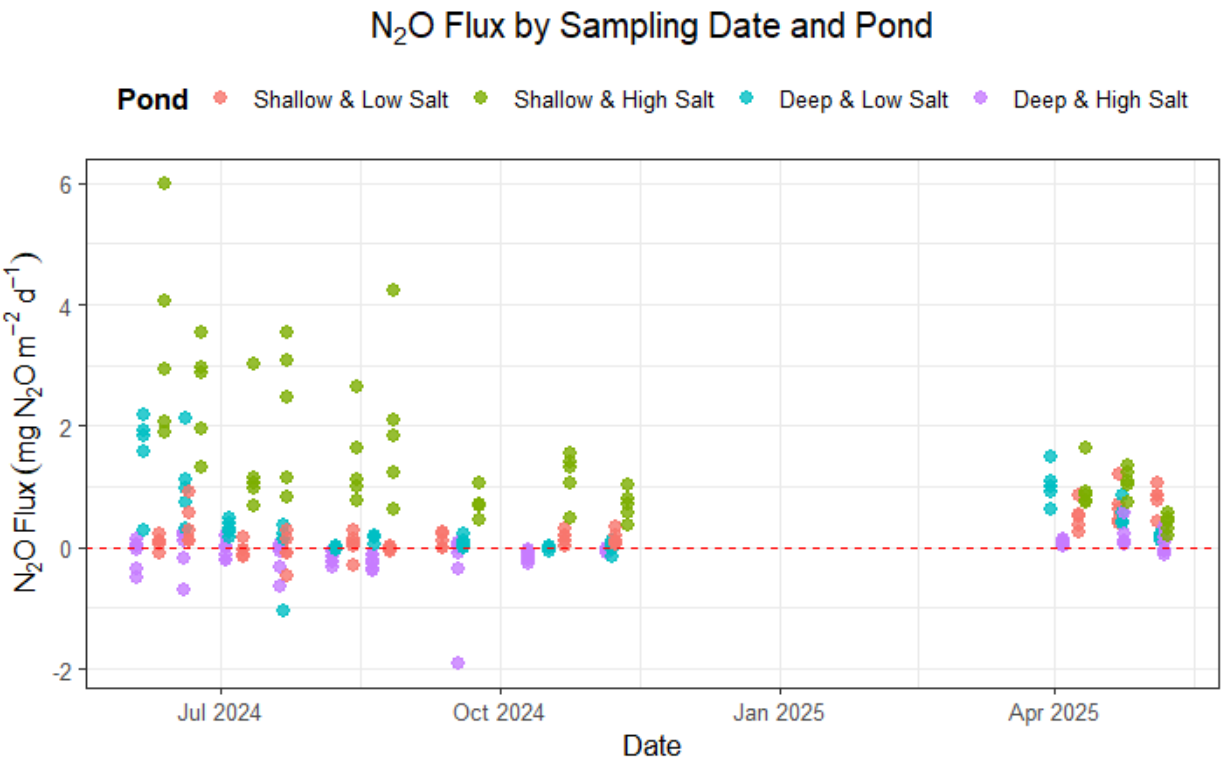


Figure B.6 N_2O fluxes by pond and sampling date. Samples below 0 indicate uptake.

Tables

Table B.1 Environmental conditions in the ponds at the ghg sampling locations

Parameter	Depth	Shallow & Low Salt			Shallow & Low Salt			Shallow & Low Salt			Shallow & Low Salt			Shallow & Low Salt		
		Inlet			Main Pond			Outlet			Main Pond			Shoreline		
		Min Value	Max Value	Mean (SD) Value	Min Value	Max Value	Mean (SD) Value	Min Value	Max Value	Mean (SD) Value	Min Value	Max Value	Mean (SD) Value	Min Value	Max Value	Mean (SD) Value
Water Column Depth (m)		0.73	0.90	0.81 (0.05)	0.95	1.10	1.02 (0.04)	0.98	1.25	1.06 (0.07)	0.78	1.00	0.88 (0.06)	0.34	0.65	0.49 (0.09)
Temperature (°C)	10 cm	7.20	25.70	17.32 (5.95)	4.90	28.20	18.17 (7.24)	4.30	27.60	17.22 (6.72)	5.30	27.60	18.13 (6.91)	5.90	29.80	18.58 (7.1)
	10 cm as	6.80	22.40	16.18 (4.95)	6.00	20.80	15.92 (4.77)	4.30	20.20	15.53 (4.89)	6.00	21.80	16.17 (4.96)	6.20	24.20	16.83 (5.42)
DO (mg/L)	10 cm	2.50	18.25	8.33 (5.08)	4.70	17.15	11.19 (3.9)	4.90	16.29	10.5 (3.71)	5.00	17.28	10.88 (3.91)	5.70	18.32	11.3 (4.27)
	10 cm as	0.90	19.11	6.29 (6.04)	0.50	17.36	7 (5.78)	0.90	20.49	6.95 (6.56)	0.80	17.20	7.47 (5.99)	2.70	18.23	8.99 (5.25)
pH	10 cm	7.56	8.85	8.39 (0.44)	7.61	9.64	8.66 (0.61)	7.64	10.17	8.71 (0.74)	7.63	9.33	8.67 (0.5)	7.65	9.20	8.65 (0.41)
	10 cm as	7.31	8.82	7.89 (0.5)	7.36	8.98	8.01 (0.55)	7.28	8.97	8.11 (0.59)	7.43	9.19	8.11 (0.59)	7.63	9.20	8.4 (0.52)
EC (us/cm)	10 cm	249.20	995.00	725.73 (213.89)	521.00	967.00	747.33 (148.69)	224.00	958.00	682.65 (207.58)	453.80	965.00	740.65 (158.02)	484.20	956.00	735.85 (163.67)
	10 cm as	401.10	1029.00	763.49 (185.49)	720.00	1002.00	830.83 (94.85)	460.90	955.00	720.55 (161.17)	624.00	962.00	791.08 (115.9)	504.80	953.00	750.27 (154.29)
Dissolved CH4 (mol/L)	Shallowest Sample Depth	1.70E-06	9.78E-06	5.42×10^{-6} (2.64×10^{-6})	1.30E-06	2.71E-05	1.05×10^{-5} (8.67×10^{-6})	1.28E-06	1.19E-05	5.17×10^{-6} (3.76×10^{-6})	1.53E-06	1.73E-05	7.67×10^{-6} (5.67×10^{-6})	2.36E-06	1.63E-05	8.16×10^{-6} (4.96×10^{-6})
	Deepest Sample Depth	6.90E-07	6.92E-05	2.48×10^{-5} (2.31×10^{-5})	4.32E-06	5.03E-04	1.09×10^{-4} (1.81×10^{-4})	1.82E-06	2.71E-04	1.11×10^{-4} (1.23×10^{-4})	3.56E-06	1.35E-04	3.94×10^{-5} (4.74×10^{-5})	2.02E-07	3.45E-05	8.91×10^{-6} (1.08×10^{-5})
Dissolved N2O mol/L	Shallowest Sample Depth	0.00E+00	9.05E-08	3.12×10^{-8} (2.91×10^{-8})	0.00E+00	3.84E-08	2.13×10^{-8} (1.49×10^{-8})	0.00E+00	3.08E-08	1.73×10^{-8} (8.93×10^{-9})	0.00E+00	1.38E-05	1.75×10^{-6} (4.87×10^{-6})	0.00E+00	4.33E-08	2.19×10^{-8} (1.53×10^{-8})
	Deepest Sample Depth	0.00E+00	1.07E-07	4.25×10^{-8} (3.44×10^{-8})	0.00E+00	1.38E-05	1.74×10^{-6} (4.87×10^{-6})	0.00E+00	1.69E-05	2.12×10^{-6} (5.97×10^{-6})	1.34E-08	1.45E-05	1.84×10^{-6} (5.12×10^{-6})	8.31E-09	1.12E-05	1.42×10^{-6} (3.95×10^{-6})
Stratification Index ($kg\,m^{-3}\,m^{-1}$)		-0.04	1.85	0.42 (0.67)	-0.02	2.41	0.67 (0.89)	0	2.13	0.46 (0.67)	-0.02	2.74	0.68 (0.82)	-0.06	7.37	1.68 (2.15)

Parameter	Depth	Shallow & High Salt			Shallow & High Salt			Shallow & High Salt			Shallow & High Salt			Shallow & High Salt		
		Inlet			Main Pond			Outlet			Main Pond			Shoreline		
		Min Value	Max Value	Mean (SD) Value	Min Value	Max Value	Mean (SD) Value	Min Value	Max Value	Mean (SD) Value	Min Value	Max Value	Mean (SD) Value	Min Value	Max Value	Mean (SD) Value
Water Column Depth (m)		0.90	1.05	0.97 (0.04)	0.80	1.15	0.89 (0.1)	1.05	1.45	1.22 (0.1)	0.70	1.15	0.93 (0.14)	0.50	0.78	0.64 (0.1)
Temperature (°C)	10 cm	5.80	22.70	15.34 (5.44)	5.80	26.80	17.07 (6.64)	6.50	27.60	17.45 (6.72)	6.80	28.20	17.95 (6.87)	7.40	28.80	18.23 (7.21)
	10 cm as	5.70	17.60	13.49 (4.1)	6.70	20.80	15.18 (4.82)	9.40	20.80	16.14 (3.9)	7.10	20.60	16.08 (4.65)	7.20	23.90	17.32 (6.2)
DO (mg/L)	10 cm	3.90	17.40	10.83 (3.74)	8.70	20.60	13.74 (3.77)	8.30	20.90	13.74 (3.72)	9.40	21.50	14.07 (3.4)	10.00	21.50	14.83 (3.26)
	10 cm as	0.00	18.55	7.1 (5.95)	1.20	15.82	7.57 (4.74)	0.00	8.09	2.34 (2.24)	1.10	16.74	6.97 (5.58)	0.80	20.78	11.56 (5.91)
pH	10 cm	7.51	8.54	7.99 (0.32)	7.68	8.76	8.13 (0.36)	7.51	8.67	8.13 (0.35)	7.63	8.69	8.17 (0.33)	7.59	8.99	8.35 (0.38)
	10 cm as	6.80	8.33	7.67 (0.46)	6.92	8.29	7.6 (0.43)	6.63	7.41	6.91 (0.24)	6.93	8.14	7.54 (0.41)	7.51	8.60	7.99 (0.36)
EC (us/cm)	10 cm	1850.00	5244.00	4212.75 (961.56)	2040.00	5246.00	4243.58 (872.1)	1852.00	5222.00	4178.25 (904.3)	1994.00	5218.00	4169.33 (879.9)	1985.00	5216.00	4241.09 (866.04)
	10 cm as	4758.00	5657.00	5031.5 (273.46)	3916.00	5495.00	4836.25 (378.18)	5488.00	16540.00	8673.83 (4042.88)	4559.00	6456.00	4981.83 (537.11)	3725.00	5230.00	4509.09 (413.74)
Dissolved CH4 (mol/L)	Shallowest Sample Depth	1.43E-06	1.22E-05	6.82×10^{-6} (3.70×10^{-6})	2.44E-06	5.46E-05	1.85×10^{-5} (2.04×10^{-5})	2.45E-06	1.12E-04	3.72×10^{-5} (3.94×10^{-5})	5.13E-06	1.55E-04	5.01×10^{-5} (4.71×10^{-5})	4.43E-08	7.10E-05	3.21×10^{-5} (2.50×10^{-5})
	Deepest Sample Depth	6.16E-06	1.33E-04	4.24×10^{-5} (4.46×10^{-5})	3.77E-06	4.63E-04	1.86×10^{-4} (1.92×10^{-4})	2.38E-08	1.40E-04	9.27×10^{-5} (4.91×10^{-5})	1.06E-05	1.87E-04	8.46×10^{-5} (5.84×10^{-5})	2.23E-06	3.45E-04	9.95×10^{-5} (1.40×10^{-4})
Dissolved N2O mol/L	Shallowest Sample Depth	4.11E-08	2.37E-05	3.06×10^{-6} (8.34×10^{-6})	3.95E-08	1.14E-05	1.50×10^{-6} (4.00×10^{-6})	4.08E-08	3.77E-06	5.48×10^{-7} (1.30×10^{-6})	0.00E+00	1.29E-07	7.49×10^{-8} (4.49×10^{-8})	0.00E+00	1.36E-07	7.30×10^{-8} (4.85×10^{-8})
	Deepest Sample Depth	1.81E-08	5.97E-06	8.62×10^{-7} (2.07×10^{-6})	0.00E+00	1.78E-05	2.31×10^{-6} (6.26×10^{-6})	0.00E+00	5.19E-07	1.07×10^{-7} (1.73×10^{-7})	9.94E-09	4.34E-06	6.42×10^{-7} (1.50×10^{-6})	0.00E+00	9.77E-06	1.44×10^{-6} (3.67×10^{-6})
Stratification Index ($kg\ m^{-3}\ m^{-1}$)		0.03	3.09	1.18 (0.93)	0.01	3.05	1.06 (0.95)	0.32	7.7	3.11 (2.61)	0.11	3.53	1.32 (1.12)	-0.04	4.5	0.99 (1.48)

Parameter	Depth	Deep & Low Salt			Deep & Low Salt			Deep & Low Salt			Deep & Low Salt			Deep & Low Salt		
		Inlet			Main Pond			Outlet			Main Pond			Shoreline		
		Min Value	Max Value	Mean (SD) Value	Min Value	Max Value	Mean (SD) Value	Min Value	Max Value	Mean (SD) Value	Min Value	Max Value	Mean (SD) Value	Min Value	Max Value	Mean (SD) Value
Water Column Depth (m)		1.37	2.30	1.82 (0.21)	1.02	2.40	1.37 (0.43)	2.75	4.00	3.17 (0.34)	1.70	2.90	2.19 (0.32)	0.49	1.25	0.76 (0.2)
Temperature (°C)	10 cm	5.80	23.20	17.18 (6.03)	6.00	23.90	17.89 (6.06)	6.60	24.20	18.28 (5.95)	6.70	25.20	18.83 (6.05)	6.90	24.80	19.13 (6.1)
	10 cm as	6.50	17.80	13.83 (3.77)	5.50	22.70	16.61 (5.63)	6.20	21.60	15.23 (5.23)	6.20	22.70	16.13 (5.35)	6.70	23.50	17.63 (5.52)
DO (mg/L)	10 cm	5.20	13.80	7.51 (2.67)	4.70	13.48	7.41 (2.49)	4.50	13.60	7.85 (2.76)	4.00	12.61	7.71 (2.41)	4.70	13.90	7.76 (2.64)
	10 cm as	0.00	8.47	2.45 (2.73)	3.70	13.34	6.57 (2.97)	0.30	19.55	4.61 (5.8)	2.00	15.47	6.37 (4.25)	4.30	13.71	7.67 (3.1)
pH	10 cm	7.63	8.64	8.15 (0.37)	7.53	8.52	8.04 (0.3)	7.62	8.54	8.09 (0.33)	7.53	8.66	8.11 (0.35)	7.60	8.55	8.12 (0.34)
	10 cm as	7.19	8.00	7.53 (0.25)	7.46	8.28	7.73 (0.26)	7.16	9.00	7.68 (0.46)	7.38	8.66	7.77 (0.35)	7.50	8.40	7.98 (0.31)
EC (us/cm)	10 cm	541.00	1127.00	852.17 (186.78)	501.00	1137.00	848.17 (202.15)	476.10	1137.00	845.84 (206.33)	483.90	1142.00	847.41 (206.8)	490.10	1205.00	855.68 (217.85)
	10 cm as	755.00	1154.00	952.17 (106.48)	515.60	1152.00	857.72 (197.63)	537.00	1139.00	871.92 (205.74)	502.10	1140.00	854.76 (207.99)	477.20	1146.00	844.35 (207.42)
Dissolved CH4 (mol/L)	Shallowest Sample Depth	1.02E-06	1.50E-05	5.32×10^{-6} (4.66×10^{-6})	9.65E-07	7.30E-06	4.12×10^{-6} (2.23×10^{-6})	1.12E-06	5.44E-06	2.88×10^{-6} (1.68×10^{-6})	7.16E-07	6.23E-06	3.63×10^{-6} (2.16×10^{-6})	9.36E-07	5.99E-06	3.29×10^{-6} (1.89×10^{-6})
	Deepest Sample Depth	2.83E-06	6.97E-05	2.31×10^{-5} (2.29×10^{-5})	7.88E-07	1.32E-05	7.24×10^{-6} (4.44×10^{-6})	1.27E-06	1.70E-04	4.68×10^{-5} (7.21×10^{-5})	1.33E-06	1.63E-05	6.86×10^{-6} (5.49×10^{-6})	0.00E+00	9.08E-06	3.49×10^{-6} (2.82×10^{-6})
Dissolved N2O mol/L	Shallowest Sample Depth	1.30E-08	1.63E-05	2.07×10^{-6} (5.75×10^{-6})	1.66E-08	8.79E-06	1.12×10^{-6} (3.10×10^{-6})	1.46E-08	7.65E-06	9.80×10^{-7} (2.70×10^{-6})	1.42E-08	7.99E-06	1.02×10^{-6} (2.81×10^{-6})	1.35E-08	7.97E-06	1.02×10^{-6} (2.81×10^{-6})
	Deepest Sample Depth	5.97E-09	7.06E-06	9.29×10^{-7} (2.48×10^{-6})	1.81E-08	8.73E-06	1.12×10^{-6} (3.08×10^{-6})	1.14E-08	9.21E-06	1.19×10^{-6} (3.24×10^{-6})	1.06E-08	7.34E-06	9.63×10^{-7} (2.58×10^{-6})	1.27E-08	7.19E-06	9.29×10^{-7} (2.53×10^{-6})
Stratification Index ($kg\ m^{-3}\ m^{-1}$)		0	1.05	0.5 (0.38)	-0.04	0.68	0.2 (0.21)	0.04	0.51	0.2 (0.16)	0.05	0.7	0.27 (0.22)	0	1.41	0.61 (0.53)

Parameter	Depth	Deep & High Salt			Deep & High Salt			Deep & High Salt			Deep & High Salt			Deep & High Salt		
		Inlet			Main Pond			Outlet			Main Pond			Main Pond		
		Min Value	Max Value	Mean (SD) Value	Min Value	Max Value	Mean (SD) Value	Min Value	Max Value	Mean (SD) Value	Min Value	Max Value	Mean (SD) Value	Min Value	Max Value	Mean (SD) Value
Water Column Depth (m)		0.20	0.62	0.51 (0.1)	3.30	3.85	3.56 (0.18)	0.50	0.95	0.81 (0.12)	2.00	3.40	2.8 (0.37)	1.30	1.81	1.6 (0.15)
Temperature (°C)	10 cm	6.30	25.70	17.86 (6.32)	7.00	27.80	19.44 (6.32)	6.70	26.00	18.23 (6.17)	8.50	27.20	19.91 (5.86)	9.30	27.00	20.29 (5.66)
	10 cm as	6.80	25.60	17.49 (5.88)	4.30	17.00	12.07 (4.37)	6.60	26.20	17.76 (6.01)	4.30	21.20	14.56 (5.74)	5.10	22.90	17.31 (5.78)
DO (mg/L)	10 cm	3.40	11.85	7.18 (2.17)	5.20	13.27	9.07 (2.75)	3.10	11.93	7.72 (2.63)	5.50	13.10	9.27 (2.71)	6.30	12.85	8.89 (2.1)
	10 cm as	0.90	10.65	4.99 (3.06)	0.00	5.90	1.51 (1.87)	0.20	7.89	4.79 (2.68)	0.11	14.76	3.37 (3.94)	1.00	16.03	5.34 (4.98)
pH	10 cm	7.67	8.98	8.23 (0.4)	7.67	9.01	8.42 (0.51)	7.72	8.80	8.35 (0.33)	7.71	9.01	8.38 (0.45)	7.69	8.78	8.39 (0.36)
	10 cm as	6.95	8.42	7.84 (0.46)	6.27	7.77	7.02 (0.52)	7.03	8.33	7.93 (0.45)	6.46	7.83	7.27 (0.37)	7.06	8.66	7.73 (0.51)
EC (us/cm)	10 cm	994.00	1745.00	1421.42 (254.13)	900.00	1712.00	1375.75 (279.37)	869.00	1718.00	1360.42 (290.21)	919.00	1713.00	1373.42 (274.88)	912.00	1716.00	1377.67 (279.2)
	10 cm as	1020.00	1785.00	1467 (249.85)	1292.00	3641.00	2820.83 (868.11)	907.00	1713.00	1374.5 (286.06)	1154.00	3487.00	2092.17 (825.6)	1081.00	1812.00	1456.33 (272.5)
Dissolved CH4 (mol/L)	Shallowest Sample Depth	5.06E-08	5.70E-06	3.46×10^{-6} (2.26×10^{-6})	7.30E-07	1.50E-05	4.79×10^{-6} (4.33×10^{-6})	3.78E-07	6.03E-06	2.48×10^{-6} (1.82×10^{-6})	2.12E-06	1.35E-04	2.64×10^{-5} (4.36×10^{-5})	1.54E-06	2.65E-05	8.86×10^{-6} (7.39×10^{-6})
	Deepest Sample Depth	1.29E-09	1.21E-04	2.86×10^{-5} (4.42×10^{-5})	0.00E+00	1.97E-04	5.17×10^{-5} (7.70×10^{-5})	3.44E-09	6.72E-05	1.72×10^{-5} (2.37×10^{-5})	5.02E-08	3.38E-04	8.77×10^{-5} (1.12×10^{-4})	1.04E-08	1.08E-04	2.01×10^{-5} (3.40×10^{-5})
Dissolved N2O mol/L	Shallowest Sample Depth	1.76E-09	6.92E-06	8.73×10^{-7} (2.44×10^{-6})	0.00E+00	1.54E-08	9.19×10^{-9} (5.18×10^{-9})	2.99E-09	9.85E-06	1.24×10^{-6} (3.48×10^{-6})	0.00E+00	1.41E-08	7.32×10^{-9} (4.57×10^{-9})	0.00E+00	1.30E-08	7.40×10^{-9} (4.99×10^{-9})
	Deepest Sample Depth	0.00E+00	6.92E-06	8.71×10^{-7} (2.44×10^{-6})	0.00E+00	1.52E-05	1.93×10^{-6} (5.36×10^{-6})	1.94E-09	1.59E-05	1.99×10^{-6} (5.62×10^{-6})	0.00E+00	1.25E-05	1.57×10^{-6} (4.42×10^{-6})	0.00E+00	1.93E-06	2.48×10^{-7} (6.80×10^{-7})
Stratification Index ($kg\ m^{-3}\ m^{-1}$)		-0.19	1.1	0.31 (0.39)	0.07	1.26	0.66 (0.36)	-0.1	0.64	0.16 (0.2)	0.05	1.13	0.55 (0.37)	0.08	1.04	0.48 (0.29)

Parameter	Depth	Deep & High Salt		
		Shoreline		
		Min Value	Max Value	Mean (SD) Value
Water Column Depth (m)		0.55	1.15	0.88 (0.17)
Temperature (°C)	10 cm	10.90	26.90	21.18 (5.55)
	10 cm as	8.20	26.10	18.92 (5.43)
DO (mg/L)	10 cm	6.70	14.50	10.41 (2.31)
	10 cm as	1.50	15.00	7.57 (3.81)
pH	10 cm	8.03	9.31	8.69 (0.36)
	10 cm as	7.57	8.82	8.21 (0.37)
EC (us/cm)	10 cm	924.00	1722.00	1372.25 (278.82)
	10 cm as	925.00	1723.00	1380.92 (275.69)
Dissolved CH4 (mol/L)	Shallowest Sample Depth	7.04E-07	1.20E-05	4.41×10^{-6} (3.44×10^{-6})
	Deepest Sample Depth	1.21E-06	3.78E-05	1.04×10^{-5} (1.24×10^{-5})
Dissolved N2O mol/L	Shallowest Sample Depth	2.52E-09	8.69E-06	1.10×10^{-6} (3.07×10^{-6})
	Deepest Sample Depth	0.00E+00	7.39E-06	9.31×10^{-7} (2.61×10^{-6})
Stratification Index ($kg\ m^{-3}\ m^{-1}$)		0.11	1.37	0.73 (0.49)